Seasonal Variation of Subgrade Support Values

Final Report

Prepared for the
STATE OF MONTANA
DEPARTMENT OF TRANSPORTATION
RESEARCH, DEVELOPMENT AND TECHNOLOGY TRANSFER PROGRAM
in cooperation with the
U.S. DEPARTMENT OF TRANSPORTATION
FEDERAL HIGHWAY ADMINISTRATION

September 30, 1996

Prepared by

Dr. Steven W. Perkins
Assistant Professor
&
Jeffrey S. Lindley
Graduate Research Assistant

Department of Civil Engineering
Montana State University
Bozeman, Montana 59717
Office Telephone: 406-994-6119
Fax: 406-994-6105
E-Mail: stevep@ce.montana.edu

TECHNICAL REPORT STANDARD PAGE

1. Report No. FHWA/MT-96/8117-4	2. Government Accession No.	3. Recipient's Catalog No.
4. Title and Subtitle Seasonal Variation of Subgrade Support Values	5. Report Date September 30, 1996 6. Performing Organization Code	
7. Author(s) Steven W. Perkins, Ph.D., P.E. Jeffrey S. Lindley	8. Performing Organization Report No.	
9. Performing Organization Name and Address Department of Civil Engineering 205 Cobleigh Hall Montana State University Bozeman, Montana 59717	10. Work Unit No. 11. Contract or Grant No. 8117	
12. Sponsoring Agency Name and Address Montana Department of Transportation 2701 Prospect Avenue P.O. Box 201001 Helena, Montana 59620-1001	13. Type of Report and Period Covered Final August 1, 1995 - September 30, 1996 14. Sponsoring Agency Code 5401	

15. Supplementary Notes
Preparation in cooperation with the Montana Department of Transportation and the U.S. Department of Transportation, Federal Highway Administration

16. Abstract

Seasonal variations in climatic conditions have long been recognized to have a significant impact on the structural response of flexible pavements. Of particular significance is the effect of subgrade moisture content on subgrade support values and potential roadway damage. The Montana Department of Transportation is conducting a project to evaluate the response of subgrade resilient modulus to seasonal changes in subgrade moisture content. Moisture content is being measured through permanent subsurface instrumentation while deflection tests are periodically being conducted to establish subgrade resilient modulus values. This report describes work performed in support of this project. The purpose of this study was to provide laboratory data on subgrade support values for the instrumented sites. This data will illustrate the variation in subgrade support with changes in moisture content and sample dry density. This information will be used to verify the accuracy of the data generated in the field and might also be used to help guide the back-calculation procedure. Laboratory testing has consisted of resilient modulus, triaxial compression, CBR and R-Value tests. Results have been generated for various combinations of sample dry density and degree of saturation. These results have been related to resilient modulus whenever possible. The results tend to show that ultimate strength related parameters are most sensitive to changes in dry density and moisture content for the cohesive subgrade soils and that deformation related parameters are most sensitive for the more non-cohesive subgrade soils.

17. Key Words Pavements, Highways, Subgrade, Support, CBR, R-Value, Seasonal, Variation, Moisture, Strength, Stiffness, Montana, Resilient Modulus, Triaxial Compression		18. Distribution Statement Unrestricted. This document is available through the National Technical Information Service, Springfield, VA 21161.	
19. Security Classif. (of this report) Unclassified	20. Security Classif. (of this page) Unclassified	21. No. of Pages 115	22. Price

DISCLAIMER STATEMENT

The information reported herein was sponsored by the Montana Department of Transportation in conjunction with the Federal Highway Administration. The opinions, findings and conclusions expressed in this publication are those of the author and not necessarily those of the Montana Department of Transportation or the Federal Highway Administration. This report does not constitute a standard, specification or regulation.

ALTERNATIVE FORMAT STATEMENT

MDT attempts to provide reasonable accommodations for any disability that may interfere with a person participating in any service, program, or activity of the Department. Alternative accessible formats of this document will be provided upon request. For further information, call (406) 444-6269 or TDD (406) 444-7696.

TABLE OF CONTENTS

LIST OF TABLES 1
LIST OF FIGURES 3
CONVERSION FACTORS 7
SUMMARY 8
INTRODUCTION 9
PROJECT OVERVIEW 10
RESEARCH APPROACH 12
SUMMARY OF SITE DATA 13
SHELBY TUBE SAMPLE LOGS 14
BASE COURSE GRAIN SIZE DISTRIBUTION 14
LABORATORY TESTING 15
- TRIAXIAL COMPRESSION TESTS 15
  - SAMPLE PREPARATION 16
  - TRIAXIAL APPARATUS 16
  - TRIAXIAL RESULTS: COHESIVE SUBGRADE SITES 20
  - TRIAXIAL RESULTS: NON-COHESIVE SUBGRADE SITES 20
- RESILIENT MODULUS TESTS 21
- CBR TESTS 21

SUMMARY OF LABORATORY RESULTS 22
- TRIAXIAL COMPRESSION TESTS 22
- RESILIENT MODULUS TESTS 23
- CBR TESTS 23

CORRELATION OF RESULTS TO RESILIENT MODULUS 23
- TRIAXIAL COMPRESSION TESTS 24
- CBR TESTS 24
- R-VALUE TESTS 25

DISCUSSION OF RESULTS 25
IMPLEMENTATION PLAN 27
CONCLUSIONS 28
REFERENCES 30
APPENDIX A: TABLES A1
APPENDIX B: FIGURES B1

LIST OF TABLES

Table 1a. Layer Thicknesses: Sunburst Site A2
Table 1b. Layer Thicknesses: Alzada Site A2
Table 1c. Layer Thicknesses: Loma Site A2
Table 1d. Layer Thicknesses: Swan Site A2
Table 1e. Layer Thicknesses: Dickey Lake Site A2
Table 2a. Subsurface Data for the Sunburst Site: Instrumentation Installed 9-22-95 A3
Table 2b. Subsurface Data for the Alzada Site: Instrumentation Installed 11-29-95 A4
Table 2c. Subsurface Data for the Loma Site: Instrumentation Installed 10-3-95 A5
Table 2d. Subsurface Data for the Swan Site: Instrumentation Installed 11-15-95 A6
Table 2e. Subsurface Data for the Dickey Lake Site: Instrumentation Installed 11-16-95 A7
Table 3. Specific Gravity and R-Value for Subgrade Soils A8
Table 4a. Triaxial Test Results: Sunburst Site A8
Table 4b. Triaxial Test Results: Alzada Site A9
Table 4c. Triaxial Test Results: Loma Site A9
Table 4d. Triaxial Test Results: Swan Site A10
Table 4e. Triaxial Test Results: Dickey Lake Site A11
Table 5a. Resilient Modulus Results: Sunburst Subgrade: γ_d = 18.7 kN/m^3 (119 lb/ft^3), ω = 12.0 %, S = 72.0 % A12
Table 5b. Resilient Modulus Results: Alzada Subgrade: γ_d = 17.5 kN/m^3 (112 lb/ft^3), ω = 18.3 %, S = 93.0 % A13
Table 5c. Resilient Modulus Results: Loma Subgrade: γ_d = 17.1 kN/m^3 (109 lb/ft^3), ω = 7.0 %, S = 33.2 % A14
Table 5d. Resilient Modulus Results: Loma Subgrade: γ_d = 17.1 kN/m^3 (109 lb/ft^3), ω = 12.0 %, S = 56.9 % A15
Table 5e. Resilient Modulus Results: Loma Subgrade: γ_d = 17.1 kN/m^3 (109 lb/ft^3), ω = 20.0 %, S = 92.8 % A16
Table 5f. Resilient Modulus Results: Swan Subgrade: γ_d = 17.1 kN/m^3 (109 lb/ft^3), ω = 8.0 %, S = 46.5 % A17
Table 5g. Resilient Modulus Results: Swan Subgrade: γ_d = 17.1 kN/m^3 (109 lb/ft^3), ω = 13.0 %, S = 75.5 % A18
Table 5h. Resilient Modulus Results: Swan Subgrade: γ_d = 17.3 kN/m^3 (110 lb/ft^3), ω = 20.0 %, S = 100 % A19
Table 5i. Resilient Modulus Results: Dickey Lake Subgrade: γ_d = 17.3 kN/m^3 (110 lb/ft^3), ω = 7.0 %, S = 37.0 % A20
Table 5j. Resilient Modulus Results: Dickey Lake Subgrade: γ_d = 17.3 kN/m^3 (110 lb/ft^3), ω =12.0 %, S = 64.0 % A21
Table 5k. Resilient Modulus Results: Dickey Lake Subgrade: γ_d = 17.3 kN/m^3 (110 lb/ft^3), ω =13.0 %, S = 70.0 % A22

Table 6a. CBR Results: Sunburst Site A23
Table 6b. CBR Results: Alzada Site A24
Table 6c. CBR Results: Loma Site A25
Table 6d. CBR Results: Swan Site A26
Table 6e. CBR Results: Dickey Lake Site A27
Table 7. Summarized Resilient Modulus Values A28
Table 8a. Texas Triaxial Class and Correlated Resilient Modulus: Sunburst Subgrade A29
Table 8b. Texas Triaxial Class and Correlated Resilient Modulus: Alzada Subgrade A29
Table 8c. Texas Triaxial Class and Correlated Resilient Modulus: Loma Subgrade A30
Table 8d. Texas Triaxial Class and Correlated Resilient Modulus: Swan Subgrade A31
Table 8e. Texas Triaxial Class and Correlated Resilient Modulus: Dickey Lake Subgrade A32
Table 9. R-Value and Correlated Resilient Modulus A33

LIST OF FIGURES

Figure 1a.	Grain Size Distribution Curves for the Sunburst Site	B2
Figure 1b.	Grain Size Distribution Curves for the Alzada Site	B2
Figure 1c.	Grain Size Distribution Curves for the Loma Site	B3
Figure 1d.	Grain Size Distribution Curves for the Swan Site	B3
Figure 1e.	Grain Size Distribution Curves for the Dickey Lake Site	B4
Figure 2.	Schematic Diagram of Triaxial Moisture Conditioning Apparatus Used for Sample Saturation	B5
Figure 3.	Schematic Diagram of Triaxial Moisture Conditioning Apparatus Used for Sample Desaturation	B6
Figure 4a.	Moisture Release Curve: Sunburst Site	B7
Figure 4b.	Moisture Release Curve: Alzada Site	B7
Figure 5a.	Triaxial Compression Results: Sunburst Subgrade, γ_d = 18.5 kN/m^3 (118 lb/ft^3), ω = 16.0 %, S = 92.7 %, σ_3 = 21.8 kPa (3.17 psi)	B8
Figure 5b.	Triaxial Compression Results: Sunburst Subgrade, γ_d = 19.4 kN/m^3 (124 lb/ft^3), ω = 15.2 %, S = 100 %, σ_3 = 20.3 kPa (2.95 psi)	B8
Figure 5c.	Triaxial Compression Results: Sunburst Subgrade, γ_d = 19.9 kN/m^3 (127 lb/ft^3), ω = 12.5 %, S = 87.5 %, σ_3 = 24.5 kPa (3.56 psi)	B9
Figure 6a.	Triaxial Compression Results: Alzada Subgrade, γ_d = 19.3 kN/m^3 (123 lb/ft^3), ω = 14.0 %, S = 99.3 %, σ_3 = 21.8 kPa (3.17 psi)	B9
Figure 6b.	Triaxial Compression Results: Alzada Subgrade, γ_d = 17.5 kN/m^3 (112 lb/ft^3), ω = 16.0 %, S = 82.6 %, σ_3 = 21.8 kPa (3.17 psi)	B10
Figure 6c.	Triaxial Compression Results: Alzada Subgrade, γ_d = 18.0 kN/m^3 (115lb/ft^3), ω = 16.0 %, S = 88.4 %, σ_3 = 23.0 kPa (3.35 psi)	B10
Figure 7a.	Triaxial Compression Results: Loma Subgrade, γ_d = 14.4 kN/m^3 (92 lb/ft^3), ω = 7.0 %, S = 25.2 %, σ_3 = 18.3 kPa (2.66 psi)	B11
Figure 7b.	Triaxial Compression Results: Loma Subgrade, γ_d = 17.3 kN/m^3 (110 lb/ft^3), ω = 7.0 %, S = 43.1 %, σ_3 = 21.3 kPa (3.10 psi)	B11
Figure 7c.	Triaxial Compression Results: Loma Subgrade, γ_d = 18.7 kN/m^3 (119 lb/ft^3), ω = 7.0 %, S = 58.2 %, σ_3 = 22.6 kPa (3.29 psi)	B12
Figure 7d.	Triaxial Compression Results: Loma Subgrade, γ_d = 15.1 kN/m^3 (96 lb/ft^3), ω = 12.0 %, S = 49.0 %, σ_3 = 18.7 kPa (2.72 psi)	B12
Figure 7e.	Triaxial Compression Results: Loma Subgrade, γ_d = 17.4 kN/m^3 (111 lb/ft^3), ω = 12.0 %, S = 76.7 %, σ_3 = 22.3 kPa (3.24 psi)	B13
Figure 7f.	Triaxial Compression Results: Loma Subgrade, γ_d = 19.0 kN/m^3 (121 lb/ft^3), ω = 12.0 %, S = 100 %, σ_3 = 24 kPa (3.49 psi)	B13
Figure 7g.	Triaxial Compression Results: Loma Subgrade, γ_d = 15.4 kN/m^3 (98.0 lb/ft^3), ω = 20.0 %, S = 86.3 %, σ_3 = 17.7 kPa (2.57 psi)	B14
Figure 7h.	Triaxial Compression Results: Loma Subgrade, γ_d = 18.0 kN/m^3 (115 lb/ft^3), ω = 20.0 %, S = 100 %, σ_3 = 24.0 kPa (3.49 psi)	B14

Figure 7i. Triaxial Compression Results: Loma Subgrade, γ_d = 19.0 kN/m^3 (121 lb/ft^3), ω = 20.0 %, S = 100 %, σ_3 = 25.2 kPa (3.67 psi) B15
Figure 8a. Triaxial Compression Results: Swan Subgrade, γ_d = 15.4 kN/m^3 (98.0 lb/ft^3), ω = 8.0 %, S = 26.7 %, σ_3 = 19.7 kPa (2.87 psi) B15
Figure 8b. Triaxial Compression Results: Swan Subgrade, γ_d = 17.4 kN/m^3 (111 lb/ft^3), ω = 8.0 %, S = 47.7 %, σ_3 = 20.7 kPa (3.01 psi) B16
Figure 8c. Triaxial Compression Results: Swan Subgrade, γ_d = 20.1 kN/m^3 (128 lb/ft^3), ω = 8.0 %, S = 69.2 %, σ_3 = 21.3 kPa (3.10 psi) B16
Figure 8d. Triaxial Compression Results: Swan Subgrade, γ_d = 14.6 kN/m^3 (93.0 lb/ft^3), ω = 13.0 %, S = 49.3 %, σ_3 = 18.7 kPa (2.72 psi) B17
Figure 8e. Triaxial Compression Results: Swan Subgrade, γ_d = 18.0 kN/m^3 (115 lb/ft^3), ω = 13.0 %, S = 94.2 %, σ_3 = 21.3 kPa (3.10 psi) B17
Figure 8f. Triaxial Compression Results: Swan Subgrade, γ_d = 19.0 kN/m^3 (121 lb/ft^3), ω = 13.0 %, S = 100 %, σ_3 = 23.1 kPa (3.36 psi) B18
Figure 8g. Triaxial Compression Results: Swan Subgrade, γ_d = 14.8 kN/m^3 (94.0 lb/ft^3), ω = 19.0 %, S = 74.4 %, σ_3 = 18.7 kPa (2.72 psi) B18
Figure 8h. Triaxial Compression Results: Swan Subgrade, γ_d = 18.0 kN/m^3 (115 lb/ft^3), ω = 19.0 %, S = 100 %, σ_3 = 20.8 kPa (3.03 psi) B19
Figure 8i. Triaxial Compression Results: Swan Subgrade, γ_d = 19.0 kN/m^3 (121 lb/ft^3), ω = 19.0 %, S = 100 %, σ_3 = 22.3 kPa (3.24 psi) B19
Figure 9a. Triaxial Compression Results: Dickey Lake Subgrade, γ_d = 15.4 kN/m^3 (98.0 lb/ft^3), ω = 7.0 %, S = 27.7 %, σ_3 = 15.2 kPa (2.21 psi) B20
Figure 9b. Triaxial Compression Results: Dickey Lake Subgrade, γ_d = 17.4 kN/m^3 (111 lb/ft^3), ω = 7.0 %, S = 39.1 %, σ_3 = 18.4 kPa (2.68 psi) B20
Figure 9c. Triaxial Compression Results: Dickey Lake Subgrade, γ_d = 20.1 kN/m^3 (128 lb/ft^3), ω = 7.0 %, S = 66.9 %, σ_3 = 20.7 kPa (3.01 psi) B21
Figure 9d. Triaxial Compression Results: Dickey Lake Subgrade, γ_d = 15.5 kN/m^3 (99.0 lb/ft^3), ω = 12.0 %, S = 48.7 %, σ_3 = 19.1 kPa (2.78 psi) B21
Figure 9e. Triaxial Compression Results: Dickey Lake Subgrade, γ_d = 17.3 kN/m^3 (110 lb/ft^3), ω = 12.0 %, S = 65.2 %, σ_3 = 20.0 kPa (2.91 psi) B22
Figure 9f. Triaxial Compression Results: Dickey Lake Subgrade, γ_d = 19.8 kN/m^3 (126 lb/ft^3), ω = 12.0 %, S = 99.0 %, σ_3 = 22.0 kPa (3.20 psi) B22
Figure 9g. Triaxial Compression Results: Dickey Lake Subgrade, γ_d = 14.6 kN/m^3 (93.0 lb/ft^3), ω = 17.0 %, S = 59.5 %, σ_3 = 17.1 kPa (2.49 psi) B23
Figure 9h. Triaxial Compression Results: Dickey Lake Subgrade, γ_d = 17.3 kN/m^3 (110 lb/ft^3), ω = 17.0 %, S = 92.4 %, σ_3 = 19.2 kPa (2.79 psi) B23
Figure 9i. Triaxial Compression Results: Dickey Lake Subgrade, γ_d = 18.8 kN/m^3 (120 lb/ft^3), ω = 17.0 %, S = 100 %, σ_3 = 21.7 kPa (3.16 psi) B24
Figure 10. Resilient Modulus Results: Sunburst Subgrade: γ_d = 18.7 kN/m^3 (119 lb/ft^3), ω = 12.0 %, S = 72.0 % B24

Figure 11. Resilient Modulus Results: Alzada Subgrade: γ_d = 17.5 kN/m^3 (112 lb/ft^3), ω = 18.3 %, S = 93.0 % B25
Figure 12a. Resilient Modulus Results: Loma Subgrade: γ_d = 17.1 kN/m^3 (109 lb/ft^3), ω = 7.0 %, S = 33.2 % B25
Figure 12b. Resilient Modulus Results: Loma Subgrade: γ_d = 17.1 kN/m^3 (109 lb/ft^3), ω = 12.0 %, S = 56.9 % B26
Figure 12c. Resilient Modulus Results: Loma Subgrade: γ_d = 17.1 kN/m^3 (109 lb/ft^3), ω = 20.0 %, S = 92.8 % B26
Figure 13a. Resilient Modulus Results: Swan Subgrade: γ_d = 17.1 kN/m^3 (109 lb/ft^3), ω = 8.0 %, S = 46.5 % B27
Figure 13b. Resilient Modulus Results: Swan Subgrade: γ_d = 17.1 kN/m^3 (109 lb/ft^3), ω = 13.0 %, S = 75.5 % B27
Figure 13c. Resilient Modulus Results: Swan Subgrade: γ_d = 17.3 kN/m^3 (110 lb/ft^3), ω = 20.0 %, S = 100 % B28
Figure 14a. Resilient Modulus Results: Dickey Lake Subgrade: γ_d = 17.3 kN/m^3 (110 lb/ft^3), ω = 7.0 %, S = 37.0 % B28
Figure 14b. Resilient Modulus Results: Dickey Lake Subgrade: γ_d = 17.3 kN/m^3 (110 lb/ft^3), ω = 12.0 %, S = 64.0 % B29
Figure 14c. Resilient Modulus Results: Dickey Lake Subgrade: γ_d = 17.3 kN/m^3 (110 lb/ft^3), ω = 13.0 %, S = 70.0 % B29
Figure 15a. Triaxial Ultimate Strength Versus Dry Density and Degree of Saturation: Sunburst Subgrade B30
Figure 15b. Triaxial Ultimate Strength Versus Dry Density and Degree of Saturation: Alzada Subgrade B30
Figure 15c. Triaxial Ultimate Strength Versus Dry Density and Degree of Saturation: Loma Subgrade B31
Figure 15d. Triaxial Ultimate Strength Versus Dry Density and Degree of Saturation: Swan Subgrade B31
Figure 15e. Triaxial Ultimate Strength Versus Dry Density and Degree of Saturation: Dickey Lake Subgrade B32
Figure 16a. Elastic Modulus Versus Dry Density and Degree of Saturation: Sunburst Subgrade B32
Figure 16b. Elastic Modulus Versus Dry Density and Degree of Saturation: Alzada Subgrade B33
Figure 16c. Elastic Modulus Versus Dry Density and Degree of Saturation: Loma Subgrade B33
Figure 16d. Elastic Modulus Versus Dry Density and Degree of Saturation: Swan Subgrade B34
Figure 16e. Elastic Modulus Versus Dry Density and Degree of Saturation: Dickey Lake Subgrade B34
Figure 17a. Resilient Modulus Versus Dry Density and Degree of Saturation: Loma Subgrade B35

Figure 17b. Resilient Modulus Versus Dry Density and Degree of Saturation: Swan Subgrade B35
Figure 17c. Resilient Modulus Versus Dry Density and Degree of Saturation: Dickey Lake Subgrade B36
Figure 18a. CBR Versus Dry Density and Degree of Saturation: Sunburst Subgrade B36
Figure 18b. CBR Versus Dry Density and Degree of Saturation: Alzada Subgrade B37
Figure 18c. CBR Versus Dry Density and Degree of Saturation: Loma Subgrade B37
Figure 18d. CBR Versus Dry Density and Degree of Saturation: Swan Subgrade B38
Figure 18e. CBR Versus Dry Density and Degree of Saturation: Dickey Lake Subgrade B38
Figure 19a. Resilient Modulus Correlated From Triaxial Ultimate Strength Via Texas Triaxial Class: Sunburst Subgrade B39
Figure 19b. Resilient Modulus Correlated From Triaxial Ultimate Strength Via Texas Triaxial Class: Alzada Subgrade B39
Figure 19c. Resilient Modulus Correlated From Triaxial Ultimate Strength Via Texas Triaxial Class: Loma Subgrade B40
Figure 19d. Resilient Modulus Correlated From Triaxial Ultimate Strength Via Texas Triaxial Class: Swan Subgrade B40
Figure 19e. Resilient Modulus Correlated From Triaxial Ultimate Strength Via Texas Triaxial Class: Dickey Lake Subgrade B41
Figure 20a. Resilient Modulus Correlated From CBR (Heukelom and Klomp, 1962): Sunburst Subgrade B41
Figure 20b. Resilient Modulus Correlated From CBR (Heukelom and Klomp, 1962): Alzada Subgrade B42
Figure 20c. Resilient Modulus Correlated From CBR (Heukelom and Klomp, 1962): Loma Subgrade B42
Figure 20d. Resilient Modulus Correlated From CBR (Heukelom and Klomp, 1962): Swan Subgrade B43
Figure 20e. Resilient Modulus Correlated From CBR (Heukelom and Klomp, 1962): Dickey Lake Subgrade B43
Figure 21a. Resilient Modulus Correlated From CBR (Van Till et al., 1972): Sunburst Subgrade B44
Figure 21b. Resilient Modulus Correlated From CBR (Van Till et al., 1972): Alzada Subgrade B44
Figure 21c. Resilient Modulus Correlated From CBR (Van Till et al., 1972): Loma Subgrade B45
Figure 21d. Resilient Modulus Correlated From CBR (Van Till et al., 1972): Swan Subgrade B45
Figure 21e. Resilient Modulus Correlated From CBR (Van Till et al., 1972): Dickey Lake Subgrade B46

CONVERSION FACTORS

The following conversion factors are required for interpretation of results in figures contained in Appendix B. Within the text of the report and in the tables in Appendix A, SI units are used with English units listed in parenthesis.

1m = 3.28 ft

1mm = 0.0394 in

1 kPa = 0.145 lb/in^2 = 20.9 lb/ft^2

1 MPa = 145 lb/in^2 = 20,900 lb/ft^2

1kN/m^3 = 6.36 lb/ft^3

SUMMARY

Seasonal variations in climatic conditions have long been recognized to have a significant impact on the structural response of flexible pavements. Of particular significance is the effect of subgrade moisture content on subgrade support values and potential roadway damage. The Montana Department of Transportation is conducting a project to evaluate the response of subgrade resilient modulus to seasonal changes in subgrade moisture content. Moisture content is being measured through permanent subsurface instrumentation while deflection tests are periodically being conducted to establish subgrade resilient modulus values. This report describes work performed in support of this project. The purpose of this study was to provide laboratory data on subgrade support values for the instrumented sites. This data will illustrate the variation in subgrade support with changes in moisture content and sample dry density. This information will be used to verify the accuracy of the data generated in the field and might also be used to help guide the back-calculation procedure. Laboratory testing has consisted of resilient modulus, triaxial compression, CBR and R-Value tests. Results have been generated for various combinations of sample dry density and degree of saturation. These results have been related to resilient modulus whenever possible. The results tend to show that ultimate strength related parameters are most sensitive to changes in dry density and moisture content for the cohesive subgrade soils and that deformation related parameters are most sensitive for the more non-cohesive subgrade soils.

INTRODUCTION

Seasonal variations in climatic conditions, such as air temperature, wind speed and precipitation, have long been recognized to have a significant impact on the structural response of flexible pavements. Air temperature and wind speed have an impact on the stiffness of the asphalt concrete. This impact is typically experienced within hours after a change in the climatic condition. Precipitation has a much slower and more long lasting impact on pavement performance. A subgrade and base course layer's moisture content can gradually increase during and well after periods of precipitation. Temperature also has a slower response time associated with the freezing and thawing of subgrade and base course pavement layers. Periods of thawing and correspondingly high moisture content levels typically lead to a weakened pavement section. Damage to the pavement section can occur during these periods if sufficient loading is applied.

Highway agencies qualitatively recognize the link between climatic conditions, loading and pavement damage. The Federal Highway Administration (FHWA) is currently attempting to quantify the relationship between these variables through the Seasonal Monitoring Program (SMP) contained within the Long Term Pavement Performance (LTPP) program (FHWA, 1994). The objective of the SMP-LTPP program is to provide data needed to attain a fundamental understanding of the magnitude and impact of temporal variations in pavement response and material properties due to separate and combined effects of temperature, moisture and frost/thaw variations.

A number of studies have examined the impact of moisture on the strength and stiffness of subgrade materials. Monismith and Finn (1977) report that the presence of water in a pavement system is one of the most important environmental considerations to be made. Thompson and Robnett (1976) have shown that the resilient modulus of partially saturated soils decreases as the moisture content increases. Black (1962) noted that the California Bearing Ratio (CBR) decreases as moisture content increases. Similar results were reported by Larry and Mahoney (1984) and Monismith et al. (1972). Basma and Al-Suleiman (1991) presented results from these studies by plotting resilient modulus versus water content for different levels of dry density and evaluated the effect on the structural number as used in the AASHTO flexible pavement design (AASHTO, 1993).

Burland (1965) emphasized the need to simulate negative pore water pressures when evaluating strength and stiffness characteristics of partially saturated soils. Elfino and Davidson (1989) examined the effect of different water retention conditions on resilient modulus for various soil classes. They found that for A-2-6 soils, the resilient modulus at optimum water content was 25 % greater than that obtained for a near saturated specimen. For A-5 soils, little difference in moduli was observed for different water retention levels. Hardcastle (1992) presented a method for estimating seasonal values of resilient moduli of subgrade soils by applying a series of adjustment coefficients to a reference resilient modulus. Ali and Lopez (1996) and Ali and Parker (1996) used results from the LTPP SMP to perform a statistical analysis to evaluate the relationship between climatic factors and pavement structural properties.

The studies above point to the importance of subgrade moisture content on the structural response of flexible pavements. These studies clearly indicate the dependance of moisture content on a subgrade's support value. The purpose of this study was to provide laboratory data on subgrade support values for particular sites that have been instrumented with senors to monitor long-term environmental changes in the pavement section. This data will be used in assessing the impact of loading on these sites during periods of adverse climatic and subsurface environmental conditions.

PROJECT OVERVIEW

The purpose of this project is to provide supporting data for a research project being conducted by the Montana Department of Transportation (MDT) titled "Spring Thaw Weakening: Design Impact, Load Restriction Impact". This project is being led by Mr. Kent Shepherd of the Non-Destructive Testing Unit at MDT and is designed to assess the structural weakening of pavement sections with increases in moisture content experienced particularly during periods of "spring thaw".

The current MDT project is being conducted to provide information which can be used to identify critical periods of low subgrade support. These periods most likely occur during Spring

months when frozen layers of soil in the subgrade begin to thaw with the water not being able to drain downwards due to deeper, still frozen frost layers. The information to be generated in the MDT project consists of surface weather data and subsurface seasonal variation data for ten sites across the State. These sites have been chosen to provide for a cross-section of subgrade soil types typical to Montana.

The weather data includes air temperature, surface pavement temperature, wind speed and precipitation. The subsurface data will consist of moisture content, temperature and salinity at various times of the year. The Non-Destructive Testing Unit at MDT will be performing deflection tests on the pavement sections at key times during the year. MDT currently uses the Road Rater for deflection testing. This information will be used to back-calculate the deformation characteristics (resilient modulus) of the subgrade and will ultimately be used to relate loss of pavement support to atmospheric or subsurface seasonal variables for the purpose of more accurately designing for and dealing with the "spring thaw" phenomenon.

A critical element to the field data collected is the information on subgrade deformation characteristics or subgrade support values. It is this piece of information which will largely control the decision on when a roadway is too weak for designed traffic loads. Under the existing MDT project, this information will be determined from deflection testing. This test allows the subgrade modulus to be back-calculated from surface deflection information. In this way, the subgrade support value is not directly measured.

The purpose of the author's project is to provide additional data to illustrate the variation of subgrade support values with changes in moisture. This information is needed primarily to verify the accuracy of the data generated in the field by the back-calculation technique for the deflection tests and might also be used to guide the back-calculation procedure. For instance, this project's data might show that certain soil types experience very little change in support values with changes in moisture content, while other soil types experience dramatic changes. This information, combined with field data showing the *in situ* variation of moisture content with depth, can be used to decide how the subgrade soil should be subdivided, such that different back-calculated moduli can be determined for various layers. The data from the author's study may also indicate different levels of subgrade strength and/or stiffness corresponding to different depths that may have been

impossible to identify by other means. This information will also be helpful in establishing an analysis approach to the deflection data.

The data generated from the author's study can also be used to examine correlations between laboratory determined values of subgrade strength or stiffness and back-calculated values. This information can be useful in determining whether certain types of tests are appropriate for routine roadway design. Hence, the objective of this project is to provide relationships between moisture content or degree of saturation, and subgrade support values for the subgrade materials located at the sites where instrumentation has been placed.

RESEARCH APPROACH

To accomplish the objective stated above, various types of laboratory experiments have been performed on subgrade samples from the field sites where subsurface instrumentation has been placed. These laboratory experiments have been conducted on both disturbed and undisturbed subgrade samples, where these samples have been conditioned to various moisture content levels. The experiments performed include triaxial compression and resilient modulus tests on undisturbed and reconstituted subgrade samples conditioned to various water content levels, and R-Value and California Bearing Ratio (CBR) tests on disturbed subgrade samples. The CBR tests were performed at various dry densities and moisture contents in an attempt to bracket the conditions anticipated at the individual sites.

The undisturbed samples were generated from the general vicinity of the instrumentation shaft used for the temperature and moisture content probes at each site. These samples were obtained by pushing shelby tubes into the subgrade soils. The intention was to obtain shelby tube samples from only the sites containing a cohesive subgrade (i.e. A-4, A-5, A-6 or A-7 soils). Originally, it was thought that of the six sites instrumented to date (Sunburst, Alzada, Loma, Swan, Dickey Lake and East Glacier), four contained cohesive subgrade. These four sites were thought to be Sunburst, Alzada, Loma and East Glacier. The Loma material turned out to be an A-2-4 soil,

while the East Glacier classified as an A-4, but was of the consistency of weathered siltstone. Shelby tubes yielding partially full samples for testing have been returned from the Sunburst and Alzada sites.

Bulk (disturbed) samples were obtained during the installation of the instrumentation directly from the instrumentation shaft. Bulk samples have been obtained from the Sunburst, Alzada, Loma, Swan, Dickey Lake and East Glacier sites. During the sampling of these sites, care was taken to also sample individual layers of the base course to assess the quantity of fines contamination.

SUMMARY OF SITE DATA

This section describes the subsurface conditions encountered at five of the six sites instrumented to date. Tables 1a-1e provide information on pavement layer thicknesses for the Sunburst, Alzada, Loma, Swan and Dickey Lake sites. Data on the East Glacier site has not been included. The subgrade at this site was the consistency of weathered siltstone. Undisturbed samples could not be obtained. It was felt that attempting to reconstitute samples would not produce results indicative of the *in situ* material. The thicknesses provided in Tables 1a - 1e were established through the boring of the instrumentation shaft at the time of sensor installation. Tables 2a-2e tabulate data on the date of instrumentation, in-place dry density, in-place moisture content at the time of instrumentation installation, percent passing the #200 sieve, liquid and plastic limits, and soil classification. This data has been accumulated from several sources. The majority of the in-place dry density and moisture content data is from nuclear density testing inside the instrumentation shaft at various depths. This data is highlighted by italicizing the corresponding measurements in Tables 2a - 2e. The data from the nuclear density tests corresponds to depth intervals ranging over 0.15 m (6 in.). Comparing the moisture contents from the nuclear tests to data from direct measurement tests (i.e. sampling and oven drying), it appears that the nuclear gauge showed water contents that were approximately 50 % higher than the direct measurements. Data from the Sunburst and Alzada sites indicates that the dry density measured from the nuclear probe is low. Where available, density

and moisture content data from the shelby tube samples is also listed in Tables 2a-2e. Table 3 provides data on specific gravity, soil classification and R-value for the subgrade from the 5 sites listed above. Grain size distribution curves for base course samples are given in Figures 1a-1e.

SHELBY TUBE SAMPLE LOGS

Shelby tubes measuring 76.2 mm (3 in.) in I.D. and 0.914 m (36 in.) in length were pushed into the subgrade at the Sunburst and Alzada sites. The same was attempted for the Loma and East Glacier sites. These tubes produced poor quality samples, or became bent due to either the strength of the subgrade at the site or the granular nature of the soil. The sampling plan called for six tubes to be taken at each site. For each tube, the subgrade was sampled by auguring a 0.102 m (4 in.) diameter hole through the AC and base. The hole was then cleaned and the tube inserted and pushed to the desired depth. The Sunburst site was sampled in mid-September, 1995. One tube was returned with a bent end, with the contents being of poor quality. The other tubes contained between 0.24 to 0.48 m (9.5 to 19 in.) of subgrade soil. The Alzada site was sampled for the first time in mid-September, 1995. Five tubes were returned, with one tube being of poor quality. The remaining tubes contained 0.23 to 0.38 m (9 to 15 in.) of subgrade soil. MDT drillers reported obtaining full tubes from the Alzada site. This discrepancy required the Alzada site to be sampled a second time in early May, 1996. The six tubes returned contained 0.38 to 0.56 m (15-22 in.) of soil. Of this material, only the bottom 0.17 to 0.36 m (6.5-14 in.) of soil appeared to be subgrade, with the upper portion ranging from 0.1 to 0.28 m (4-11 in.) being what appeared to be base course.

BASE COURSE GRAIN SIZE DISTRIBUTION

Figures 1a-1e provide grain size distribution curves for various depth intervals in the base course layers for the five sites. The percentage passing the number 200 sieve for each depth interval

is listed in Table 2a-2e. The Sunburst and Alzada sites show an increase in fines of 4 to 6.5 %, respectively, from the top to the bottom of the base. The grain size distribution of the various layers at the time of construction and the amount of mixing with the subgrade during construction is not known. Detailed information is not available for the Loma or Swan sites, although the fines content of the base course sample tested appears to be close to that which would have been specified, while the subgrade contained over 25 % fines. Data from the Dickey Lake site indicates that fines from the subgrade have not intruded into the base course soils. In summary, it appears that the potential for contamination of the base course layer is most appreciable for the cohesive soil sites.

LABORATORY TESTING

Triaxial compression, resilient modulus, CBR and R-Value tests were performed on the subgrade soils. In addition, standard index tests, such as specific gravity, liquid and plastic limits, and grain size distribution, were performed to supplement data supplied by MDT. A summary of the index tests is provided in Tables 2 and 3.

Triaxial Compression Tests

Triaxial compression tests have been performed on undisturbed subgrade samples from the sites containing cohesive subgrade and on reconstituted subgrade samples from the sites containing non-cohesive subgrade. The goal of these tests was to provide a measure of strength and stiffness for various moisture contents, or degrees of saturation, and for various dry density levels.

For the sites containing cohesive subgrade (Sunburst and Alzada), triaxial compression tests were to be conducted on undisturbed shelby tube samples at three different depths within the subgrade. For each depth level, three samples were to be conditioned to different moisture content levels without disturbing the sample. This required three shelby tubes nearly full (i.e. at least 0.76 m (30 in.) of soil per shelby tube) for each cohesive site. These nine tests would have provided

information on stiffness and strength with changes in moisture content for depths of approximately 0.25, 0.5 and 0.75 m (6, 18 and 30 in.) into the subgrade. With the samples returned, it has been possible to only partially carry out these tests on the upper most layer of the subgrade. For the sites containing a non-cohesive subgrade, samples were reconstituted and prepared to three moisture contents and at three different levels of dry density. This matrix of nine tests was performed for the Loma, Swan and Dickey Lake sites. The three dry densities for each site were chosen to bracket the *in situ* values measured during instrumentation installation. Moisture content levels were chosen to bracket values anticipated in the field.

Sample Preparation

Samples from cohesive subgrade sites were directly extruded from the shelby tubes and placed in the triaxial device described below for moisture conditioning. Bulk samples were obtained from the non-cohesive subgrade sites. For these sites, this required that triaxial samples be reconstituted in the laboratory. Samples were prepared to three moisture contents and three values of dry density. The range of moisture content and dry density was chosen to bracket conditions anticipated at the specific sites. In order to achieve the target dry density at its specified water content a mold was constructed to prepare the samples. The mold was fabricated from PVC pipe with an inside diameter measuring 70 mm (2.8 in.) and a height large enough to produce a 140 mm (5.5 in.) high sample. The non-cohesive soil was compacted in five even lifts, where a standard proctor hammer was used to compact the sample. The number of blows used per layer depended on the target dry density. By weighing the apparatus before and after packing the mold with soil, it was possible to determine the soil's dry density knowing the weight, height, diameter, and moisture content of the soil sample. A precut seam in the mold allowed for easy removal and assisted in keeping the sample intact for subsequent triaxial testing.

Triaxial Apparatus

The moisture conditioning process for the triaxial samples has required that a special triaxial apparatus be assembled. This apparatus allows for samples to be initially saturated and subsequently desaturated to a desired water content level. This moisture conditioning process was used only for

the cohesive subgrade sites (i.e. Sunburst and Alzada). The samples from the non-cohesive subgrade sites were compacted to the target water contents desired. Saturation is accomplished by driving water into and up through the sample by a small positive pore water pressure gradient. Desaturation is achieved by driving water out of the sample using air pressure and a pressure-plate assembly. The saturation-desaturation process can take 3-4 weeks for cohesive samples. The triaxial apparatus allows for the saturation-desaturation process to occur under stress conditions comparable to that in the field.

A schematic diagram of the triaxial moisture conditioning apparatus is shown in Figures 2 and 3. Figure 2 shows the device configured for the saturation stage, while Figure 3 corresponds to the desaturation stage. The device consists of a conventional triaxial cell which accommodates a sample measuring 70 mm (2.8 in.) in diameter by 140 mm (5.5 in.) in height. A latex membrane is used to encase the sample. Water pressure can be applied to the cell chamber, thereby supplying an all-around confinement to the sample. The chamber water pressure is supplied through an air-water interface device consisting of a double cylinder volume change burette. The burrette allows for volume changes of the sample to be monitored during saturation and desaturation. Sample volume changes are indirectly measured by water entering or leaving the cell chamber as the sample compresses or expands, respectively.

For purposes of sample saturation, a pore water pressure can be applied to the sample through a port connected to the bottom platen (Figure 2). This water pressure is applied through a second air-water pressure interface device consisting of a capped PVC tube with a clear tube attached to the outside for monitoring the water level inside the pipe. Air pressure is applied to each interface device through two separate pressure regulators. A pressure gage is used to monitor pressure applied to the specimen. Pressure from each interface device is routed to opposite sides of a Sensotec (Worthington, OH) model A-5 differential pressure transducer having a range of 69 kPa (10 psi). A gagemaster signal conditioner is used as a readout for the device. The transducer measures the difference in pressure between that applied to the outside and inside of the specimen.

Samples are saturated by applying a small pore water pressure to the bottom of the sample. This pressure is no greater than 3.5 kPa (0.51 psi). A confinement is applied to the sample at the same time. The difference between the confinement and the pore water pressure is set to the value

of the total vertical stress corresponding to the point in the ground where the sample was taken. The total unit weight of the various layers above the sample location are used to calculate this vertical stress. This allows the sample to become saturated and possibly swell by an amount which approximates that which would occur in the field. For the samples tested, typically representing the upper 150 to 200 mm (6 to 8 in.) of the subgrade, total vertical stresses calculated ranged from 17 to 25 kPa (355 to 522 psf). Samples are assumed to be saturated when water is seen dripping from the connection to the top of the sample. Water is flushed through the sample for an additional two days once the first drops of water are observed.

Due to the need to have a positive pore water pressure gradient through the sample, the effective stress state in the sample will be different from one end of the sample to the other. For example, if 6.9 kPa (1 psi) of water pressure is applied to the bottom of the sample and 27.6 kPa (4 psi) of confinement is applied, the effective stress in the sample at the bottom is the difference between these two values, i.e. 20.7 kPa (3 psi). Since the top of the sample is open to the atmosphere, such that water can drain from the top, the pore water pressure at this point is zero. The effective stress at the top of the sample is then equal to the confinement, which for this example is 27.6 kPa (4 psi). From this example it is seen that because of the need to flush water though the sample to achieve saturation, it is not possible to maintain a uniform state of effective stress throughout the sample duplicating that which would be experienced in the field. This difference is minimized by reducing the pore water pressure applied to the sample, which in turn increases the time necessary for saturation.

Figure 3 shows the configuration of the device when samples are desaturated. Water is driven from the sample by applying air pressure to the top of the specimen. A high air-entry porous stone is fit to the bottom platen. This stone allows water to pass but not air, provided the air pressure is less than 500 kPa (72.5 psi). Higher air pressures cause more moisture to exit the sample and hence lower the moisture content. As air pressure was applied to the sample, the confining pressure was increased by an amount necessary to maintain a difference between the confinement and the air pressure equal to the total stress corresponding to the point in the ground where the sample was taken. Volume changes of the sample were monitored during this period.

Since a target moisture content at the end of the desaturation process was desired, it was

necessary to know the relationship between the applied air pressure (also know as the matrix suction) and the resulting equilibrium moisture content. This relationship was accomplished by conducting pressure-plate tests to establish the soil's moisture retention curve. Samples were originally brought to a fully saturated state by allowing them to soak in a consolidation device for 6 days. The sample volume was monitored during this period such that the degree of saturation could be calculated at the end of the soaking period. A degree of saturation ranging from 87 - 93 % was obtained. Moisture content was then determined at increasing levels of matrix suction application to establish the moisture retention curves given in Figures 4a and 4b. These curves were used to establish the air pressure needed during the triaxial desaturation process to achieve a particular sample water content.

Once the desaturation process was complete, the samples were allowed to sit with only the confinement applied to the sample for a period of 2 days. The confinement applied during this stage was set to the total vertical stress corresponding to the point in the ground where the sample was taken. This step allowed for the sample to reach equilibrium under the applied state of confinement. Volume changes of the sample were also monitored during this period. The continual monitoring of sample volume changes allowed for the sample dry density to be determined immediately prior to shearing. Once the sample was sheared and removed from the triaxial device, water content was determined and degree of saturation was calculated.

Shearing of the samples took place under the same confinement prescribed during the equilibrium period (i.e. a value equal to the total vertical stress corresponding to the point in the ground where the sample was taken). Shearing was accomplished with the drainage lines to the sample being open, however water was not seen to leave the sample. Shearing was carried out at an approximate rate of 6 %/min. The shearing sequence was the same for both the cohesive and non-cohesive subgrade sites. During each test, the load was released and reapplied to provide for 5 unloading-reloading cycles. These cycles were typically conducted between axial strain levels ranging from 3-5 %. The elastic modulus (similar to the resilient modulus) was measured from each of these unloading-reloading loops. The peak strength of the specimen was also measured from each test.

Triaxial Results: Cohesive Subgrade Sites

Three triaxial tests were performed on samples from the top of the subgrade at the Sunburst and Alzada sites. Since these sites were sampled in the Fall, it was felt that the *in situ* moisture content represented the lowest water content that might be experienced during seasonal monitoring. For this reason, one sample from each site was tested at the moisture content at the time of sampling. Saturation and desaturation was not required for these two samples. An additional sample from each site was saturated using the technique described above and sheared in a saturated state. The remaining sample from each site was saturated and subsequently desaturated to achieve a moisture content greater than the *in situ* moisture content and less than the saturated value. From the three triaxial tests performed on the Sunburst site, the water content varied from 12.5 % to 16.0 % with a degree of saturation of 87.5 % to 100 %, respectively. From the three triaxial tests performed on the Alzada site, the water content varied from 14 % to 16 % with a degree of saturation of 82 % to 99 %, respectively.

Figures 5 and 6 provide results from each test. Figures 5c and 6b correspond to the *in situ* condition at the time of sampling. Tables 4a and 4b provide results of the experiments, listing ultimate strength and elastic modulus along with dry density, moisture content, degree of saturation of the samples immediately prior to testing and the confining stress applied during shear testing.

Triaxial Results: Non-Cohesive Subgrade Sites

Subgrade samples from the non-cohesive sites (i.e. Loma, Swan and Dickey Lake) were prepared to three dry densities and three moisture contents as described in an earlier section. The highest water content for each site was typically achieved by preparing the sample to the desired dry density at a lower moisture content and allowing the sample to saturate by the same means used for the cohesive subgrade samples. Water contents of approximately 7, 12 and 19 % were achieved for each of the three materials. Dry densities ranging from 14 to 20 kN/m^3 (89 to 128 lb/ft) were obtained. Figures 7 - 9 provide results of the experiments. Tables 4c - 4e provide summary data from these tests.

Resilient Modulus Tests

The proposal called for conducting resilient modulus tests only on undisturbed samples from the sites containing cohesive subgrade. Resilient modulus tests were to be performed on undisturbed samples from one depth level (i.e. the middle of the shelby tube or 0.4 m (16 in.) into the subgrade) and for three different water content levels. Due to the limited number of undisturbed samples from the cohesive sites, only one sample from the Sunburst and one sample from the Alzada site was tested. These samples corresponded to the top of the subgrade. Results from the resilient modulus tests on the Sunburst and Alzada samples are given in Tables 5a and 5b and in Figures 10 and 11.

Resilient modulus tests were also performed on subgrade soils from the non-cohesive sites. Bulk soils were sent to the testing laboratory with instructions on a dry density and moisture content to which the samples should be compacted. Three tests on subgrade from each site were performed. Each sample was compacted to the same density and at three different water contents. Tables 5c-5k and Figures 12 - 14 summarize results from these tests. All resilient modulus tests were performed in accordance to SHRP Protocol P46 (AASHTO, 1992).

CBR Tests

CBR tests were performed on subgrade samples in an attempt to generate CBR strengths for the range of *in situ* dry densities and moisture contents anticipated at the different sites. CBR tests have been performed for all five sites. The majority of the CBR samples were prepared by compacting the samples to different dry densities with the soil prepared at a particular water content. CBR tests were then performed on these samples without soaking the samples. In this way, the CBR penetration strength represents the moisture condition of the as-compacted sample. To achieve higher moisture content levels, samples were prepared to desired densities and allowed to soak. CBR strengths for these samples are reported along with the water content of the sample after the soaking occurred. Tables 6a-6e summarize the CBR strengths for the five different sites.

SUMMARY OF LABORATORY RESULTS

Strength and deformation parameters obtained from the triaxial compression, resilient modulus and CBR tests were determined for subgrade samples at various dry densities and water contents. From the triaxial tests, ultimate strength and elastic modulus were obtained. The resilient modulus tests provide 15 values of resilient modulus from a given test on a single sample for various combinations of confinement and axial stress application. To summarize these results and allow them to be compared to results from the other tests, a single value of resilient modulus was interpolated from Figures 10 - 14 for a level of confining pressure representative of that for the top of the subgrade for each particular site. The axial stress used in Figures 10 - 14 corresponded to the middle value (approximately 42 kPa, 6.1 psi). This value typically represented the point at which the variation in resilient modulus with axial stress was no longer appreciable.

Triaxial ultimate strength, elastic modulus, resilient modulus and CBR were plotted individually against the sample dry density and water content and against the sample dry density and degree of saturation. More consistent trends were noted by plotting each parameter against dry density and degree of saturation. Water content itself is not a precise indicator of strength or stiffness since the water content can be the same for two samples at different dry densities with correspondingly different strengths. The degree of saturation reflects both the change in water content and the change in density. In each summary presentation of the data, dry density is plotted on the ordinate with degree of saturation plotted on the abscissa. Where possible, contours of each parameter have been drawn from the available data.

Triaxial Compression Tests

Figures 15a - 15b present triaxial ultimate strength data from the Sunburst and Alzada sites. Since only three data points are available from each site, drawing contours of constant peak strength was not attempted. Figures 15c -15e present triaxial ultimate strength results for the three non-cohesive subgrade sites. Nine data points were available for each site, from which the contours were

constructed. In many cases, there was an appreciable amount of scatter to the results. These contours should be taken as approximate. Figures 16a - 16e present triaxial elastic modulus data for all five sites. The elastic modulus used in these figures was a calculated average from the five cycles performed on each sample.

Resilient Modulus Tests

A single resilient modulus test was performed for the subgrade from the Sunburst and Alzada sites. For the three remaining non-cohesive subgrade sites, three resilient modulus tests for each site were performed. A single value of resilient modulus was determined from each test corresponding to a particular confinement and axial stress level as described at the beginning of this section. Table 7 presents resilient modulus results from each test. Figures 17a - 17c present results from the three non-cohesive subgrade sites.

CBR Tests

Nine CBR tests were performed for each of the five sites. Figures 18a - 18e present contours of constant CBR for combinations of dry density and degree of saturation. As with the triaxial results, these contour results should be considered approximate.

CORRELATION OF RESULTS TO RESILIENT MODULUS

To compare results, an attempt has been made to relate the various strength and deformation parameters to resilient modulus values. Where possible, correlations existing in the literature have been used. Correlations specific for each site could also be developed. This possibility is discussed in the section on *Discussion of Results*.

Triaxial Compression Tests

Correlation of the triaxial ultimate strength results to resilient modulus values was accomplished by relating the ultimate strength to the Texas Triaxial Class (Texas Department of Transportation, 1995). A Texas Triaxial Class of 6 corresponds to a very weak subgrade, while a class of 1 corresponds to a good flexible base material. The class is obtained by plotting the peak strength from the triaxial test against the normal stress on a Mohr diagram, which has been divided into six regions corresponding to the six classes. The triaxial tests performed as part of this study were performed in general accordance with the Texas standard. The Texas standard calls for performing a sufficient number of tests to develop a Mohr-Coulomb failure envelope, which is then plotted on the classification diagram. The most critical point on the envelope is then used to interpolate the class. From the triaxial tests performed as part of this study, only one point on the Mohr-Coulomb failure envelope is available. This single point was used to determine the Texas Triaxial Class. The Texas Triaxial Class was then converted to a resilient modulus value using the correlation provided by Van Til et al. (1972). Tables 8a - 8e summarize the Texas Triaxial Class and resulting resilient modulus values from each test. New diagrams of resilient modulus versus dry density and degree of saturation were then generated, as shown in Figure 19a - 19e.

A conversion of the elastic modulus from the triaxial tests to resilient modulus values was not attempted and is not necessary due to the similarity between the two parameters. The contours of elastic modulus given in Figures 16a - 16e should be compared directly to other resilient modulus values.

CBR Tests

CBR values were converted to resilient modulus values by two approaches. The simple conversion of multiplying CBR by 1500 to get a resilient modulus in units of psi (Heukelom and Klomp, 1962) was first used. This conversion is designed to apply to CBR values less than 10. The second approach used a correlation diagram provided by Van Til et al. (1972). Results from these two correlations are presented in Figures 20a -20e and 21a-21e, respectively.

R-Value Tests

The R-Values given in Table 3 were correlated to resilient modulus using the diagram provided by Van Til et al. (1972). Unlike the other tests used in this study, the R-Value test does not allow for the examination of density and water content variations on subgrade support. Table 9 provides a summary of the R-Values and correlated resilient modulus values for the subgrade of each site.

DISCUSSION OF RESULTS

The resilient modulus test results, to which other results should be compared, have been presented in Figures 17a -17c and summarized in Table 7. Contours of constant resilient modulus have not been sketched on Figures 17a -17c due to the limited number of data points available. Due to the similarity of testing conditions between the resilient modulus test and the test used to determine the elastic modulus, and the similarity of the type of parameter being determined (i.e. each is a measure of stiffness), it is expected that these two parameters would be comparable. Taking the single resilient modulus data point for the Sunburst and Alzada sites from Table 7 and plotting these points on Figures 16a and 16b, respectively, it is seen that the correlation does not appear to be one -to-one. The resilient modulus appears to be on the order of three times the value of the elastic modulus. On the other hand, overlaying Figures 16c - 16e and 17a -17c, it is seen that the three resilient modulus values for each non-cohesive site compare reasonably well to the contours of elastic modulus from the triaxial tests. Due to the similarity of the two parameters, it is reasoned that the trend of elastic modulus with dry density and degree of saturation seen in Figures 16c - 16e is comparable to that which would have been observed for resilient modulus values had more resilient modulus tests been performed. Additional resilient modulus tests are necessary to substantiate this argument.

Figures 15a - 15e and 16a - 16e can be used to compare trends in triaxial ultimate strength to elastic modulus. For the limited data from the cohesive subgrade sites, it appears that the two

parameters exhibit similar trends. For the non-cohesive sites, the general trend is similar, however the ultimate strength results tend to show a flattening trend at low degree of saturation, which is not seen to this degree in the elastic modulus contours. This tends to indicate that the ultimate strength may be a suitable parameter for correlation to resilient modulus for the cohesive subgrades, but is not as appropriate as elastic modulus for the non-cohesive subgrades.

Resilient modulus data from Figures 17a - 17c and Table 7 can be compared to resilient modulus values correlated from triaxial ultimate strength via the Texas Triaxial Class from Figures 19a - 19e. For the cohesive subgrade sites, it is seen that the correlations from the Texas Triaxial Class overpredict the actual resilient modulus values by a factor of 3-4. For the non-cohesive sites, the overprediction of the correlations ranged by a factor of 4-6. Since the trend in the results are similar, site specific correlations appear possible.

Comparing CBR results from Figures 18a - 18e to the elastic modulus curves in Figures 16a - 16e, it is seen that the trends in the CBR curves for the cohesive soil sites are like those expected for the modulus results. Additional elastic and resilient modulus testing is necessary to substantiate this argument. The shape of the CBR curves for the non-cohesive sites (Figures 18c - 18e) are not like those of the elastic modulus results in Figures 16c - 16e. If the argument that the shape of the elastic modulus curves is similar to that of the resilient modulus curves is valid, it would follow that the CBR test is less appropriate for developing correlations to resilient modulus for non-cohesive subgrades in comparison to other tests. This argument needs to be supported by additional resilient modulus tests.

The CBR to resilient modulus correlations are examined by comparing CBR correlations given in Figures 20a - 20e and 21a - 21e to resilient modulus results from Figures 17a - 17c and Table 7. Using the first CBR correlation (Heukelom and Klomp, 1962), it is seen that the correlations overpredict resilient modulus by a factor ranging from 3-6 for the higher CBR values. The correlations appear to work reasonably well for the lower CBR values. For the Alzada site, an underprediction was observed. The correlations in Van Til et al. (1972) (Figures 21a - 21e) appear to be reasonably close to the actual resilient modulus values.

R-Values from Table 9 can be compared to Figures 17a - 17c and Table 7. The value for the Sunburst site is close to the resilient modulus value given in Table 7. The correlated value for the

Alzada site is 2.5 times the value given in Table 7. For the non-cohesive sites, the correlated values appear to be high in comparison to the values given in Figures 17a - 17c.

IMPLEMENTATION PLAN

The objective of this research was to provide laboratory data describing the variation of subgrade support values with moisture content for the sites instrumented as part of an on-going research project at MDT. Subgrade support values in the form of resilient modulus have been ascertained from the results of the laboratory tests described above (i.e. triaxial strength, elastic modulus, resilient modulus, CBR or R-Value). Resilient modulus values will also be obtained by back-calculation through deflection tests. The purpose of this section is to offer suggestions on how the laboratory data contained in this report might be used by MDT.

As described in the introductory section, this data should be first used to check the reasonableness of the back-calculation modulus values coming from the deflection tests. The resilient modulus tests will provide the best data for this comparison. Due to the lack of undisturbed samples from different depths, it appears that this comparison will only be possible for the upper level of the subgrade for the cohesive subgrade sites. The other laboratory data can also be used to see if trends in the deflection data are reasonable. Had undisturbed samples been available for different depths, it would have been possible to comment on the variation of support values with moisture content for three depth levels in the subgrade. This information would have aided in establishing the analysis approach used for the back-calculation program by indicating how the subgrade should be broken into different layers. It does not appear that this will be possible for the cohesive subgrade sites given the lack of samples at deeper depths. These steps can still be carried out for the non-cohesive subgrade sites, while it is remembered that laboratory results pertain to reconstituted samples.

The goal of the MDT project is to evaluate the damage that occurs to roadways as subgrade moisture content increases. It is believed that the laboratory data can aid in this goal beyond the

items discussed above. The diagrams generated in this report will allow for the subgrade support value (or resilient modulus) to be determined at any time of the season by knowing moisture content and dry density from the site. It is suggested that these diagrams be used in a pavement life prediction model to establish diagrams of pavement life versus subgrade moisture content. Such diagrams should be compared to similar diagrams generated using the deflection data. Comparison of these diagrams will indicate whether the use of certain input parameters for subgrade support are better suited (i.e. more sensitive) for predicting effective pavement design life as subgrade moisture content changes. These diagrams can then be used to indicate roadway damage and establish load restrictions for a given threshold moisture content and acceptable damage ceiling.

CONCLUSIONS

The data collected during this project has provided the type of information called for in the author's proposal. Several problems have developed which have not allowed the desired quantity of data to be collected. The lack of full, good quality shelby tube samples has not allowed MSU to perform the number of triaxial or resilient modulus tests proposed. This development has made it difficult to directly compare correlated resilient modulus to actual values. The remaining laboratory data can be used to examine the reasonableness of data generated from the deflection tests conducted at the various sites.

From the data generated, the following conclusions can be made.

1. Strength and deformation parameters from the laboratory tests illustrate the significance of moisture content and dry density on subgrade support values.
2. Trends in subgrade support measures appear more consistent by plotting degree of saturation rather than moisture content.
3. Ultimate strength parameters (such as triaxial ultimate strength and CBR) appear to be more sensitive to changes in density and degree of saturation for the cohesive subgrade sites than do stiffness parameters (resilient and elastic moduli). The opposite appears to be true for the

non-cohesive subgrade sites.

4. Laboratory generated values of resilient modulus compare reasonably well to values of elastic modulus from triaxial compression tests for the non-cohesive subgrade sites. This comparison does not appear to be as good for the cohesive subgrade sites, although this conclusion is based on only one resilient modulus test for each of the two cohesive subgrade sites. Additional resilient modulus and triaxial compression tests are needed on undisturbed cohesive subgrade samples to make proper comparisons.
5. Due to the similarity of the resilient modulus test and the triaxial compression test used to establish an elastic modulus, it has been assumed that the trends observed for elastic modulus with changes in dry density and degree of saturation are similar to those for resilient modulus. Additional resilient modulus tests are required to validate this assumption.
6. Assuming item 5 to be valid, it appears that both the ultimate strength from the triaxial tests and the CBR strength for the cohesive subgrade sites can be used to establish good correlations to resilient modulus. These tests do not appear to be appropriate for the non-cohesive subgrade sites. These statements were made by comparing trends in the modulus values from the triaxial tests to trends in the uncorrelated data from these tests.
7. The existing correlations used in this study showed varying degrees of success. It appears that site specific correlations would offer much better results.
8. The R-Value test does not allow for variations in subgrade support with changes in moisture content and dry density to be examined.

The true utility of the data generated in this report will not become apparent until it is used to help interpret the data from deflection tests conducted at the sites where subgrade moisture content will be known. It is suggested that this exercise be conducted prior to conducting any additional laboratory tests. If it is found that this data is useful, and that additional data is needed, then further laboratory testing should be considered for the sites described in this report and for those sites that have been instrumented but for which no laboratory testing has been performed.

REFERENCES

American Association of State Highway and Transportation Officials, AASHTO (1993), "Guide for Design of Pavement Structures", Washington, D.C.

American Association of State Highway and Transportation Officials, AASHTO (1992), "Standard Method of Test for Resilient Modulus of Subgrade Soils", AASHTO Designation: T 274-82, Washington, D.C.

Ali, H.A., and Parker, N.A. (1996), "Using Time Series to Incorporate Seasonal Variations in Pavement Design", Transportation Research Board Preprint Paper No. 960122.

Ali, H.A., and Lopez, A. (1996), "Statistical Analysis of Temperature and Moisture Effects on Pavement Structural Properties Based on Seasonal Monitoring Data", Transportation Research Board Preprint Paper No. 960124.

Basma, A.A., and Al-Suleiman, T. I. (1991), "Climatic Considerations in New AASHTO Flexible Pavement Design", *Journal of Transportation Engineering*, V. 117, No.2, pp.210-223.

Black, W.P.M. (1962), "A Method of Estimating the California Bearing Ratio of Cohesive Soils From Plasticity Data", *Geotechnique*, V.12, No.4, pp.271-282.

Burland, J.B. (1965), "Some Aspects of the Mechanical Behavior of Partly Saturated Soils", *Symposium Moisture Equilibria and Moisture Changes in Soils Beneath Covered Areas*, Butterworth, Australia.

Elfino, M.K., and Davidson, J.L. (1989), "Modeling Field Moisture in Resilient Moduli Testing", *Resilient Moduli of Soils: Laboratory Conditions, ASCE Special Technical Publication No.24*, D.J.

Elton and R.P. Ray, editiors, pp.31-51.

FHWA (1994), LTPP Seasonal Monitoring Program: Instrumentation and Data Collection Guidelines, FHWA-RD-94-110.

Hardcastle, J.H. (1992), "Subgrade Resilient Modulus for Idaho Pavements", FHWA Report No. RP110-D.

Heukelom, W. And Klomp, J.J.G. (1962), "Dymanic Testing as a Means of Controlling Pavements During and After Construction", *Proceedings First International Conference on Structural Design of Asphalt Pavements*, University of Michigan.

Larry, J.A., and Mahoney, J.P. (1984), "Seasonal Effects on the Strength of Pavement Structures", *Transportation Research Record*, 954, pp.88-94.

Monismith, C.L., Hicks, R.G., and Salem, Y.M. (1972), "Basic Properties of Pavement Components", *Report No. FHWA-RD-72-19*, Federal Highway Administration, Washington, D.C.

Monismith, C.L., and Finn, F.N. (1977), "Flexible Pavement Design: State-of-the-Art", *Transportation Engineering Journal*, ASCE, V.103, No. TE1, pp. 1-51.

Texas Department of Transportation, Materials and Test Division (1995), *Manual of Testing Procedures*, Volume 1, Test Method Tex-117-E, "Triaxial Compression Tests for Distrubed Soils and Base Materials".

Thompson, M.R., and Robnett, Q. L. (1976), "Data Summary: Resilient Properties of Subgrade Soils", *Transportation Engineering Series 14, Illinois Cooperative Highway and Transportation Series 160, Final Report*, Dept. Of Civil Eng., Univ. Of Illinois, Urbana, Ill.

Van Til, C.J., McCullough, B.F., Vallerga, B.A., and Hicks, R.G. (1972), "Evaluation of AASHO Interim Guides for Design of Pavement Structures", National Cooperative Highway Research Program (NCHRP), No. 128.

APPENDIX A: TABLES

Table 1a. Layer Thicknesses: Sunburst Site

Layer	Thickness, m (in)
AC	0.330 (13.0)
Base	0.483 (19.0)
Subgrade	-

Table 1b. Layer Thicknesses: Alzada Site

Layer	Thickness, m (in)
AC	0.235 (9.25)
Base	0.604 (23.75)
Subgrade	-

Table 1c. Layer Thicknesses: Loma Site

Layer	Thickness, m (in)
AC	0.152 (6.0)
Base	0.686 (27.0)
Subgrade	-

Table 1d. Layer Thicknesses: Swan Site

Layer	Thickness, m (in)
AC	0.244 (9.6)
Base	0.127 (5.0)
Subgrade	1.10 (43.4)

Table 1e. Layer Thicknesses: Dickey Lake Site

Layer	Thickness, m (in)
AC	0.127 (5.0)
Base	0.427 (16.8)
Subgrade	0.919 (36.2)

Table 2a. Subsurface Data for the Sunburst Site: Instrumentation Installed 9-22-95

Layer	Depth Below Pavement m (in)	Depth Within Layer m (in)	Dry Density kN/m³ (pcf)	Moisture Content (%)	% Passing # 200 Sieve	LL	PL	Soil Class
Base	.33 - .48 (13 - 19)	0 - .15 (0 - 6)	*16.3 (105)*	*6.4*	7.5	-	-	A-1-a(0)
	.48 - .64 (19 - 25)	.15 - .30 (6 - 12)	*19.0 (121)*	*8.0*	8.8	-	-	A-1-a(0)
	.64 - .79 (25 - 31)	.30 - .46 (12 - 18)	*18.8 (120)*	*13.0*	11.8	21	NP	A-1-b(0)
Sub-grade	.89 (35)	.076 (3)	18.5 (118)	13.6	-	-	-	-
	.48 - .61 (32 -37)	0 - .13 (0 - 5)	*15.0 (95.8)*	*25.7*	-	-	-	-
	1.07 (42)	.254 (10)	-	13.6	-	-	-	-
	1.09 (43)	.28 (11)	19.4 (123)	15.6	-	-	-	-
	1.22 (48)	.406 (16)	-	13.9	-	-	-	-
	1.37 (54)	.559 (22)	-	14.2	-	-	-	-
	1.57 (62)	.762 (30)	-	14.2	-	-	-	-
	1.88 (74)	1.07 (42)	-	12.5	-	-	-	-
	2.29 (90)	1.47 (58)	-	12.5	-	-	-	-
	.91 - 1.52 (36 - 60)	.43 - 1.04 (17 - 41)	-	10.0	-	29	24	A-4(0)

Table 2b. Subsurface Data for the Alzada Site: Instrumentation Installed 11-29-95

Layer	Depth Below Pavement m (in)	Depth Within Layer m (in)	Dry Density kN/m³ (pcf)	Moisture Content (%)	% Passing # 200 Sieve	LL	PL	Soil Class
Base	.23 - .38 (9 - 15)	0 - .15 (0 - 6)	*19.7 (126)*	*9.1*	7.3	-	-	-
	.38 - .53 (15 -21)	.15 - .30 (6 - 12)	*18.3 (117)*	*11.3*	10.6	-	-	-
	.53 - .69 (21 - 27)	.30 - .46 (12 - 18)	*18.7 (119)*	*11.5*	10.8	-	-	-
	.69 - .84 (27 - 33)	.46 - .61 (18 - 24)	*20.0 (128)*	*11.6*	13.9	-	-	-
Sub-grade	.91 (36)	.076 (3)	19.3 (123)	12.3	-	-	-	-
	.91 (36)	.076 (3)	17.5 (111)	12.9	-	-	-	-
	.91 (36)	.076 (3)	17.5 (111)	18.3	-	-	-	-
	.84 - .99 (33 - 39)	0 - .15 (0 - 6)	*14.8 (94.3)*	*20.0*	-	-	-	-
	0.96 (37.8)	0.12 (4.8)	-	12.7	36.6	-	-	-
	1.04-1.19 (41 - 47)	.20 - .36 (8 - 14)	*12.7 (81.2)*	*27.8*	-	-	-	-
	1.14 (44.8)	0.30 (11.8)	-	10.4	26.9	-	-	-
	1.29 (50.7)	0.45 (17.7)	-	6.8	20.7	-	-	-
	1.44 (56.6)	0.60 (23.6)	-	8.9	17.7	-	-	-
	1.64 (64.5)	0.80 (31.5)	-	8.6	14.4	-	-	-
	1.94 (76.3)	1.10 (43.3)	-	8.2	12.7	-	-	-
	2.34 (92.1)	1.50 (59.1)	-	7.7	11.1	-	-	-
	Bulk Sample	Bulk Sample	-	-	-	19	18	A-1-b(0)

Table 2c. Subsurface Data for the Loma Site: Instrumentation Installed 10-3-95

Layer	Depth Below Pavement m (in)	Depth Within Layer m (in)	Dry Density kN/m³ (pcf)	Moisture Content (%)	% Passing # 200 Sieve	LL	PL	Soil Class
Base	.15 - .30 (6 - 12)	0 - .15 (0 - 6)	*16.3 (104)*	*7.0*	-	-	-	-
	.30 - .46 (12 - 18)	.15 - .30 (6 - 12)	*19.64 (124)*	*6.5*	-	-	-	-
	.46 - .61 (18 - 24)	.30 - .46 (12 - 18)	*19.9 (127)*	*9.1*	-	-	-	-
	.61 - .76 (24 - 30)	.46 - 61 (18 - 24)	*14.9 (95)*	*22.5*	-	-	-	-
	Bulk Sample	Bulk Sample	-	-	7.3	NP	NP	A-1-a(0)
Sub-grade	Bulk Sample	Bulk Sample	-	-	22.7	NP	NP	A-2-4(0)

NP = Non - Plastic

Table 2d. Subsurface Data for the Swan Site: Instrumentation Installed 11-15-95

Layer	Depth Below Pavement m (in)	Depth Within Layer m (in)	Dry Density kN/m^3 (pcf)	Moisture Content (%)	% Passing # 200 Sieve	LL	PL	Soil Class
Crushed PMS	.12 - .27 (4.6-10.6)	.12 - .27 (4.6-10.6)	*18.0 (115)*	*8.3*	9.0	NP	NP	-
Base	.24 - .40 (9.6-15.6	0 - .15 (0 - 6)	*19.7 (126)*	*9.2*	6.5	NP	NP	A-1-a(0)
Sub grade	.38 -.53 (15 - 21)	.01 - .16 (.4 -6.4)	*18.0 (115)*	*13.5*	-	-	-	-
	.67 (26.5)	.30 (11.9)	-	14.3	25.1	NP	NP	A-2-4(0)
	.69 - .84 (27 - 33)	.31 - .47 (12.-18.)	*14.6 (93.2)*	*18.4*	-	-	-	-
	.81 (32)	.44 (17.4)	-	9.1	11.7	NP	NP	A-1-a(0)
	.96 (38)	.59 (23.4)	-	16.5	22.9	NP	NP	A-1-b(0)
	.99 - 1.14 (39 - 45)	.62 - .77 (24.- 30.)	*12.8 (81.7)*	*28.0*	-	-	-	-
	1.17 (46)	.80 (31.4)	-	16.2	18.8	NP	NP	A-1-b(0)
	1.47 (58)	1.10 (43.4)	-	10.0	8.6	NP	NP	A-1-a(0)
	1.87 (73.5)	1.50 (58.9)	-	6.8	2.4	NP	NP	A-1-a(0)
	Bulk Sample	Bulk Sample	-	-	14.4	29	NP	A-1-a(0)

Table 2e. Subsurface Data for the Dickey Lake Site: Instrumentation Installed 11-16-95

Layer	Depth Below Pavement m (in)	Depth Within Layer m (in)	Dry Density kN/m^3 (pcf)	Moisture Content (%)	% Passing # 200 Sieve	LL	PL	Soil Class
Base	.13 - .28 (5 - 11)	0 - .15 (0 - 6)	*20.8 (133)*	*8.2*	13.2	NP	NP	A-1-a(0)
	.28 - .43 (11 - 17)	.15 - .30 (6 - 12)	*19.3 (123)*	*8.9*	11.3	NP	NP	A-1-a(0)
	.43 - .58 (17 - 23)	.30 - .46 (12 - 18)	*17.7 (113)*	*10.3*	9.60	NP	NP	A-1-a(0)
Sub-grade	.58 (23)	.03 (1.2)	-	7.10	27.5	19	NP	A-2-4(0)
	.69 -.84 (27 - 33)	.13 - .28 (5.2-11.2)	*15.8 (101)*	*14.5*	-	-	-	-
	.81 (32)	.26 (10.2)	-	12.7	37.3	22	20	-
	.10 - .12 (41 - 47)	.48 - .64 (19 - 25)	*14.7 (93.5)*	*18.5*	-	-	-	-
	1.17 (46)	.61 (24.2)	-	7.6	23.5	22	20	A-1-b(0)
	1.27-1.42 (50 -56)	.71 - .86 (28 - 34)	*14.6 (93.0)*	*17.7*	-	-	-	-
	1.47 (58)	.91 (36)	-	5.7	18.3	22	19	A-1-b(0)
	1.60 (63)	1.05 (41)	-	2.2	27.7	20	18	A-2-4(0)
	Bulk Sample	Bulk Sample	-	-	33.8	21	NP	A-2-4(0)

Table 3. Specific Gravity and R-Value for Subgrade Soils

Site Location	Depth Sampled Within Layer m (in)	Specific Gravity	Composite Classification	R-Value
Sunburst	.102 - .711 (4.0 - 28.0)	2.80	A-4 (0)	46
Alzada	Not Indicated	2.75	A-1-b (0)	61
Dickey Lake	Not Indicated	2.63	A-2-4 (0)	52
Swan	Not Indicated	2.49	A-1-a (0)	71
Loma				
Base Course	Not Indicated		A-1-a (0)	71
Subgrade	Not Indicated	2.79	A-2-4 (0)	59

Table 4a. Triaxial Test Results: Sunburst Site

SITE	Moisture Content (%)	Dry Density kN/m^3 (lb/ft^3)	Degree of Saturation (%)	σ_3 kPa (psi)	Ultimate Strength kPa (psi)	Young's Modulus MPa (ksi) cycle number 1	2	3	4	5
Sunburst	16.0	18.5 (118)	92.7	22 (3.2)	245 (35.5)	22 (3.2)	30 (4.4)	30 (4.4)	30 (4.4)	27 (3.9)
	15.2	19.4 (124)	100	20 (2.9)	200 (29.0)	20 (2.9)	30 (4.4)	27 (3.9)	30 (4.4)	30 (4.4)
	12.5	19.9 (127)	87.5	25 (3.6)	273 (39.6)	14 (2.0)	10 (1.5)	32 (4.7)	32 (4.7)	20 (2.9)

Table 4b. Triaxial Test Results: Alzada Site

SITE	Moisture Content (%)	Dry Density kN/m^3 (lb/ft^3)	Degree of Saturation (%)	σ_3 kPa (psi)	Ultimate Strength kPa (psi)	Young's Modulus MPa (ksi) cycle number 1	2	3	4	5
Alzada	14.0	19.3 (123)	98.5	22 (3.2)	245 (35.5)	25 (3.6)	28 (4.1)	30 (4.4)	27 (3.9)	29 (4.2)
	16.0	17.5 (111)	82.2	22 (3.1)	140 (20.3)	16 (2.3)	12 (1.7)	14 (2.0)	14 (2.0)	18 (2.6)
	16.0	18.1 (115)	88.0	23 (3.3)	190 (27.5)	12 (1.7)	15 (2.2)	19 (2.8)	20 (2.9)	20 (2.9)

Table 4c. Triaxial Test Results: Loma Site

SITE	Moisture Content (%)	Dry Density kN/m^3 (lb/ft^3)	Degree of Saturation (%)	σ_3 kPa (psi)	Ultimate Strength kPa (psi)	Young's Modulus MPa (ksi) cycle number 1	2	3	4	5
Loma	7.00	14.4 (91.4)	25.2	18 (2.7)	93.0 (13.5)	30 (4.4)	27 (3.9)	40 (5.8)	27 (3.9)	40 (5.8)
	7.00	17.3 (110)	43.0	21 (3.1)	420 (60.9)	83 (12)	88 (13)	80 (12)	83 (12)	80 (12)
	7.00	18.7 (119)	58.4	23 (3.3)	550 (79.7)	100 (15)	150 (22)	125 (18)	125 (18)	125 (18)
	12.0	15.1 (96.0)	49.0	19 (2.7)	92.0 (13.3)	30 (4.4)	35 (5.1)	30 (4.4)	20 (2.9)	20 (2.9)
	12.0	17.4 (111)	76.2	22 (3.2)	198 (28.7)	30 (4.4)	33 (4.8)	28 (4.1)	20 (2.9)	29 (4.2)
	12.0	18.8 (120)	100	24 (3.5)	350 (50.7)	40 (5.8)	30 (4.4)	25 (3.6)	33 (4.8)	33 (4.8)
	20.0	15.4 (98.0)	86.3	18 (2.6)	34.0 (4.93)	20 (2.9)	20 (2.9)	20 (2.9)	17 (2.5)	20 (2.9)
	20.0	17.6 (112)	100	24 (3.5)	127 (18.4)	38 (5.5)	38 (5.5)	38 (5.5)	26 (3.8)	15 (2.2)
	20.0	18.8 (120)	100	25 (3.7)	320 (46.4)	37 (5.4)	40 (5.8)	38 (5.5)	46 (6.7)	57 (8.3)

Table 4d. Triaxial Test Results: Swan Site

SITE	Moisture Content (%)	Dry Density kN/m³ (lb/ft³)	Degree of Saturation (%)	σ_3 kPa (psi)	Ultimate Strength kPa (psi)	Young's Modulus MPa (ksi) cycle number 1	2	3	4	5
Swan	8.00	13.9 (88.6)	26.8	20 (2.9)	118 (17.1)	50 (7.4)	57 (8.4)	52 (7.7)	67 (9.9)	67 (9.9)
	8.00	17.1 (109)	47.7	21 (3.0)	313 (45.3)	75 (11)	80 (12)	75 (11)	70 (10)	83 (12)
	8.00	18.8 (120)	69.2	21 (3.1)	626 (90.7)	67 (9.9)	83 (12)	86 (13)	88 (13)	87 (13)
	13.0	14.6 (93.0)	48.9	19 (2.7)	100 (14.5)	27 (4.0)	27 (4.0)	27 (4.0)	30 (4.4)	27 (4.0)
	13.0	17.0 (109)	76.3	20 (2.8)	275 (39.9)	56 (8.3)	57 (8.4)	48 (7.1)	19 (2.8)	16 (2.4)
	13.0	18.1 (115)	94.2	21 (3.1)	328 (47.5)	50 (7.4)	50 (7.4)	36 (5.3)	42 (6.2)	20 (3.0)
	13.0	18.8 (120)	100	23 (3.3)	350 (50.7)	50 (7.4)	40 (5.9)	38 (5.6)	31 (4.6)	25 (3.7)
	19.0	14.8 (94.0)	73.5	19 (2.7)	31.1 (4.51)	12 (1.8)	15 (2.2)	15 (2.2)	18 (2.7)	20 (3.0)
	19.0	17.7 (113)	100	21 (3.0)	398 (57.7)	50 (7.4)	50 (7.4)	50 (7.4)	50 (7.4)	40 (5.9)
	19.0	18.8 (120)	100	22 (3.2)	451 (65.4)	50 (7.4)	58 (8.6)	50 (7.4)	63 (9.3)	46 (6.8)

Table 4e. Triaxial Test Results: Dickey Lake Site

SITE	Moisture Content (%)	Dry Density kN/m³ (lb/ft³)	Degree of Saturation (%)	σ_3 kPa (psi)	Ultimate Strength kPa (psi)	Young's Modulus MPa (ksi) cycle number 1	2	3	4	5
Dickey Lake	7.00	15.4 (98.0)	27.7	15 (2.2)	118 (17.10)	45 (6.6)	45 (6.6)	50 (7.4)	50 (7.4)	50 (7.4)
	7.00	17.4 (111)	39.1	18 (2.7)	312.5 (45.29)	75 (11)	83 (12)	80 (12)	86 (13)	90 (13)
	7.00	20.1 (128)	66.9	21 (3.0)	626 (90.72)	150 (22)	147 (22)	150 (22)	163 (24)	164 (24)
	12.0	15.5 (99.0)	48.7	19 (2.8)	121 (17.54)	22 (3.2)	20 (3.0)	20 (3.0)	20 (3.0)	13 (1.9)
	12.0	17.3 (110)	65.2	20 (2.9)	150 (21.74)	56 (8.3)	57 (8.4)	48 (7.1)	19 (2.8)	16 (2.4)
	12.0	19.8 (126)	99.0	22 (3.2)	452 (65.5)	42 (6.2)	39 (5.8)	47 (6.9)	45 (6.6)	50 (7.4)
	17.0	14.6 (93.2)	59.5	17 (2.5)	23.75 (3.44)	45 (6.6)	45 (6.6)	50 (7.4)	50 (7.4)	50 (7.4)
	17.0	17.3 (110)	92.4	19 (2.8)	223 (32.3)	75 (11)	83 (12)	80 (12)	86 (13)	90 (13)
	17.0	18.8 (120)	100	22 (3.1)	323 (46.8)	150 (22)	147 (22)	150 (22)	163 (24)	164 (24)

Table 5a. Resilient Modulus Results: Sunburst Subgrade: γ_d = 18.7 kN/m^3 (119 lb/ft^3), ω = 12.0 %, S = 72.0 %

Chamber Confining Pressure, kPa (psi)	Nominal Maximum Axial Stress, kPa (psi)	Resilient Modulus MPa (ksi)
41.4 (6.11)	12.4 (1.83)	101 (14.9)
41.4 (6.11)	24.7 (3.65)	91.9 (13.6)
41.4 (6.11)	36.7 (5.42)	77.1 (11.4)
41.4 (6.11)	48.6 (7.17)	65.7 (9.70)
41.4 (6.11)	60.6 (8.95)	56.8 (8.38)
27.5 (4.06)	12.4 (1.83)	92.3 (13.6)
27.5 (4.06)	24.7 (3.65)	80.8 (11.9)
27.5 (4.06)	36.6 (5.40)	68.9 (10.2)
27.5 (4.06)	48.6 (7.17)	60.3 (8.90)
27.5 (4.06)	60.6 (8.95)	54.3 (8.02)
13.8 (2.04)	12.5 (1.85)	84.3 (12.4)
13.8 (2.04)	24.6 (3.63)	73.5 (10.9)
13.8 (2.04)	36.5 (5.39)	62.9 (9.29)
13.8 (2.04)	48.5 (7.16)	55.4 (8.18)
13.8 (2.04)	60.6 (8.95)	50.7 (7.48)

Table 5b. Resilient Modulus Results: Alzada Subgrade: γ_d = 17.5 kN/m^3 (112 lb/ft^3), ω = 18.3 %, S = 93.0 %

Chamber Confining Pressure, kPa (psi)	Nominal Maximum Axial Stress, kPa (psi)	Resilient Modulus MPa (ksi)
41.4 (6.11)	12.6 (1.86)	73.6 (10.9)
41.4 (6.11)	25.2 (3.72)	67.7 (9.99)
41.4 (6.11)	37.5 (5.54)	60.5 (8.93)
41.4 (6.11)	49.8 (7.35)	55.7 (8.22)
41.4 (6.11)	62.3 (9.20)	52.8 (7.79)
27.6 (4.07)	12.6 (1.86)	67.0 (9.89)
27.6 (4.07)	25.2 (3.72)	58.1 (8.58)
27.6 (4.07)	37.5 (5.54)	52.2 (7.71)
27.6 (4.07)	49.8 (7.35)	49.0 (7.23)
27.6 (4.07)	62.3 (9.20)	47.6 (7.03)
13.8 (2.04)	12.6 (1.86)	57.0 (8.41)
13.8 (2.04)	25.2 (3.72)	49.0 (7.23)
13.8 (2.04)	37.5 (5.54)	44.4 (6.55)
13.8 (2.04)	49.8 (7.35)	42.2 (6.23)
13.8 (2.04)	62.3 (9.20)	41.4 (6.11)

Table 5c. Resilient Modulus Results: Loma Subgrade: γ_d = 17.1 kN/m^3 (109 lb/ft^3), ω = 7.0 %, S = 33.2 %

Chamber Confining Pressure, kPa (psi)	Nominal Maximum Axial Stress, kPa (psi)	Resilient Modulus MPa (ksi)
41.4 (6.11)	14.2 (2.11)	108 (15.9)
41.4 (6.11)	28.1 (4.15)	105 (15.5)
41.4 (6.11)	41.8 (6.17)	97.7 (14.4)
41.4 (6.11)	55.4 (8.18)	94.0 (13.9)
41.4 (6.11)	69.2 (10.2)	92.5 (13.7)
27.5 (4.06)	14.2 (2.11)	95.5 (14.1)
27.5 (4.06)	27.6 (4.07)	89.6 (13.2)
27.5 (4.06)	41.2 (6.08)	85.8 (12.7)
27.5 (4.06)	55.0 (8.12)	84.0 (12.4)
27.5 (4.06)	68.6 (10.1)	83.7 (12.4)
13.8 (2.04)	14.2 (2.11)	80.0 (11.8)
13.8 (2.04)	27.0 (3.99)	74.7 (11.0)
13.8 (2.04)	40.8 (6.02)	72.7 (10.7)
13.8 (2.04)	54.4 (8.03)	71.8 (10.6)
13.8 (2.04)	68.0 (10.0)	72.4 (10.7)

Table 5d. Resilient Modulus Results: Loma Subgrade: γ_d = 17.1 kN/m^3 (109 lb/ft^3), ω = 12.0 %, S = 56.9 %

Chamber Confining Pressure, kPa (psi)	Nominal Maximum Axial Stress, kPa (psi)	Resilient Modulus MPa (ksi)
41.4 (6.11)	14.2 (2.07)	66.7 (9.85)
41.4 (6.11)	27.8 (4.10)	62.9 (9.29)
41.4 (6.11)	41.4 (6.11)	59.3 (8.75)
41.4 (6.11)	55.1 (8.13)	57.7 (8.52)
41.4 (6.11)	68.8 (10.2)	58.2 (8.59)
27.5 (4.06)	14.0 (2.07)	55.7 (8.22)
27.5 (4.06)	27.1 (4.00)	49.9 (7.37)
27.5 (4.06)	40.8 (6.02)	47.8 (7.06)
27.5 (4.06)	54.5 (8.05)	48.3 (7.13)
27.5 (4.06)	68.2 (10.1)	49.3 (7.28)
13.8 (2.04)	13.8 (2.04)	41.5 (6.13)
13.8 (2.04)	26.6 (3.93)	36.8 (5.43)
13.8 (2.04)	40.3 (5.95)	36.4 (5.37)
13.8 (2.04)	53.8 (7.94)	37.9 (5.59)
13.8 (2.04)	67.4 (9.95)	39.2 (5.79)

Table 5e. Resilient Modulus Results: Loma Subgrade: γ_d = 17.1 kN/m^3 (109 lb/ft^3), ω = 20.0 %, S = 92.8 %

Chamber Confining Pressure, kPa (psi)	Nominal Maximum Axial Stress, kPa (psi)	Resilient Modulus MPa (ksi)
41.4 (6.11)	14.2 (2.10)	55.4 (8.18)
41.4 (6.11)	27.7 (4.09)	49.7 (7.34)
41.4 (6.11)	41.2 (6.08)	45.0 (6.64)
41.4 (6.11)	54.5 (8.05)	42.0 (6.20)
41.4 (6.11)	68.2 (10.1)	41.5 (6.12)
27.5 (4.06)	14.5 (2.14)	43.1 (6.36)
27.5 (4.06)	27.2 (4.02)	36.1 (5.33)
27.5 (4.06)	41.1 (6.07)	33.8 (4.99)
27.5 (4.06)	54.5 (8.05)	33.5 (4.95)
27.5 (4.06)	68.1 (10.1)	33.5 (4.95)
13.8 (2.04)	14.0 (2.07)	29.9 (4.41)
13.8 (2.04)	26.4 (3.90)	23.9 (3.53)
13.8 (2.04)	40.2 (5.93)	23.1 (3.41)
13.8 (2.04)	53.5 (7.90)	23.6 (3.48)
13.8 (2.04)	67.3 (9.93)	24.3 (3.59)

Table 5f. Resilient Modulus Results: Swan Subgrade: γ_d = 17.1 kN/m^3 (109 lb/ft^3), ω = 8.0 %, S = 46.5 %

Chamber Confining Pressure, kPa (psi)	Nominal Maximum Axial Stress, kPa (psi)	Resilient Modulus MPa (ksi)
41.4 (6.11)	14.8 (2.18)	119 (17.6)
41.4 (6.11)	28.4 (4.19)	107 (15.8)
41.4 (6.11)	42.0 (6.20)	94.0 (13.9)
41.4 (6.11)	55.7 (8.22)	88.4 (13.0)
41.4 (6.11)	69.5 (10.3)	86.8 (12.8)
27.5 (4.06)	14.5 (2.14)	102 (15.1)
27.5 (4.06)	27.7 (4.09)	87.9 (13.0)
27.5 (4.06)	41.4 (6.11)	80.1 (11.8)
27.5 (4.06)	55.2 (8.15)	76.9 (11.4)
27.5 (4.06)	68.7 (10.1)	75.9 (11.2)
13.8 (2.04)	14.3 (2.11)	79.3 (11.7)
13.8 (2.04)	27.1 (4.00)	67.7 (9.99)
13.8 (2.04)	40.9 (6.04)	62.8 (9.27)
13.8 (2.04)	54.3 (8.02)	61.4 (9.06)
13.8 (2.04)	68.1 (10.1)	62.0 (9.15)

Table 5g. Resilient Modulus Results: Swan Subgrade: γ_d = 17.1 kN/m^3 (109 lb/ft^3), ω = 13.0 %, S = 75.5 %

Chamber Confining Pressurem, kPa (psi)	Nominal Maximum Axial Stress, kPa (psi)	Resilient Modulus MPa (ksi)
41.4 (6.11)	14.2 (2.10)	73.4 (10.8)
41.4 (6.11)	27.8 (4.10)	66.7 (9.85)
41.4 (6.11)	41.3 (6.10)	58.6 (8.65)
41.4 (6.11)	55.0 (8.12)	54.8 (8.09)
41.4 (6.11)	68.5 (10.1)	51.4 (7.59)
27.7 (4.09)	13.9 (2.05)	46.1 (6.81)
27.7 (4.09)	26.9 (3.97)	39.8 (5.88)
27.7 (4.09)	40.6 (5.99)	40.1 (5.92)
27.7 (4.09)	54.2 (8.00)	42.2 (6.23)
27.7 (4.09)	67.7 (9.99)	41.3 (6.10)
14.0 (2.07)	13.6 (2.01)	28.6 (4.22)
14.0 (2.07)	26.2 (3.87)	25.0 (3.69)
14.0 (2.07)	40.1 (5.92)	28.1 (4.15)
14.0 (2.07)	53.4 (7.88)	31.2 (4.61)
14.0 (2.07)	66.8 (9.86)	31.0 (4.58)

Table 5h. Resilient Modulus Results: Swan Subgrade: γ_d = 17.3 kN/m^3 (110 lb/ft^3), ω = 20.0 %, S = 100 %

Chamber Confining Pressure, kPa (psi)	Nominal Maximum Axial Stress, kPa (psi)	Resilient Modulus MPa (ksi)
41.3 (6.10)	14.4 (2.13)	67.7 (9.99)
41.3 (6.10)	28.1 (4.15)	59.0 (8.71)
41.3 (6.10)	41.6 (6.14)	51.8 (7.65)
41.3 (6.10)	55.2 (8.15)	49.2 (7..26)
41.3 (6.10)	68.7 (10.1)	48.3 (7.13)
27.5 (4.06)	14.2 (2.10)	49.2 (7.26)
27.5 (4.06)	27.1 (4.00)	40.5 (5.98)
27.5 (4.06)	40.8 (6.02)	38.6 (5.70)
27.5 (4.06)	54.6 (8.06)	39.1 (5.77)
27.5 (4.06)	67.9 (10.0)	37.3 (5.51)
13.7 (2.02)	13.9 (2.05)	28.1 (4.15)
13.7 (2.02)	26.5 (3.91)	23.6 (3.48)
13.7 (2.02)	40.3 (5.95)	25.1 (3.71)
13.7 (2.02)	53.8 (7.94)	26.2 (3.87)
13.7 (2.02)	66.5 (9.82)	24.7 (3.65)

Table 5i. Resilient Modulus Results: Dickey Lake Subgrade: γ_d = 17.3 kN/m^3 (110 lb/ft^3), ω = 7.0 %, S = 37.0 %

Chamber Confining Pressure, kPa (psi)	Nominal Maximum Axial Stress, kPa (psi)	Resilient Modulus MPa (ksi)
41.5 (6.13)	14.3 (2.11)	115 (17.0)
41.5 (6.13)	28.0 (4.13)	108 (15.9)
41.5 (6.13)	41.7 (6.16)	100 (14.8)
41.5 (6.13)	55.1 (8.13)	95.2 (14.1)
41.5 (6.13)	69.1 (10.2)	96.4 (14.2)
27.7 (4.10)	13.7 (2.02)	100 (14.8)
27.7 (4.10)	27.5 (4.06)	90.8 (13.4)
27.7 (4.10)	41.6 (6.14)	85.8 (12.7)
27.7 (4.10)	55.2 (8.15)	84.7 (12.5)
27.7 (4.10)	68.9 (10.2)	85.8 (12.7)
14.0 (2.07)	14.3 (2.11)	81.9 (12.1)
14.0 (2.07)	27.2 (4.02)	72.8 (10.7)
14.0 (2.07)	41.0 (6.05)	70.2 (10.4)
14.0 (2.07)	54.8 (8.09)	71.2 (10.5)
14.0 (2.07)	68.4 (10.1)	73.0 (10.8)

Table 5j. Resilient Modulus Results: Dickey Lake Subgrade: γ_d = 17.3 kN/m^3 (110 lb/ft^3), ω =12.0 %, S = 64.0 %

Chamber Confining Pressure, kPa (psi)	Nominal Maximum Axial Stress, kPa (psi)	Resilient Modulus MPa (ksi)
41.3 (6.10)	13.9 (2.05)	72.8 (10.7)
41.3 (6.10)	27.6 (4.07)	68.5 (10.1)
41.3 (6.10)	41.1 (6.07)	59.3 (8.75)
41.3 (6.10)	54.5 (9.52)	53.6 (7.91)
41.3 (6.10)	68.0 (10.0)	50.1 (7.40)
27.7 (4.09)	13.5 (1.99)	38.6 (5.70)
27.7 (4.09)	27.3 (4.03)	39.0 (5.76)
27.7 (4.09)	41.1 (6.07)	43.5 (6.42)
27.7 (4.09)	54.8 (8.09)	46.6 (6.88)
27.7 (4.09)	67.9 (10.0)	44.9 (6.63)
13.7 (2.02)	13.7 (2.02)	23.0 (3.40)
13.7 (2.02)	26.5 (3.91)	24.1 (3.56)
13.7 (2.02)	40.5 (5.98)	30.2 (4.46)
13.7 (2.02)	54.0 (7.97)	34.4 (5.08)
13.7 (2.02)	67.1 (9.91)	34.4 (5.08)

Table 5k. Resilient Modulus Results: Dickey Lake Subgrade: γ_d = 17.3 kN/m^3 (110 lb/ft^3), ω =13.0 %, S = 70.0 %

Chamber Confining Pressure, kPa (psi)	Nominal Maximum Axial Stress, kPa (psi)	Resilient Modulus MPa (ksi)
41.5 (6.13)	14.3 (2.11)	67.2 (9.92)
41.5 (6.13)	28.0 (4.13)	63.6 (9.39)
41.5 (6.13)	41.2 (6.08)	54.0 (7.97)
41.5 (6.13)	54.2 (8.00)	43.1 (6.36)
41.5 (6.13)	67.9 (10.0)	33.2 (4.90)
27.6 (4.07)	13.0 (1.92)	15.9 (2.35)
27.6 (4.07)	27.0 (3.99)	23.6 (3.48)
27.6 (4.07)	40.8 (6.02)	30.8 (4.55)
27.6 (4.07)	54.3 (8.02)	35.6 (5.26)
27.6 (4.07)	67.5 (9.96)	36.2 (5.34)
13.7 (2.02)	11.0 (1.62)	11.8 (1.74)
13.7 (2.02)	26.0 (3.84)	18.2 (2.69)
13.7 (2.02)	40.4 (5.96)	26.0 (3.84)
13.7 (2.02)	53.8 (7.94)	31.7 (4.68)

Table 6a. CBR Results: Sunburst Site

SITE	Dry Density kN/m^3 (lb/ft^3)	Moisture Content (%)	Degree of Saturation (%)	CBR
Sunburst	15.7 (100)	6.00	21.0	11
	16.6 (106)	6.00	24.0	29
	16.9 (108)	6.00	26.0	35
	17.2 (109)	12.0	53.0	19
	18.2 (116)	12.0	62.0	25
	18.7 (119)	12.0	71.0	27
	15.7 (100)	18.0	64.0	3.4
	17.6 (112)	14.0	66.0	13
	18.3 (117)	14.0	73.8	25

Table 6b. CBR Results: Alzada Site

SITE	Dry Density kN/m^3 (lb/ft^3)	Moisture Content (%)	Degree of Saturation (%)	CBR
Alzada	16.2 (103)	9.00	35.4	15
	16.9 (108)	9.00	39.2	25
	20.0 (127)	9.00	65.8	73
	17.1 (109)	12.0	56.0	7.4
	17.5 (112)	12.0	60.3	10
	18.0 (115)	12.0	64.8	14
	15.7 (100)	19.0	69.7	3.6
	17.2 (110)	12.5	70.0	5.4
	19.0 (121)	12.0	73.0	11

Table 6c. CBR Results: Loma Site

SITE	Dry Density kN/m^3 (lb/ft^3)	Moisture Content (%)	Degree of Saturation (%)	CBR
Loma	15.0 (95.5)	7.00	23.0	15
	15.8 (100)	7.00	26.0	36
	16.5 (105)	7.00	29.0	69
	15.8 (101)	12.0	44.4	9.1
	16.6 (106)	12.0	50.0	14
	17.4 (111)	12.0	57.4	19
	15.6 (99.4)	17.0	61.0	16
	15.8 (101)	17.0	64.0	19
	16.2 (103)	17.0	67.0	24

Table 6d. CBR Results: Swan Site

SITE	Dry Density kN/m^3 (lb/ft^3)	Moisture Content (%)	Degree of Saturation (%)	CBR
Swan	16.4 (104)	8.00	38.2	20
	17.0 (108)	8.00	44.1	41
	17.8 (113)	8.00	48.7	70
	15.3 (97.1)	13.0	52.0	6.7
	16.8 (106)	13.0	69.4	11
	17.6 (112)	13.0	74.9	15
	16.3 (104)	18.0	86.5	2.4
	16.8 (107)	18.0	92.7	3.9
	17.3 (110)	18.0	98.0	5.2

Table 6e. CBR Results: Dickey Lake Site

SITE	Dry Density kN/m^3 (lb/ft^3)	Moisture Content (%)	Degree of Saturation (%)	CBR
Dickey Lake	17.7 (113)	7.00	35.4	26
	19.0 (121)	7.00	44.4	49
	19.5 (124)	7.00	48.8	76
	18.0 (115)	12.0	70.1	2.2
	18.5 (118)	12.0	78.3	5.2
	19.0 (121)	12.0	83.1	8.3
	17.5 (112)	17.0	86.0	2.5
	17.9 (114)	17.0	90.6	4.9
	18.3 (116)	17.0	96.6	7.1

Table 7. Summarized Resilient Modulus Values

Site	Moisture Content (%)	Dry Unit Weight kN/m^3 (lb/ft^3)	Degree of Saturation (%)	Resilient Modulus MPa (ksi)
Sunburst	12.0	18.7 (119)	71.4	67.5 (9.79)
Alzada	18.3	17.5 (111)	92.9	49.5 (7.18)
Loma	7.0	17.1 (109)	32.5	80.0 (11.6)
	12.0	17.1 (109)	55.7	42.5 (6.16)
	20.0	17.1 (109)	92.9	30.0 (4.35)
Swan	8.0	17.1 (109)	46.5	73.0 (10.6)
	13.0	17.3 (110)	78.6	35.0 (5.08)
	20.0	17.3 (110)	100	32.0 (4.64)
Dickey Lake	7.0	17.3 (110)	37.5	79.0 (11.5)
	12.0	17.3 (110)	64.2	37.5 (5.44)
	13.0	17.3 (110)	70.0	27.5 (3.99)

Table 8a. Texas Triaxial Class and Correlated Resilient Modulus: Sunburst Subgrade

Site	Moisture Content (%)	Dry Unit Weight kN/m³ (lb/ft³)	Degree of Saturation (%)	Ultimate Strength kPa (psi)	Normal Stress kPa (psi)	Texas Triaxial Class	Resilient Modulus MPa (ksi)
Sunburst	16.0	18.5 (118)	92.7	245 (35.5)	133 (19.3)	2.0	276 (40.0)
	15.2	19.42 (124)	100	200 (29.0)	110 (16.0)	2.4	217 (31.5)
	12.5	19.9 (127)	87.5	273 (39.6)	149 (21.6)	1.8	299 (43.4)

Table 8b. Texas Triaxial Class and Correlated Resilient Modulus: Alzada Subgrade

Site	Moisture Content (%)	Dry Unit Weight kN/m³ (lb/ft³)	Degree of Saturation (%)	Ultimate Strength kPa (psi)	Normal Stress kPa (psi)	Texas Triaxial Class	Resilient Modulus MPa (ksi)
Alzada	14.0	19.3 (123)	98.5	245 (35.5)	133 (19.3)	2.0	276 (40.0)
	16.0	17.5 (111)	82.2	140 (20.3)	80.9 (11.7)	2.9	169 (24.5)
	16.0	18.0 (115)	88.0	190 (27.5)	106 (15.4)	2.4	221 (32.0)

Table 8c. Texas Triaxial Class and Correlated Resilient Modulus: Loma Subgrade

Site	Moisture Content (%)	Dry Unit Weight kN/m³ (lb/ft³)	Degree of Saturation (%)	Ultimate Strength kPa (psi)	Normal Stress kPa (psi)	Texas Triaxial Class	Resilient Modulus MPa (ksi)
Loma	7.00	14.4 (91.4)	25.2	93.0 (13.5)	57.2 (8.30)	3.4	118 (17.1)
	7.00	17.3 (110)	43.0	420 (60.9)	221 (32.1)	1.1	422 (61.2)
	7.00	18.7 (119)	58.4	550 (79.7)	284 (41.2)	1.0	441 (64.0)
	12.0	15.1 (96)	49.0	92.0 (13.3)	55.4 (8.00)	3.4	118 (17.2)
	12.0	17.4 (111)	76.2	198 (28.7)	110 (16.0)	2.5	200 (29.0)
	12.0	18.8 (120)	100	350 (50.7)	187 (27.1)	1.3	400 (58.0)
	20.0	15.4 (98)	86.3	34 (4.90)	25.9 (3.75)	4.0	79.3 (11.5)
	20.0	17.6 (112)	100	127 (18.4)	75.5 (10.9)	3.1	153 (22.1)
	20.0	18.8 (120)	100	320 (46.4)	173 (25.0)	1.6	341 (49.5)

Table 8d. Texas Triaxial Class and Correlated Resilient Modulus: Swan Subgrade

Site	Moisture Content (%)	Dry Unit Weight kN/m³ (lb/ft³)	Degree of Saturation (%)	Ultimate Strength kPa (psi)	Normal Stress kPa (psi)	Texas Triaxial Class	Resilient Modulus MPa (ksi)
Swan	8.00	13.9 (88.6)	26.8	118 (17.1)	68.9 (9.98)	3.1	148 (21.5)
	8.00	17.1 (109)	47.7	313 (45.3)	167 (24.1)	1.7	324 (47.0)
	8.00	18.8 (120)	69.2	626 (90.7)	324 (46.9)	1.0	441 (64.0)
	13.0	14.6 (93.0)	48.9	100 (14.5)	59.4 (8.6)	3.3	125 (18.1)
	13.0	18.1 (115)	94.2	328 (47.5)	175 (25.3)	1.7	324 (47.0)
	13.0	18.8 (120)	100	350 (50.7)	187 (27.0)	1.6	341 (49.5)
	19.0	14.8 (94.0)	73.5	31.1 (4.51)	24.9 (3.60)	4.0	78.9 (11.5)
	19.0	17.7 (113)	100	398 (57.7)	209 (30.4)	1.6	348 (50.5)
	19.0	18.8 (120)	100	451 (65.4)	237 (34.3)	1.1	435 (63.1)

Table 8e. Texas Triaxial Class and Correlated Resilient Modulus: Dickey Lake Subgrade

Site	Moisture Content (%)	Dry Unit Weight kN/m³ (lb/ft³)	Degree of Saturation (%)	Ultimate Strength kPa (psi)	Normal Stress kPa (psi)	Texas Triaxial Class	Resilient Modulus MPa (ksi)
Dickey Lake	7.00	15.4 (98.0)	27.7	118 (17.1)	66.5 (9.65)	3.1	159 (23.1)
	7.00	17.4 (111)	39.1	313 (45.3)	166 (24.0)	1.8	318 (46.1)
	7.00	20.1 (128)	66.9	626 (90.7)	323 (46.9)	1.0	441 (64.0)
	12.0	15.5 (99.0)	48.7	121 (17.5)	70.1 (10.2)	3.1	148 (21.5)
	12.0	17.3 (110)	65.2	150 (21.7)	85.0 (12.3)	2.8	180 (26.1)
	12.0	19.8 (126)	99.0	452 (65.5)	237 (34.3)	1.1	435 (63.1)
	17.0	14.6 (93.2)	59.5	23.8 (3.44)	20.4 (2.96)	4.1	71.9 (10.4)
	17.0	17.3 (110)	92.4	223 (32.3)	121 (17.6)	1.9	284 (41.2)
	17.0	18.8 (120)	100	323 (46.8)	172 (25.0)	1.7	320 (46.4)

Table 9. R-Value and Correlated Resilient Modulus

Site Location	R-Value	Resilient Modulus MPa (ksi)
Sunburst	46	75.2 (10.9)
Alzada	61	122 (17.7)
Dickey Lake	52	91.0 (13.2)
Swan	71	172 (25.0)
Loma	59	120 (17.4)

APPENDIX B: FIGURES

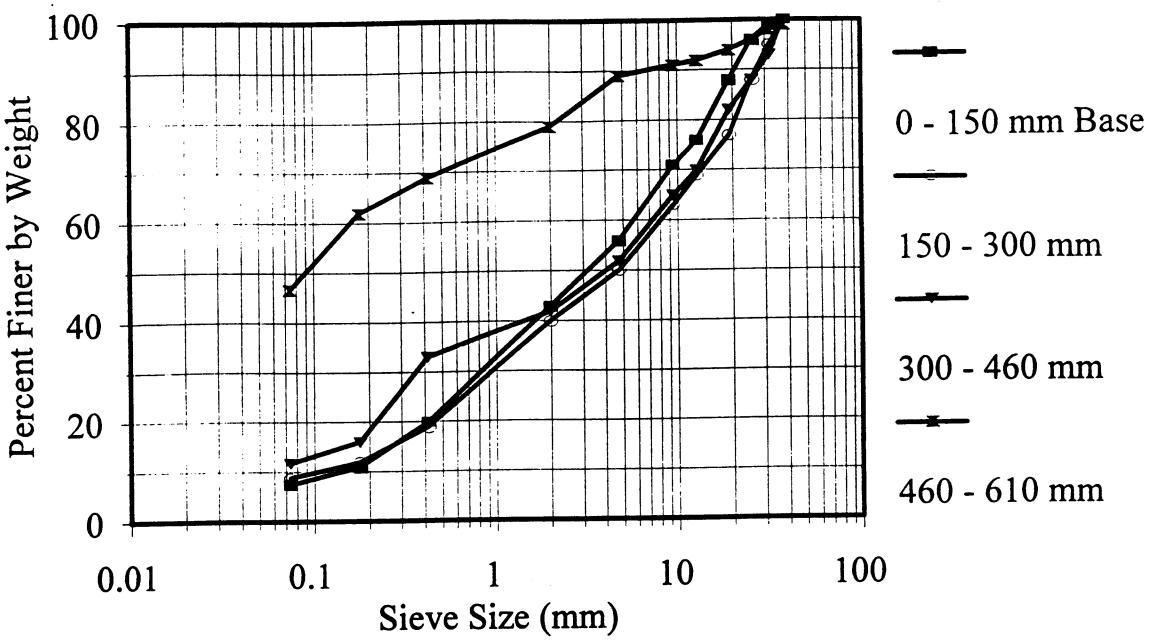

Figure 1a. Grain Size Distribution Curves for the Sunburst Site

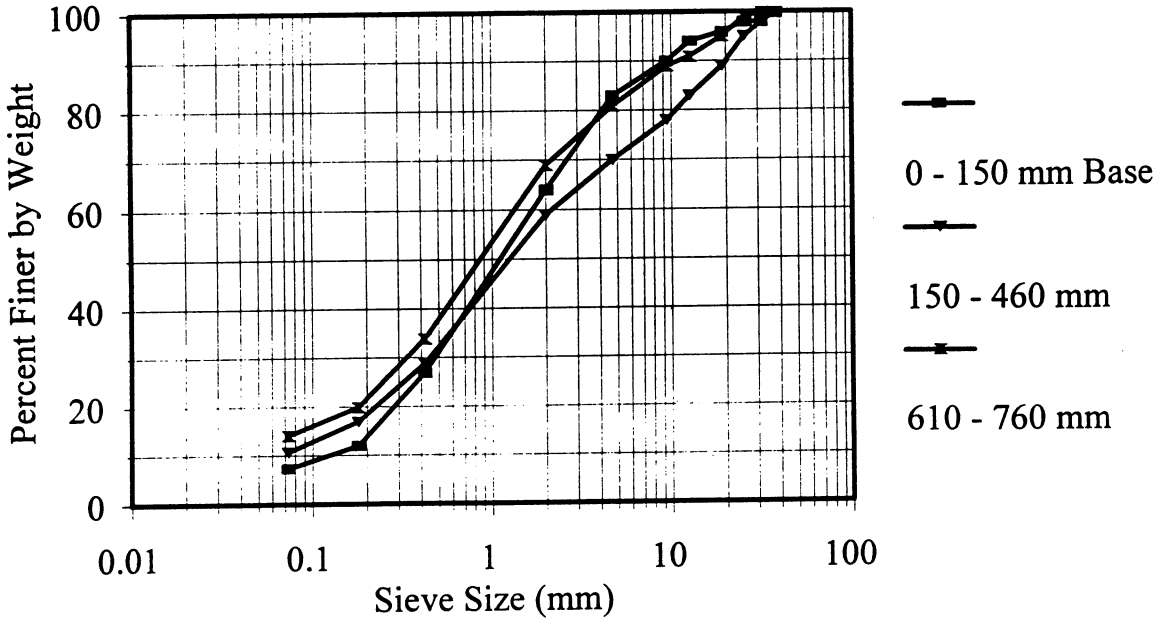

Figure 1b. Grain Size Distribution Curves for the Alzada Site

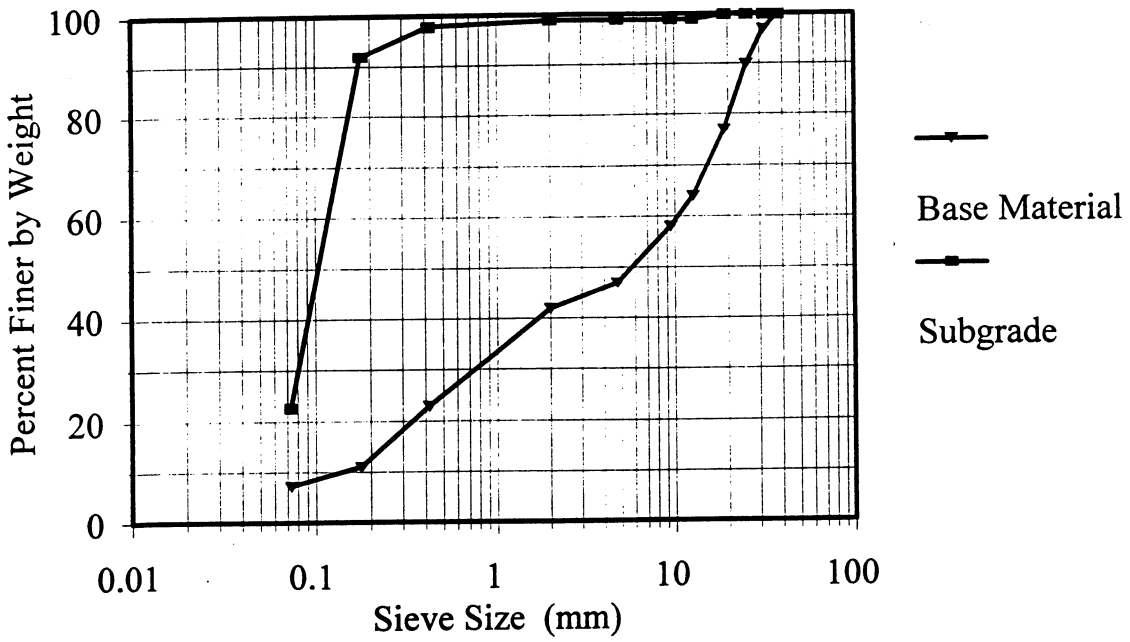

Figure 1c. Grain Size Distribution Curves for the Loma Site

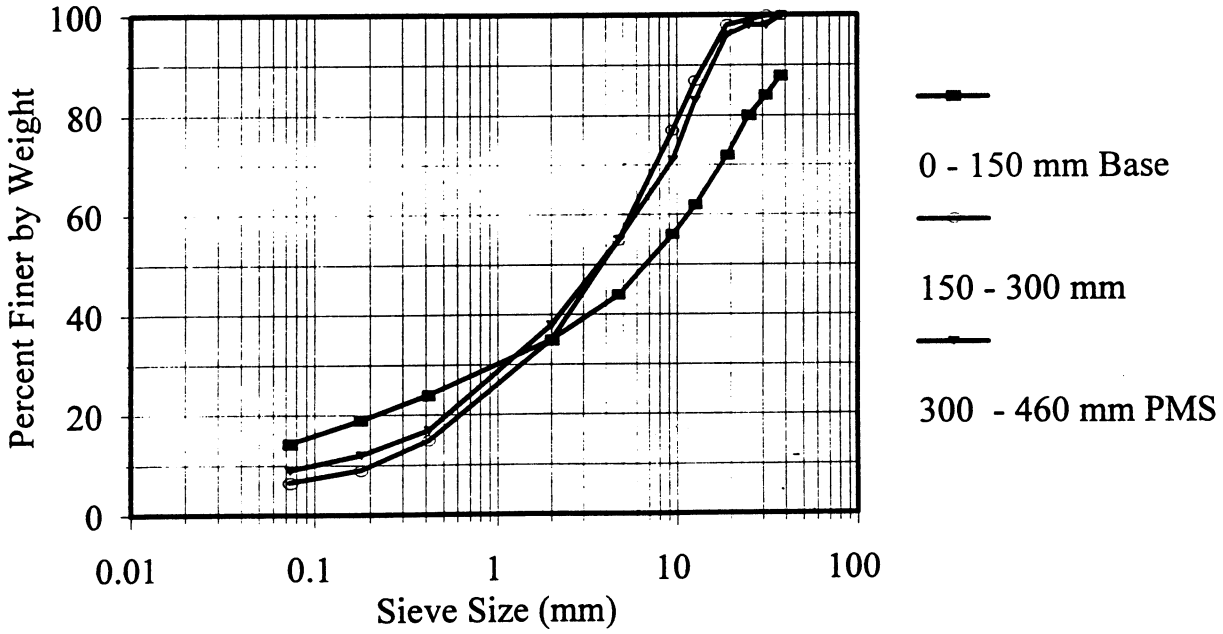

Figure 1d. Grain Size Distribution Curves for the Swan Site

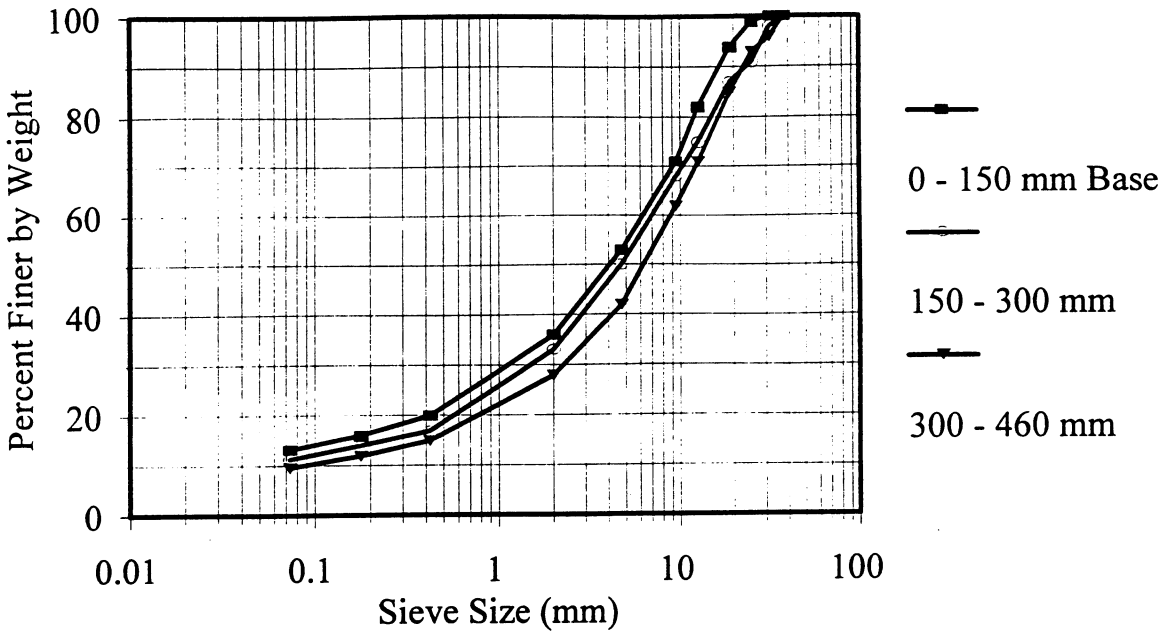

Figure 1e. Grain Size Distribution Curves for the Dickey Lake Site

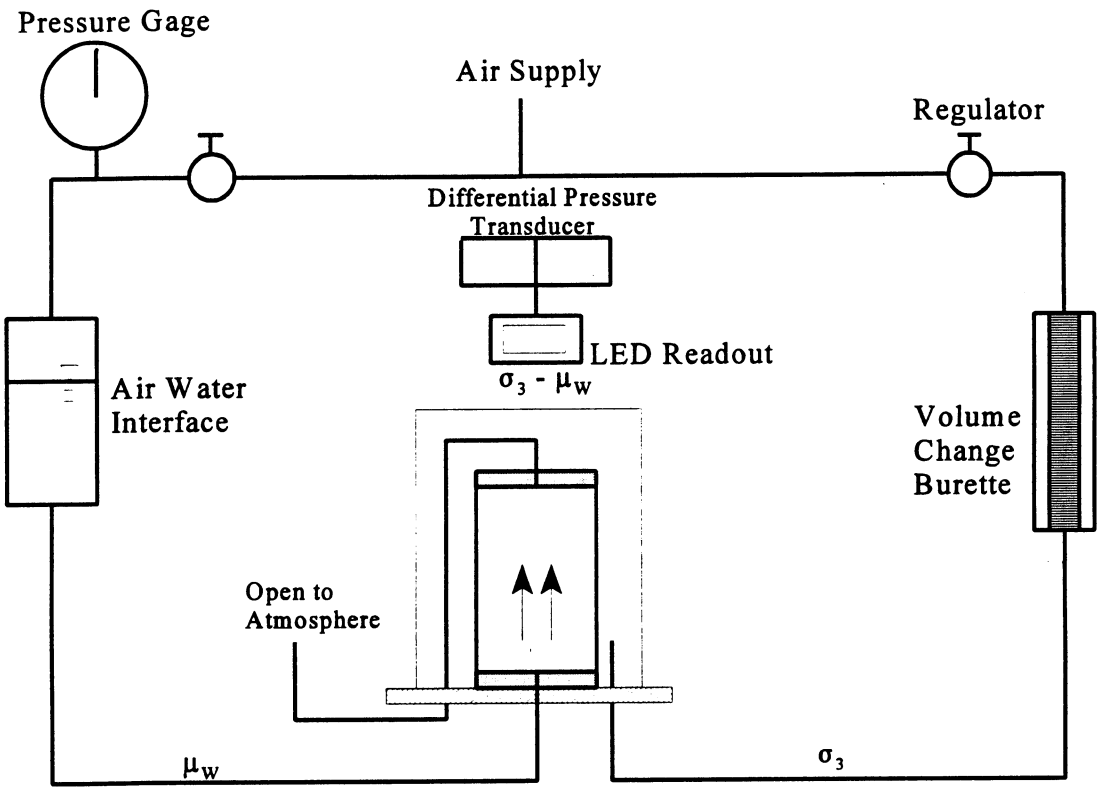

Figure 2. Schematic Diagram of Triaxial Moisture Conditioning Apparatus Used for Sample Saturation

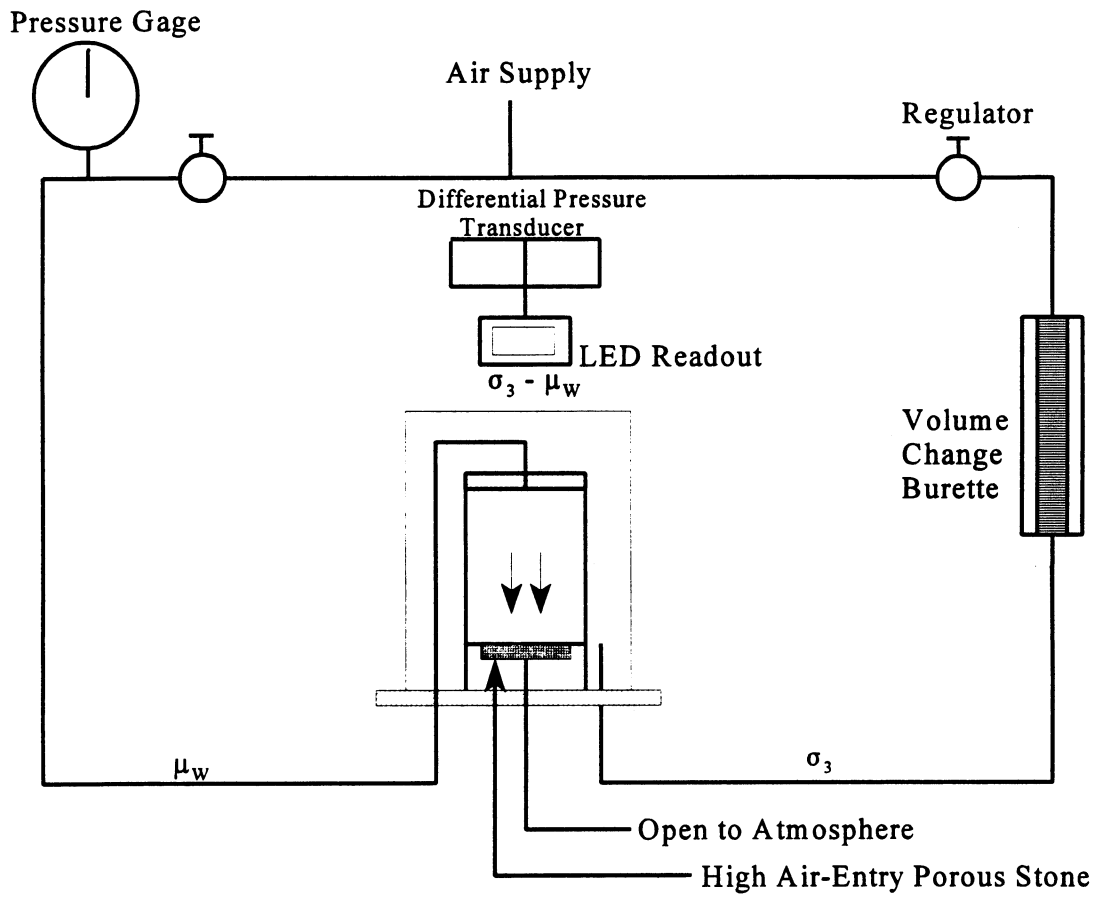

Figure 3. Schematic Diagram of Triaxial Moisture Conditioning Apparatus Used for Sample Desaturation

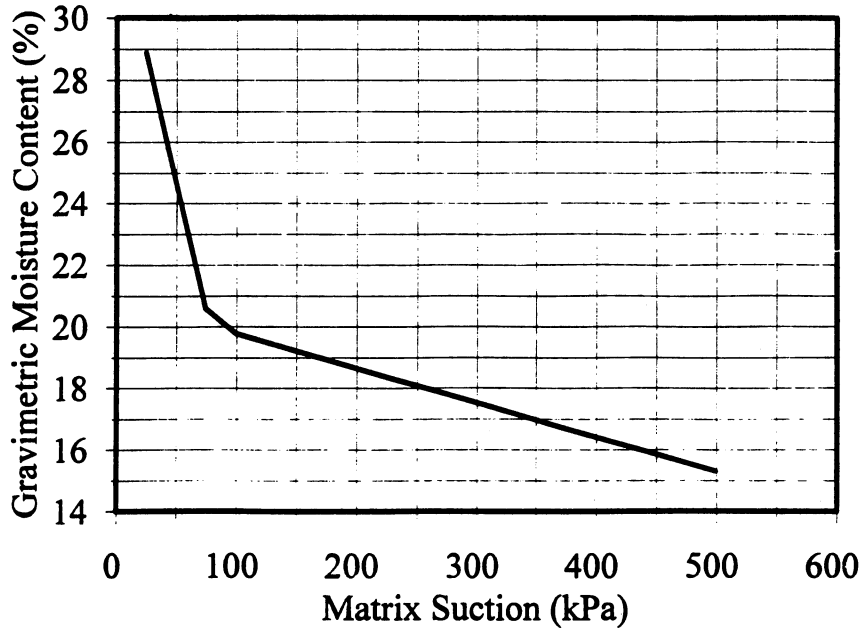

Figure 4a. Moisture Release Curve: Sunburst Site

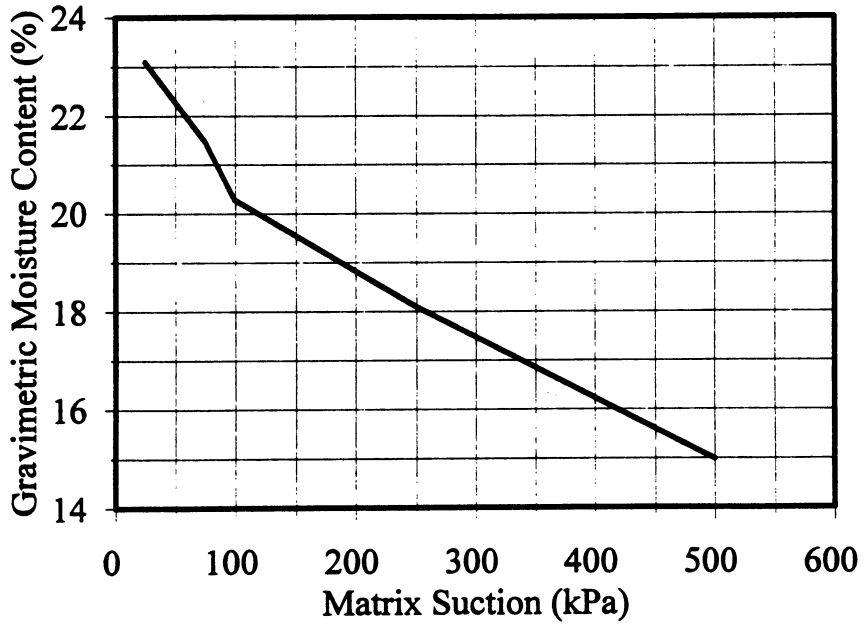

Figure 4b. Moisture Release Curve: Alzada Site

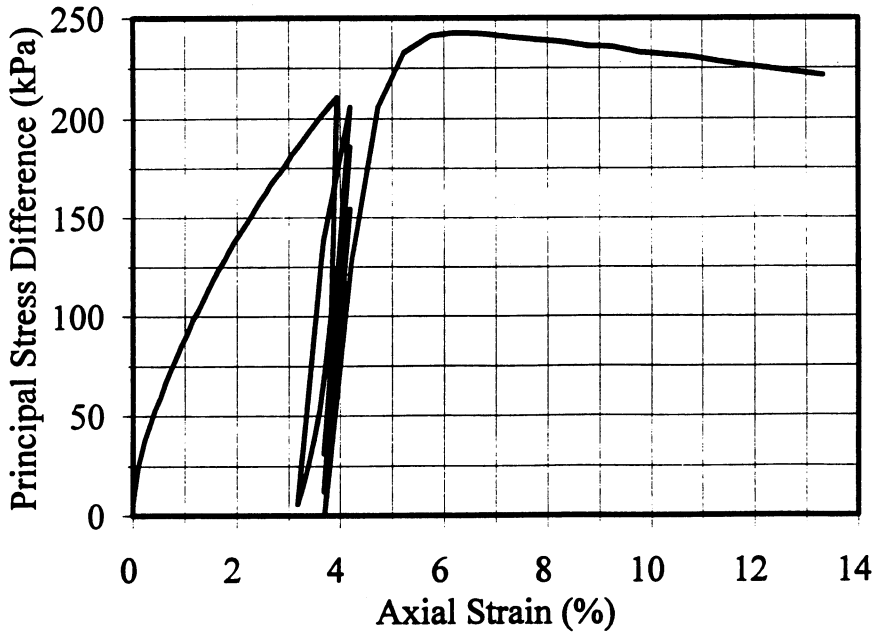

Figure 5a. Triaxial Compression Results: Sunburst Subgrade, γ_d = 18.5 kN/m^3 (118 lb/ft^3), ω = 16.0 %, S = 92.7 %, σ_3 = 21.8 kPa (3.17 psi)

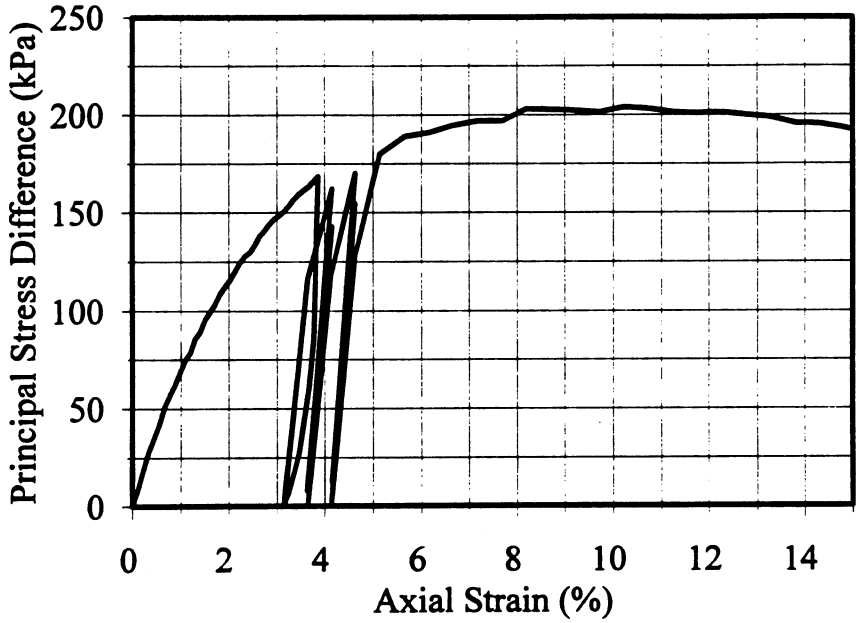

Figure 5b. Triaxial Compression Results: Sunburst Subgrade, γ_d = 19.4 kN/m^3 (124 lb/ft^3), ω = 15.2 %, S = 100 %, σ_3 = 20.3 kPa (2.95 psi)

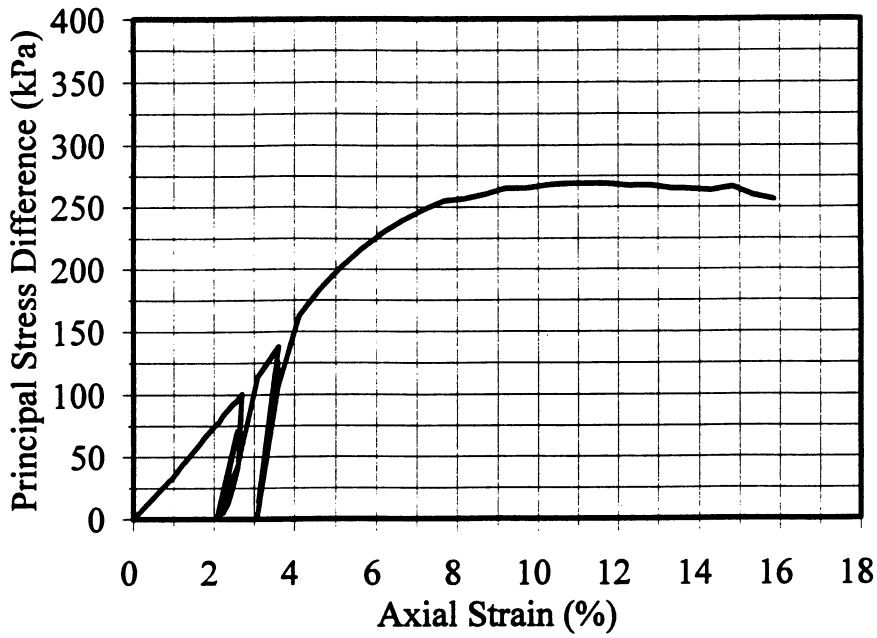

Figure 5c. Triaxial Compression Results: Sunburst Subgrade, γ_d = 19.9 kN/m^3 (127 lb/ft^3), ω = 12.5 %, S = 87.5 %, σ_3 = 24.5 kPa (3.56 psi)

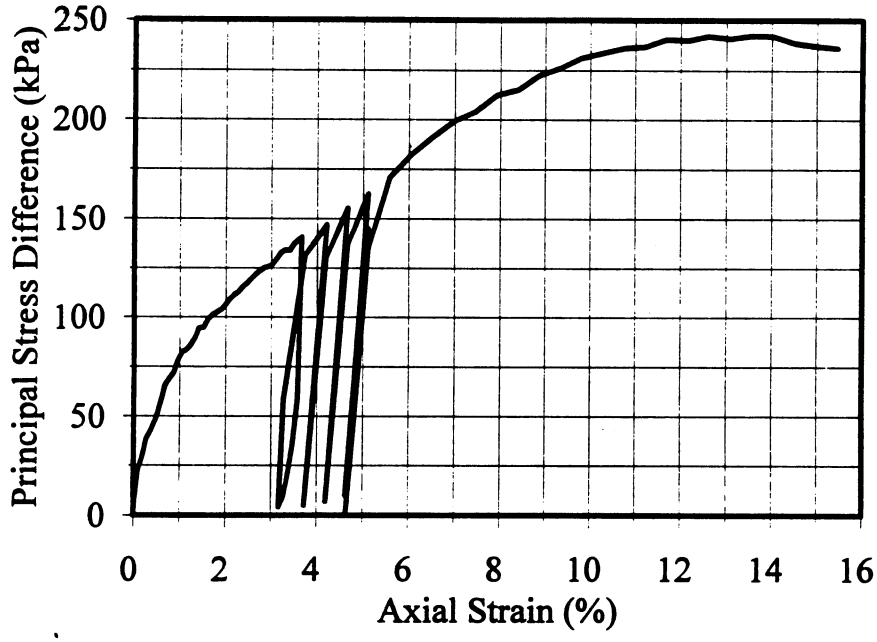

Figure 6a. Triaxial Compression Results: Alzada Subgrade, γ_d = 19.3 kN/m^3 (123 lb/ft^3), ω = 14.0 %, S = 99.3 %, σ_3 = 21.8 kPa (3.17 psi)

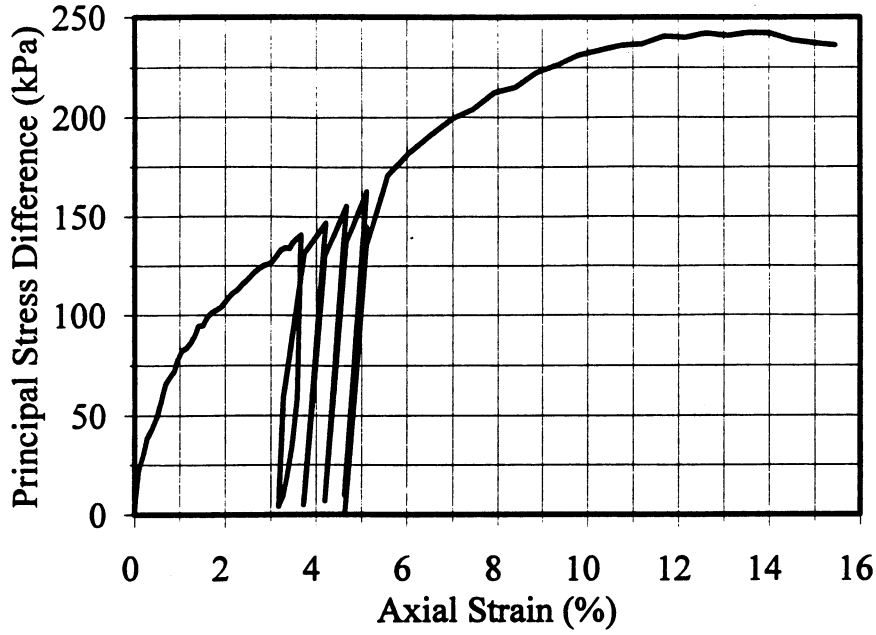

Figure 6b. Triaxial Compression Results: Alzada Subgrade, γ_d = 17.5 kN/m^3 (112 lb/ft^3), ω = 16.0 %, S = 82.6 %, σ_3 = 21.8 kPa (3.17 psi)

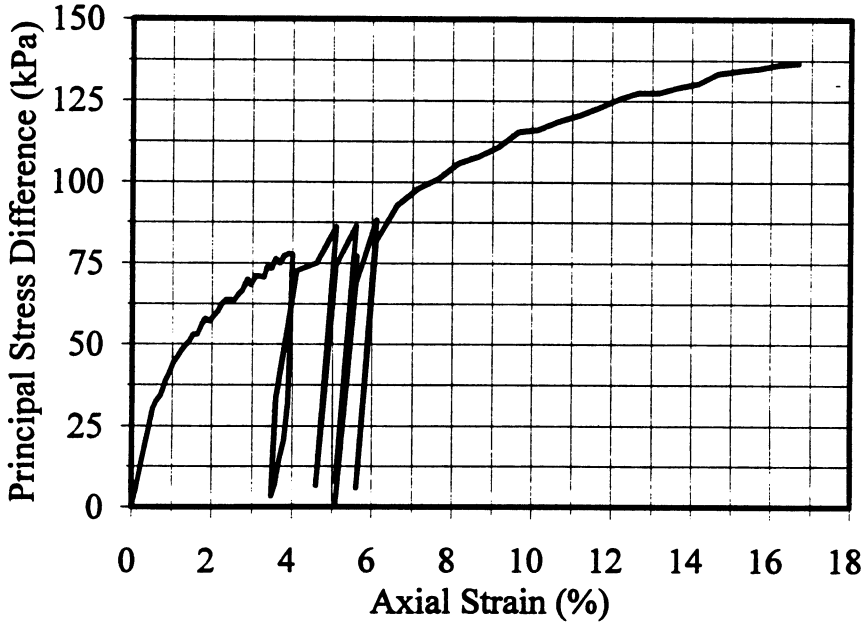

Figure 6c. Triaxial Compression Results: Alzada Subgrade, γ_d = 18.0 kN/m^3 (115lb/ft^3), ω = 16.0 %, S = 88.4 %, σ_3 = 23.0 kPa (3.35 psi)

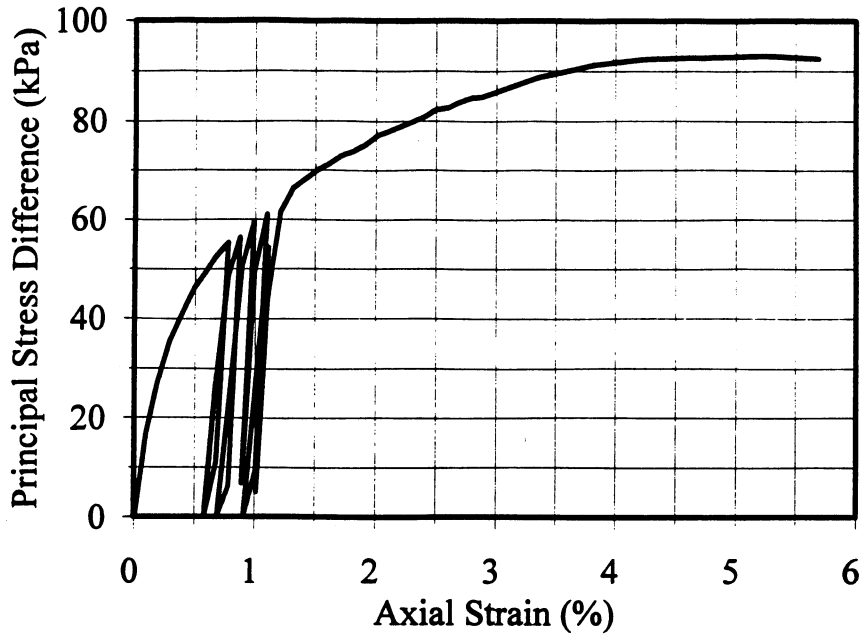

Figure 7a. Triaxial Compression Results: Loma Subgrade, γ_d = 14.4 kN/m^3 (92 lb/ft^3), ω = 7.0 %, S = 25.2 %, σ_3 = 18.3 kPa (2.66 psi)

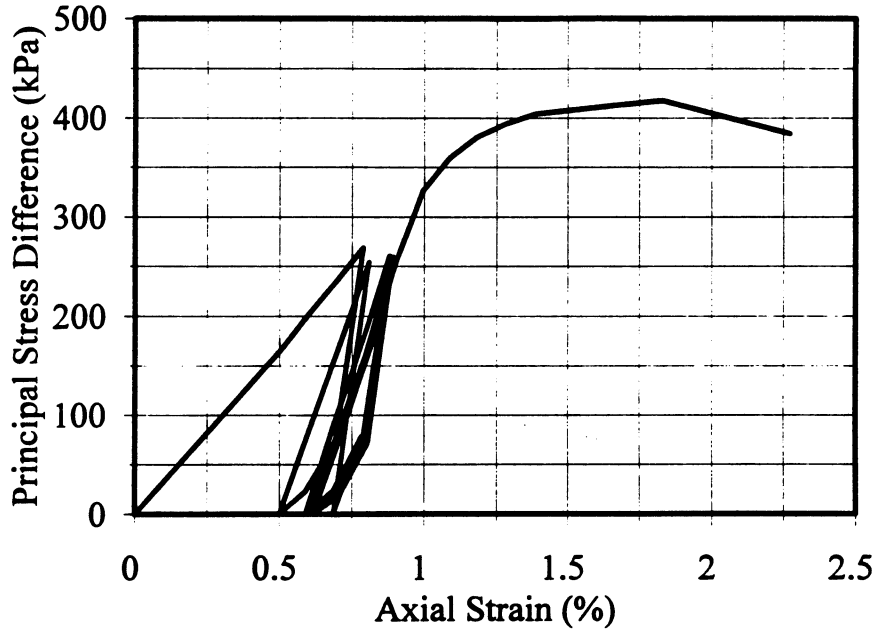

Figure 7b. Triaxial Compression Results: Loma Subgrade, γ_d = 17.3 kN/m^3 (110 lb/ft^3), ω = 7.0 %, S = 43.1 %, σ_3 = 21.3 kPa (3.10 psi)

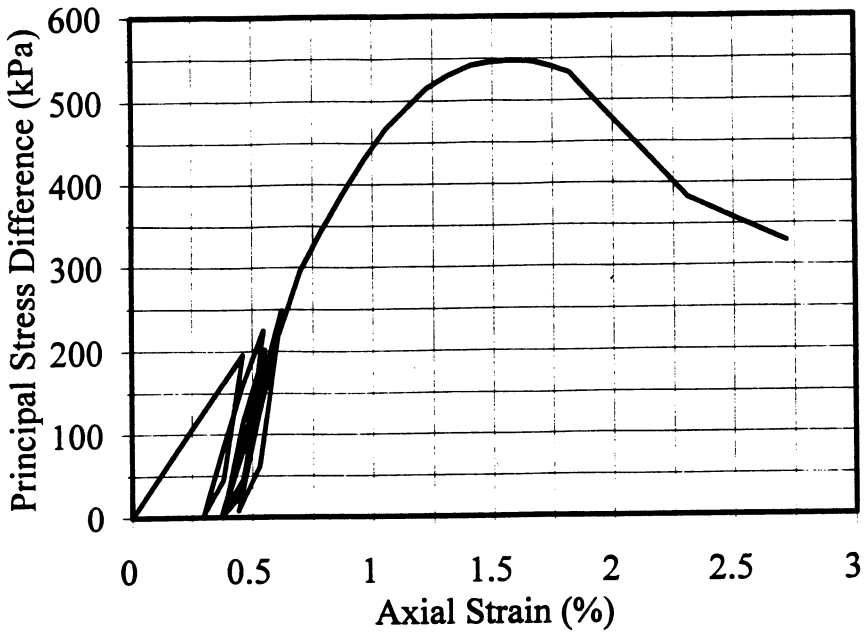

Figure 7c. Triaxial Compression Results: Loma Subgrade, γ_d = 18.7 kN/m^3 (119 lb/ft^3), ω = 7.0 %, S = 58.2 %, σ_3 = 22.6 kPa (3.29 psi)

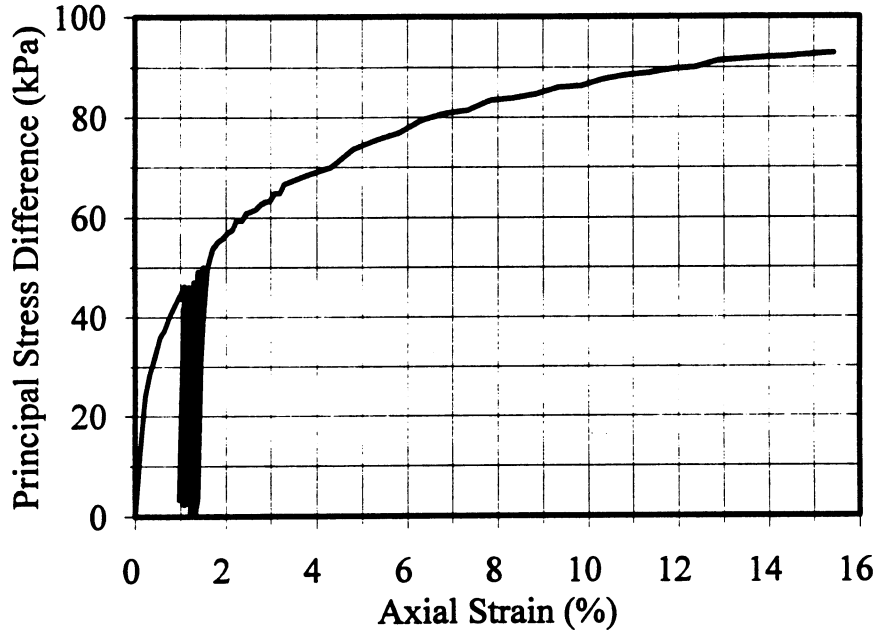

Figure 7d. Triaxial Compression Results: Loma Subgrade, γ_d = 15.1 kN/m^3 (96 lb/ft^3), ω = 12.0 %, S = 49.0 %, σ_3 = 18.7 kPa (2.72 psi)

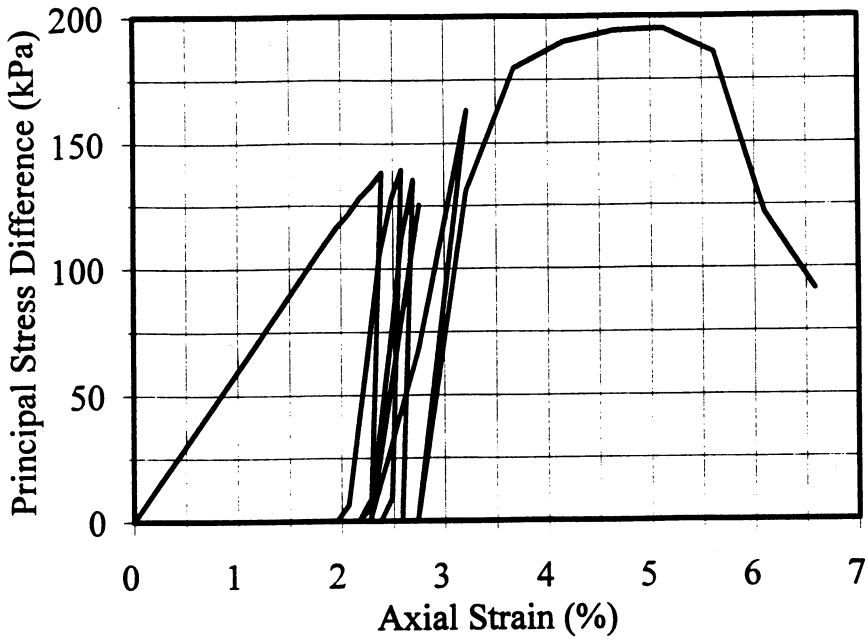

Figure 7e. Triaxial Compression Results: Loma Subgrade, γ_d = 17.4 kN/m^3 (111 lb/ft^3), ω = 12.0 %, S = 76.7 %, σ_3 = 22.3 kPa (3.24 psi)

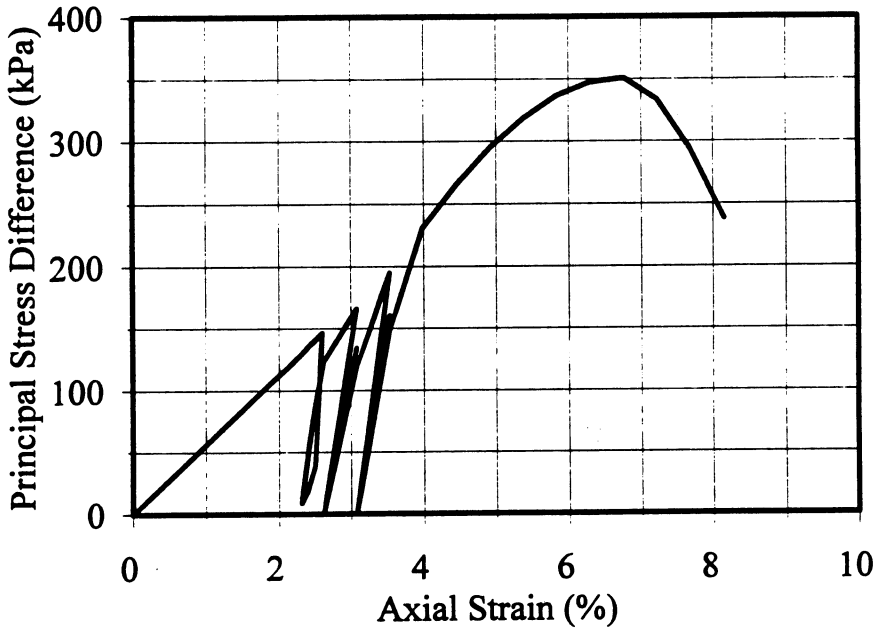

Figure 7f. Triaxial Compression Results: Loma Subgrade, γ_d = 19.0 kN/m^3 (121 lb/ft^3), ω = 12.0 %, S = 100 %, σ_3 = 24 kPa (3.49 psi)

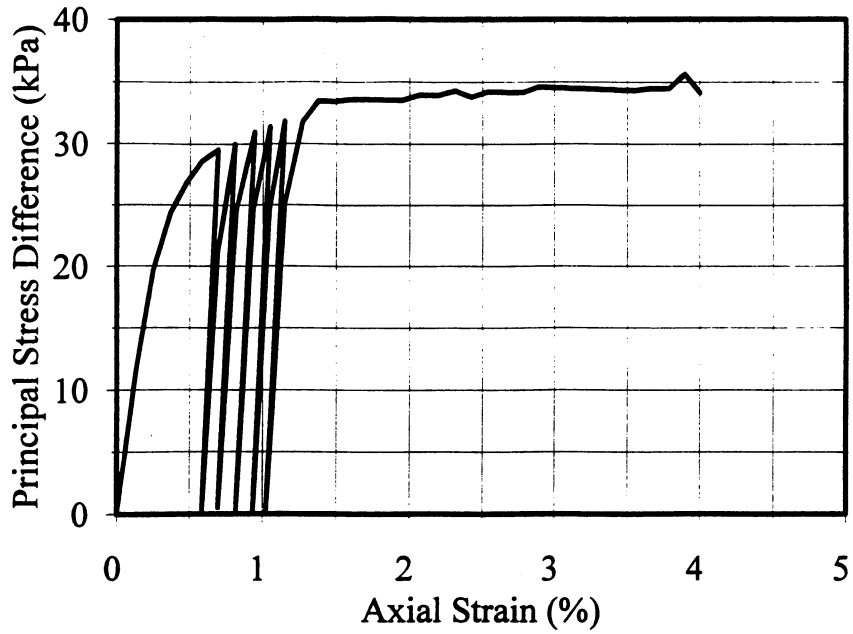

Figure 7g. Triaxial Compression Results: Loma Subgrade, γ_d = 15.4 kN/m^3 (98.0 lb/ft^3), ω = 20.0 %, S = 86.3 %, σ_3 = 17.7 kPa (2.57 psi)

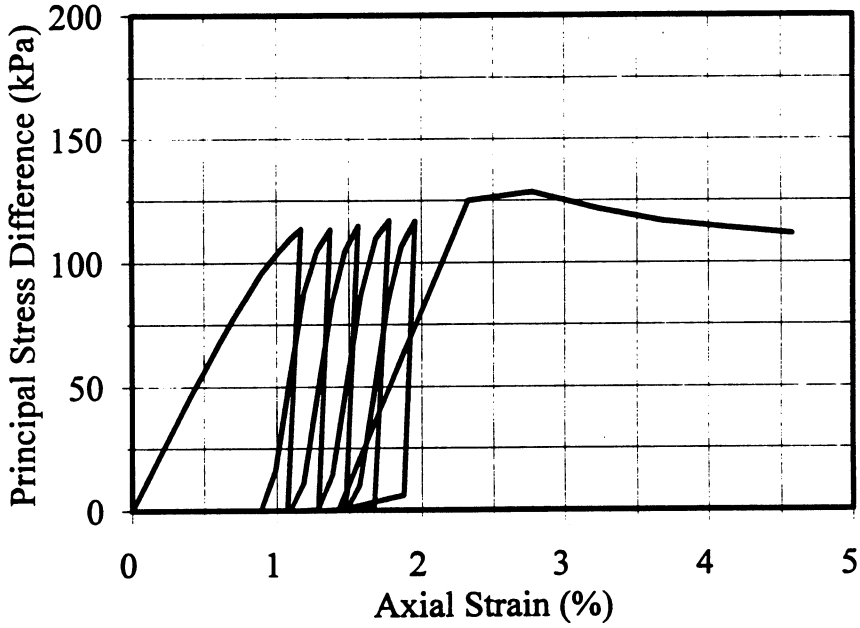

Figure 7h. Triaxial Compression Results: Loma Subgrade, γ_d = 18.0 kN/m^3 (115 lb/ft^3), ω = 20.0 %, S = 100 %, σ_3 = 24.0 kPa (3.49 psi)

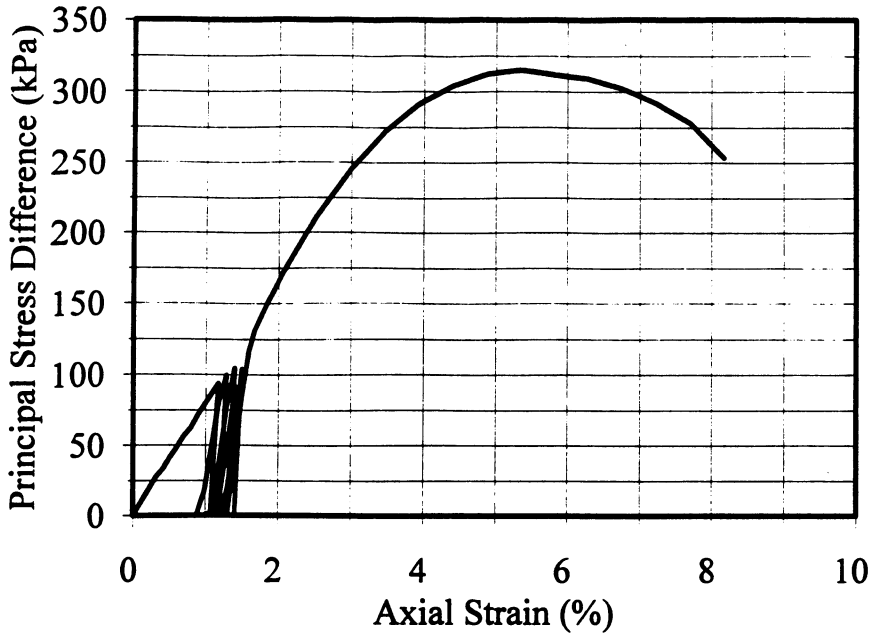

Figure 7i. Triaxial Compression Results: Loma Subgrade, γ_d = 19.0 kN/m^3 (121 lb/ft^3), ω = 20.0 %, S = 100 %, σ_3 = 25.2 kPa (3.67 psi)

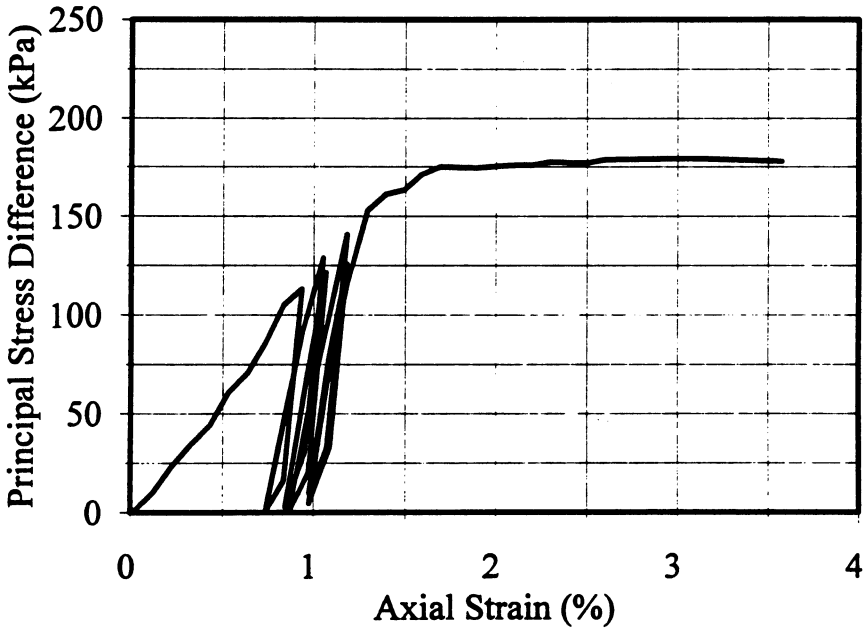

Figure 8a. Triaxial Compression Results: Swan Subgrade, γ_d = 15.4 kN/m^3 (98.0 lb/ft^3), ω = 8.0 %, S = 26.7 %, σ_3 = 19.7 kPa (2.87 psi)

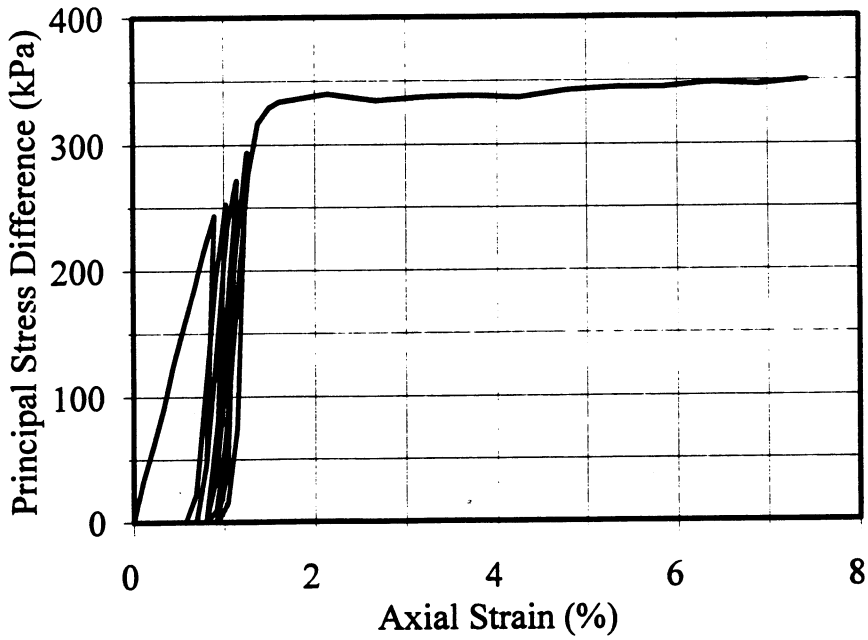

Figure 8b. Triaxial Compression Results: Swan Subgrade, γ_d = 17.4 kN/m^3 (111 lb/ft^3), ω = 8.0 %, S = 47.7 %, σ_3 = 20.7 kPa (3.01 psi)

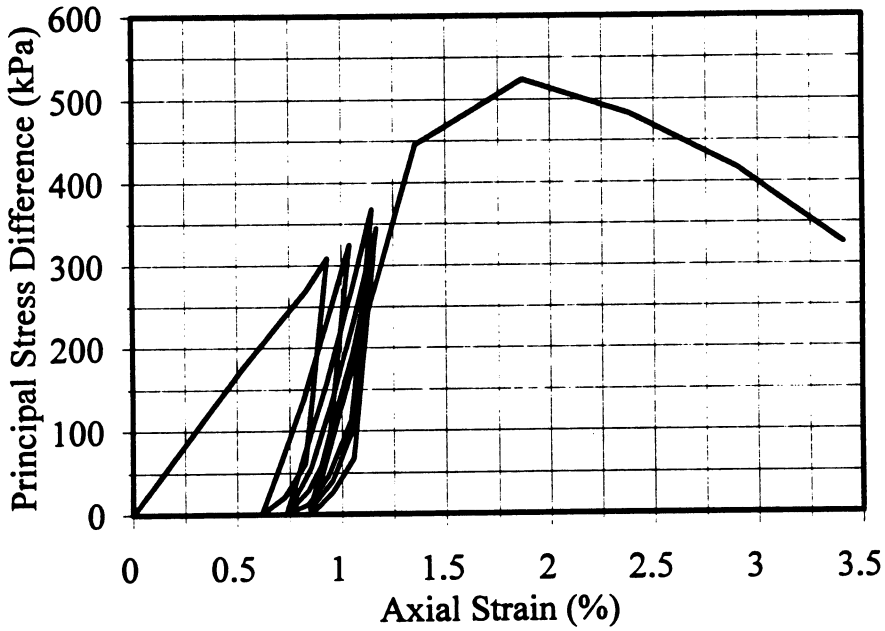

Figure 8c. Triaxial Compression Results: Swan Subgrade, γ_d = 20.1 kN/m^3 (128 lb/ft^3), ω = 8.0 %, S = 69.2 %, σ_3 = 21.3 kPa (3.10 psi)

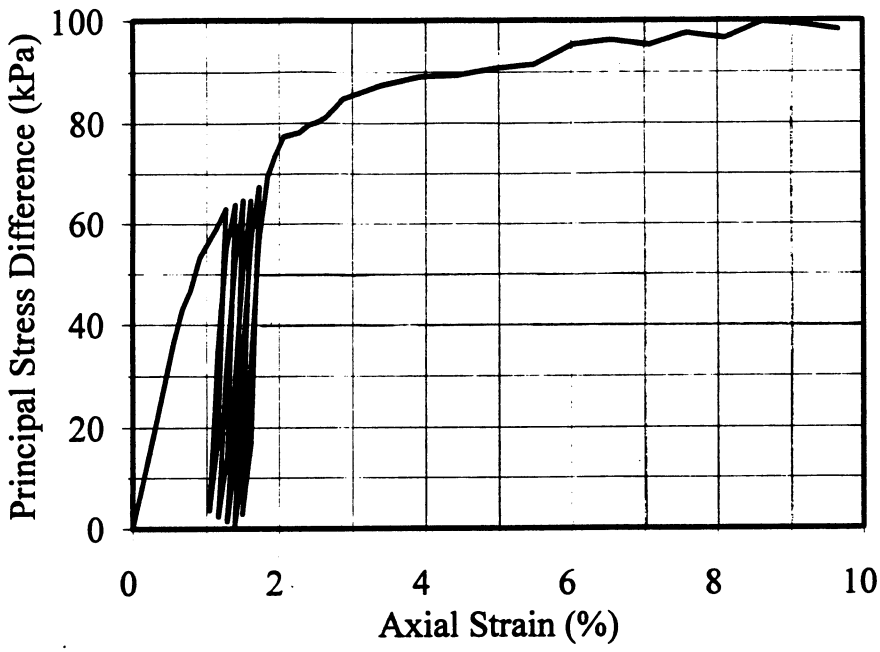

Figure 8d. Triaxial Compression Results: Swan Subgrade, γ_d = 14.6 kN/m^3 (93.0 lb/ft^3), ω = 13.0 %, S = 49.3 %, σ_3 = 18.7 kPa (2.72 psi)

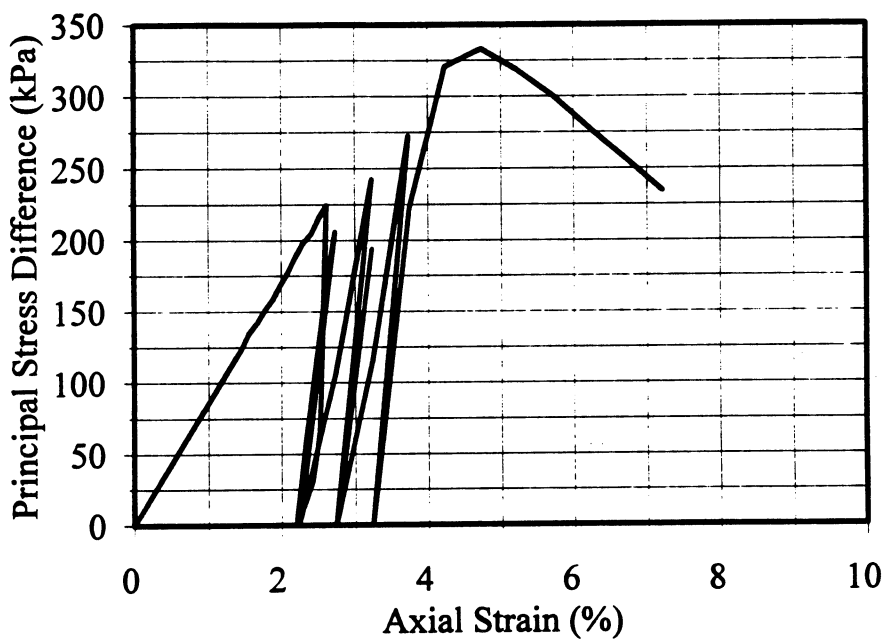

Figure 8e. Triaxial Compression Results: Swan Subgrade, γ_d = 18.0 kN/m^3 (115 lb/ft^3), ω = 13.0 %, S = 94.2 %, σ_3 = 21.3 kPa (3.10 psi)

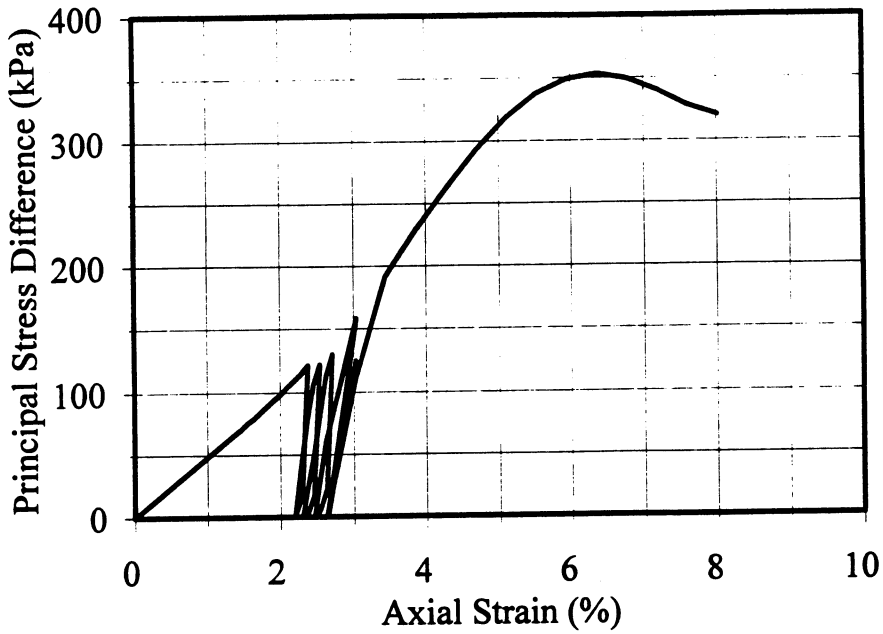

Figure 8f. Triaxial Compression Results: Swan Subgrade, γ_d = 19.0 kN/m^3 (121 lb/ft^3), ω = 13.0 %, S = 100 %, σ_3 = 23.1 kPa (3.36 psi)

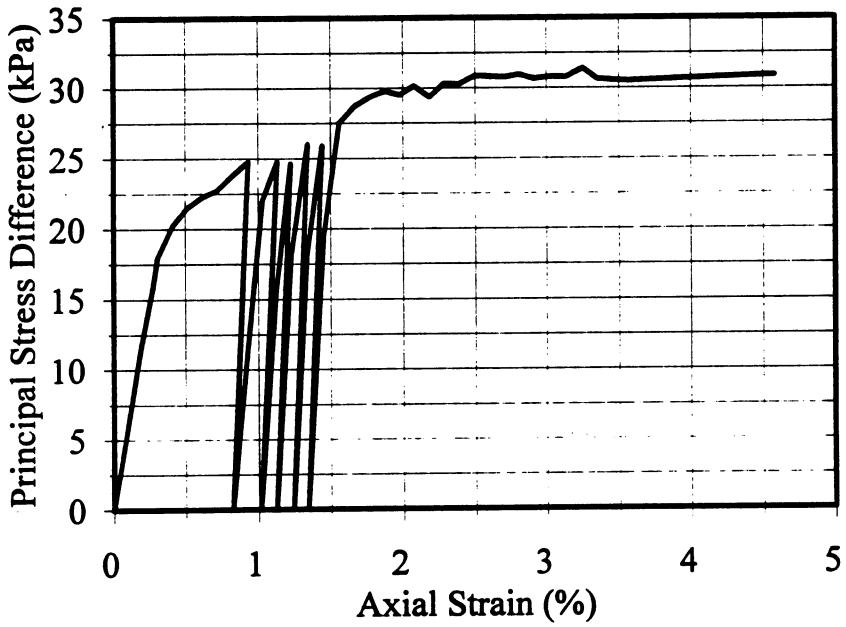

Figure 8g. Triaxial Compression Results: Swan Subgrade, γ_d = 14.8 kN/m^3 (94.0 lb/ft^3), ω = 19.0 %, S = 74.4 %, σ_3 = 18.7 kPa (2.72 psi)

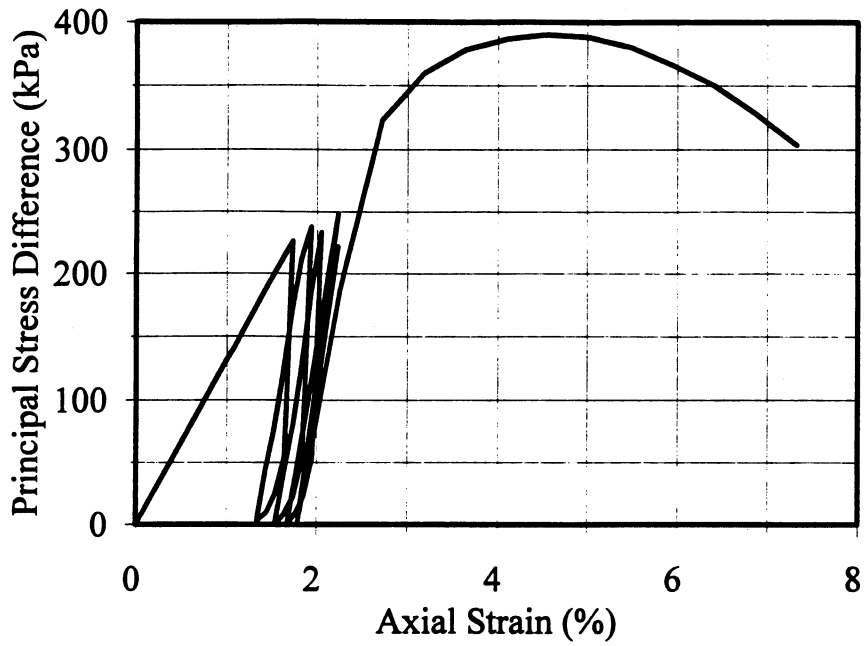

Figure 8h. Triaxial Compression Results: Swan Subgrade, γ_d = 18.0 kN/m^3 (115 lb/ft^3); ω = 19.0 %, S = 100 %, σ_3 = 20.8 kPa (3.03 psi)

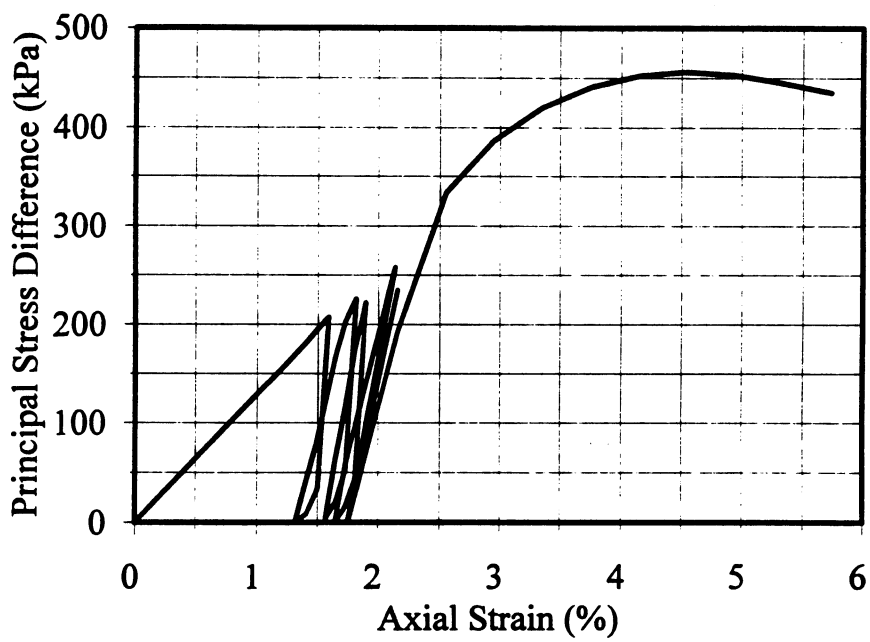

Figure 8i. Triaxial Compression Results: Swan Subgrade, γ_d = 19.0 kN/m^3 (121 lb/ft^3), ω = 19.0 %, S = 100 %, σ_3 = 22.3 kPa (3.24 psi)

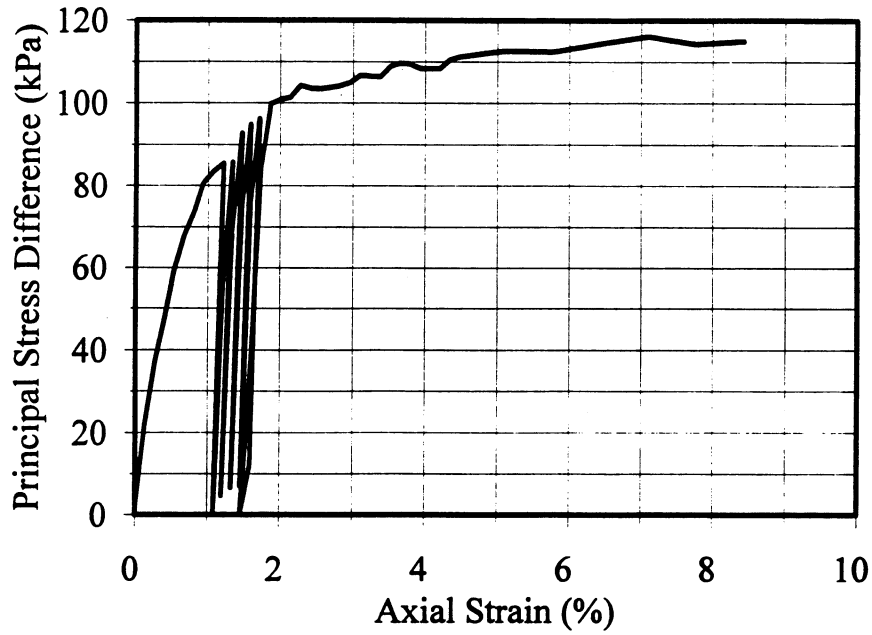

Figure 9a. Triaxial Compression Results: Dickey Lake Subgrade, γ_d = 15.4 kN/m^3 (98.0 lb/ft^3), ω = 7.0 %, S = 27.7 %, σ_3 = 15.2 kPa (2.21 psi)

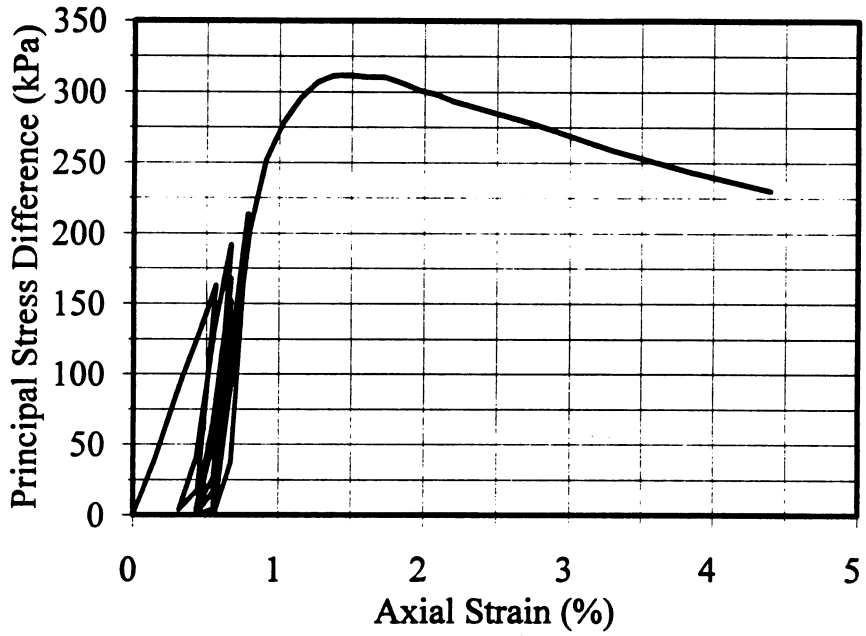

Figure 9b. Triaxial Compression Results: Dickey Lake Subgrade, γ_d = 17.4 kN/m^3 (111 lb/ft^3), ω = 7.0 %, S = 39.1 %, σ_3 = 18.4 kPa (2.68 psi)

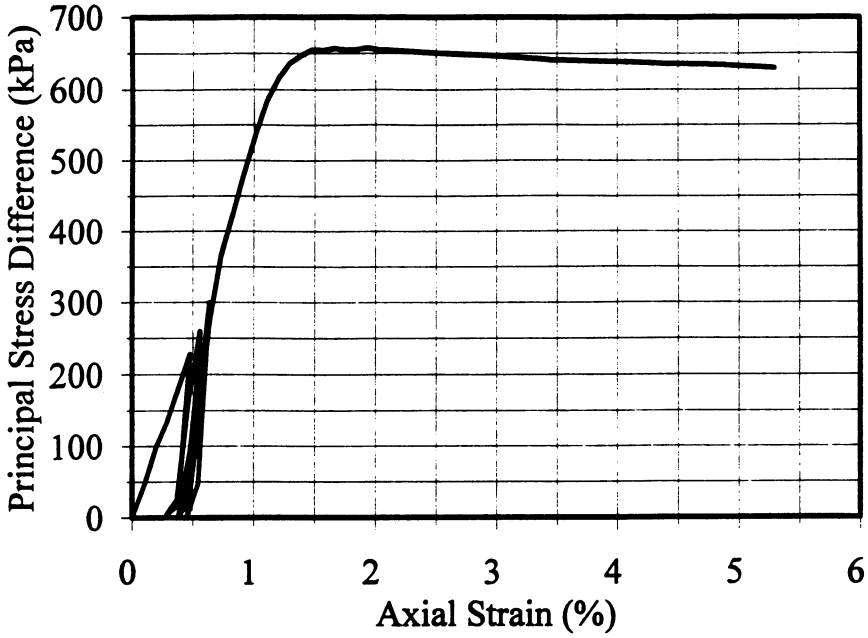

Figure 9c. Triaxial Compression Results: Dickey Lake Subgrade, γ_d = 20.1 kN/m^3 (128 lb/ft^3), ω = 7.0 %, S = 66.9 %, σ_3 = 20.7 kPa (3.01 psi)

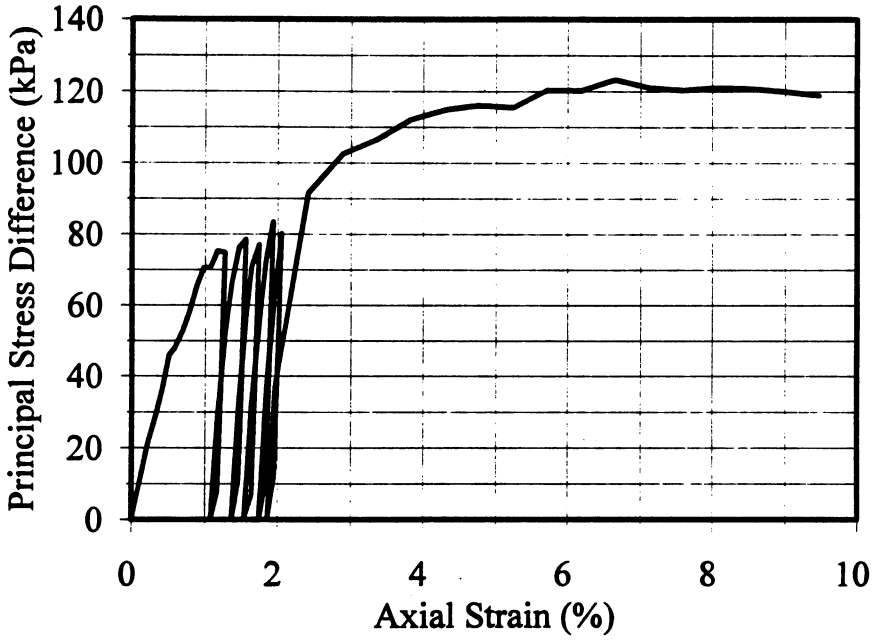

Figure 9d. Triaxial Compression Results: Dickey Lake Subgrade, γ_d = 15.5 kN/m^3 (99.0 lb/ft^3), ω = 12.0 %, S = 48.7 %, σ_3 = 19.1 kPa (2.78 psi)

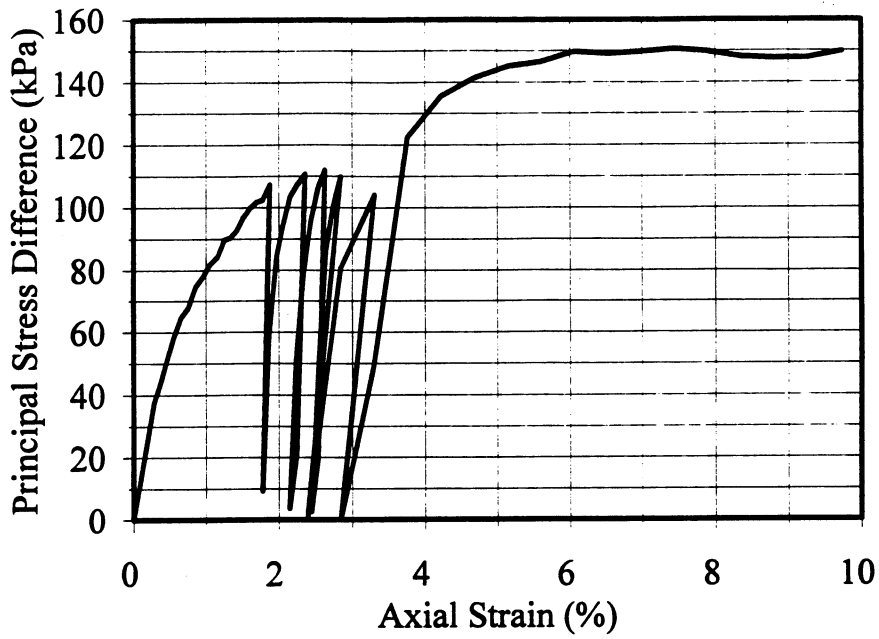

Figure 9e. Triaxial Compression Results: Dickey Lake Subgrade, γ_d = 17.3 kN/m^3 (110 lb/ft^3), ω = 12.0 %, S = 65.2 %, σ_3 = 20.0 kPa (2.91 psi)

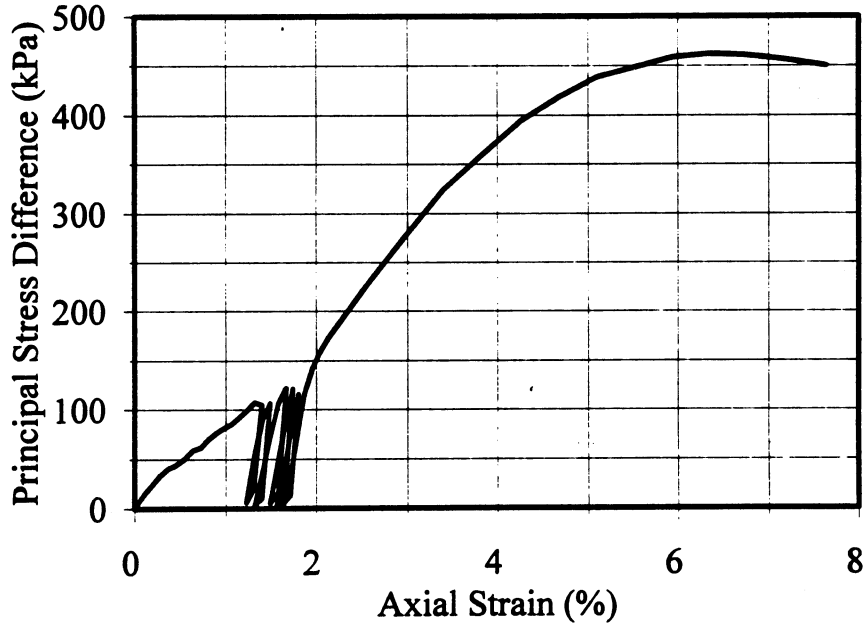

Figure 9f. Triaxial Compression Results: Dickey Lake Subgrade, γ_d = 19.8 kN/m^3 (126 lb/ft^3), ω = 12.0 %, S = 99.0 %, σ_3 = 22.0 kPa (3.20 psi)

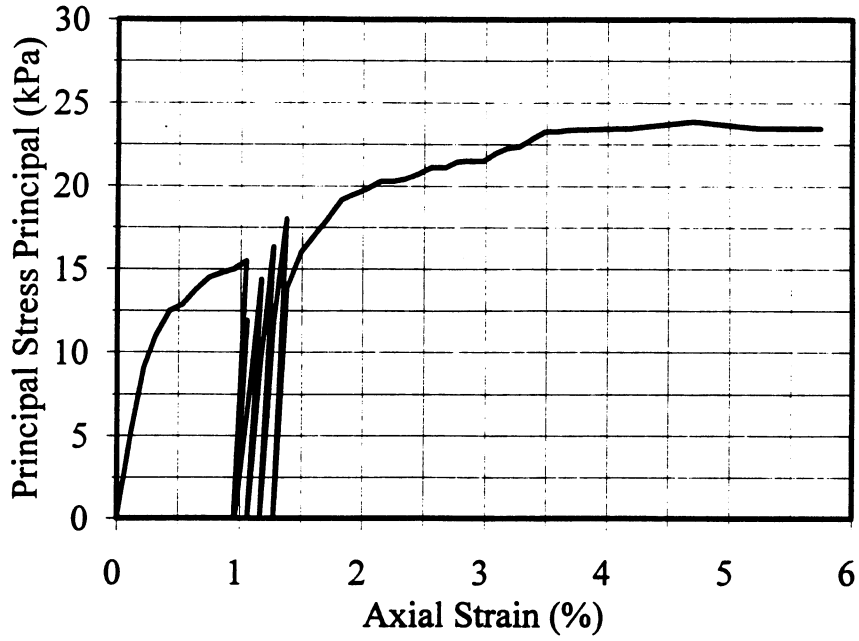

Figure 9g. Triaxial Compression Results: Dickey Lake Subgrade, γ_d = 14.6 kN/m^3 (93.0 lb/ft^3), ω = 17.0 %, S = 59.5 %, σ_3 = 17.1 kPa (2.49 psi)

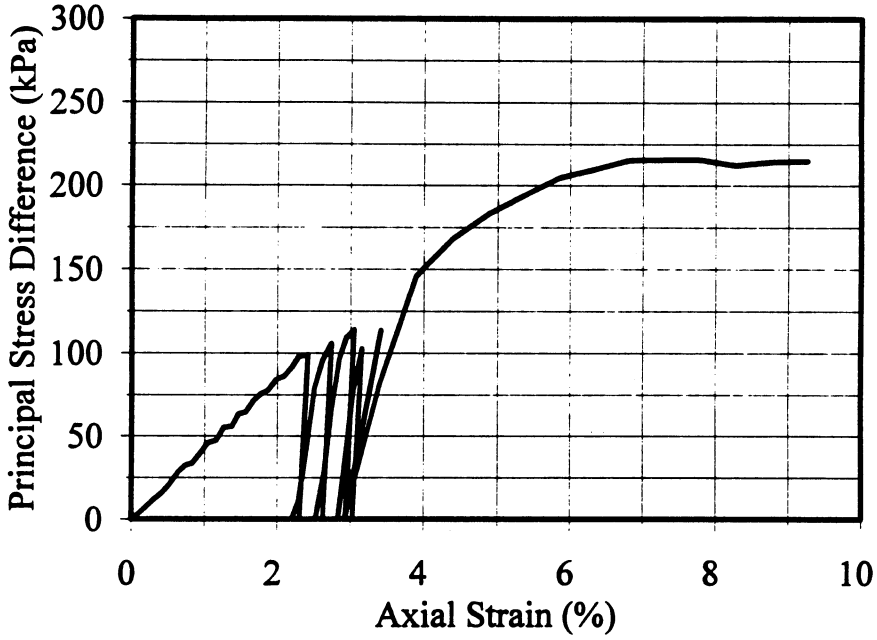

Figure 9h. Triaxial Compression Results: Dickey Lake Subgrade, γ_d = 17.3 kN/m^3 (110 lb/ft^3), ω = 17.0 %, S = 92.4 %, σ_3 = 19.2 kPa (2.79 psi)

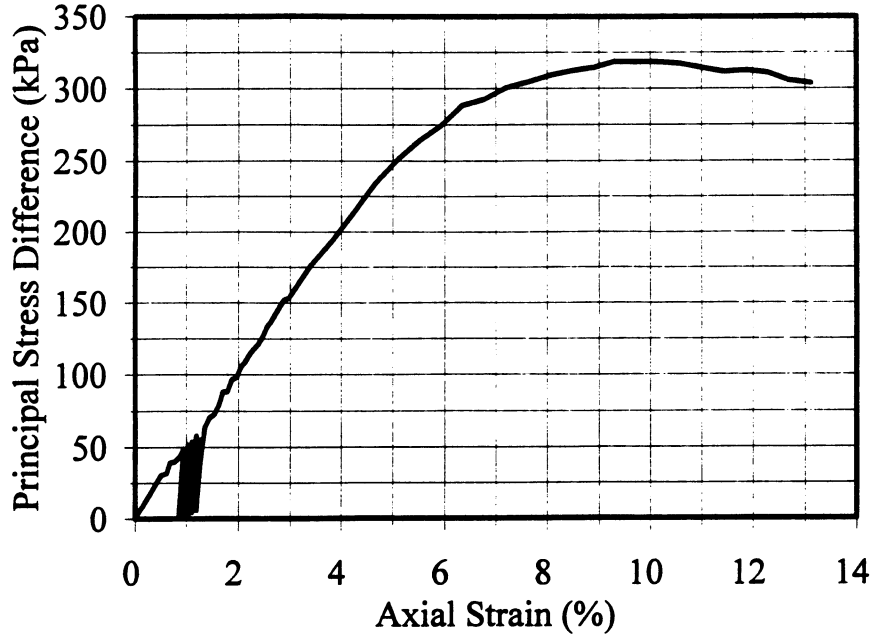

Figure 9i. Triaxial Compression Results: Dickey Lake Subgrade, γ_d = 18.8 kN/m^3 (120 lb/ft^3), ω = 17.0 %, S = 100 %, σ_3 = 21.7 kPa (3.16 psi)

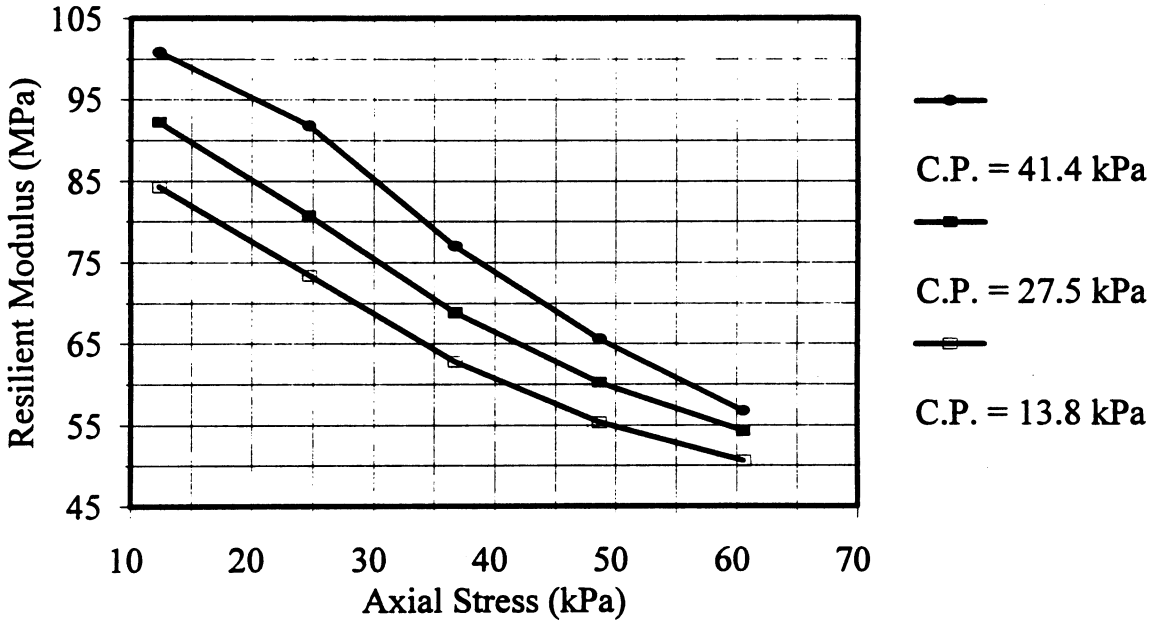

Figure 10. Resilient Modulus Results: Sunburst Subgrade: γ_d = 18.7 kN/m^3 (119 lb/ft^3), ω = 12.0 %, S = 72.0 %

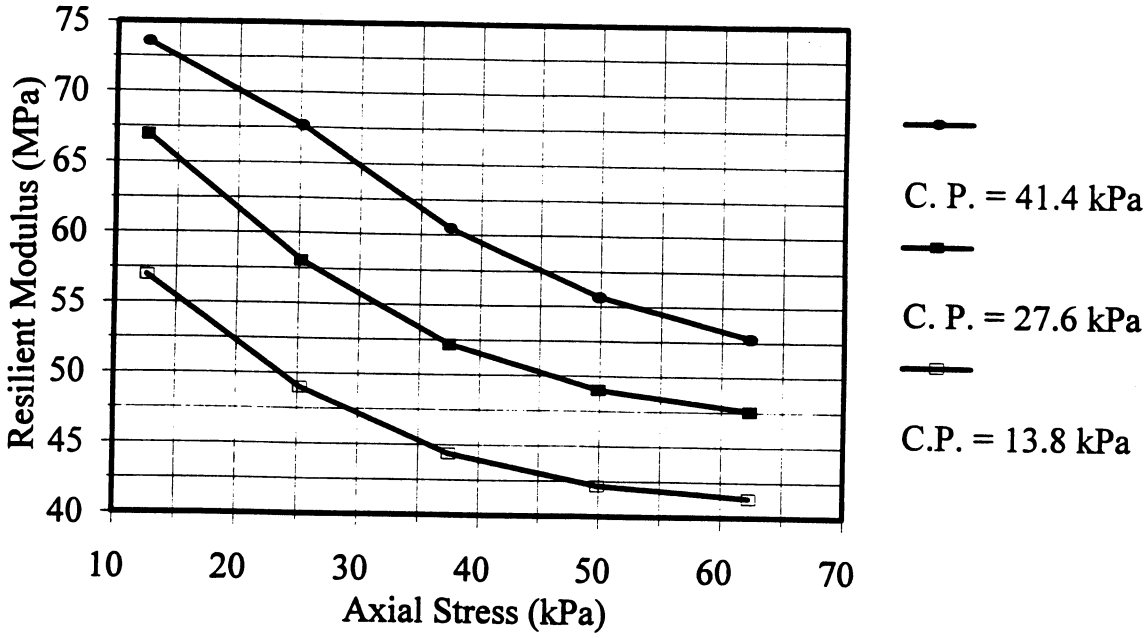

Figure 11. Resilient Modulus Results: Alzada Subgrade: γ_d = 17.5 kN/m^3 (112 lb/ft^3), ω = 18.3 %, S = 93.0 %

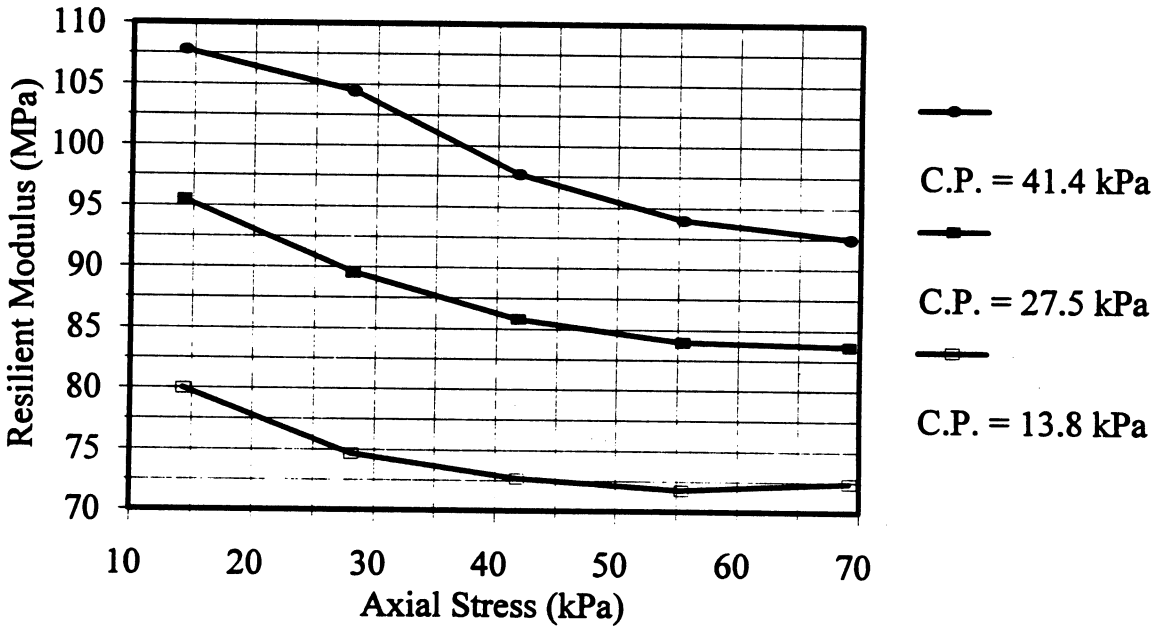

Figure 12a. Resilient Modulus Results: Loma Subgrade: γ_d = 17.1 kN/m^3 (109 lb/ft^3), ω = 7.0 %, S = 33.2 %

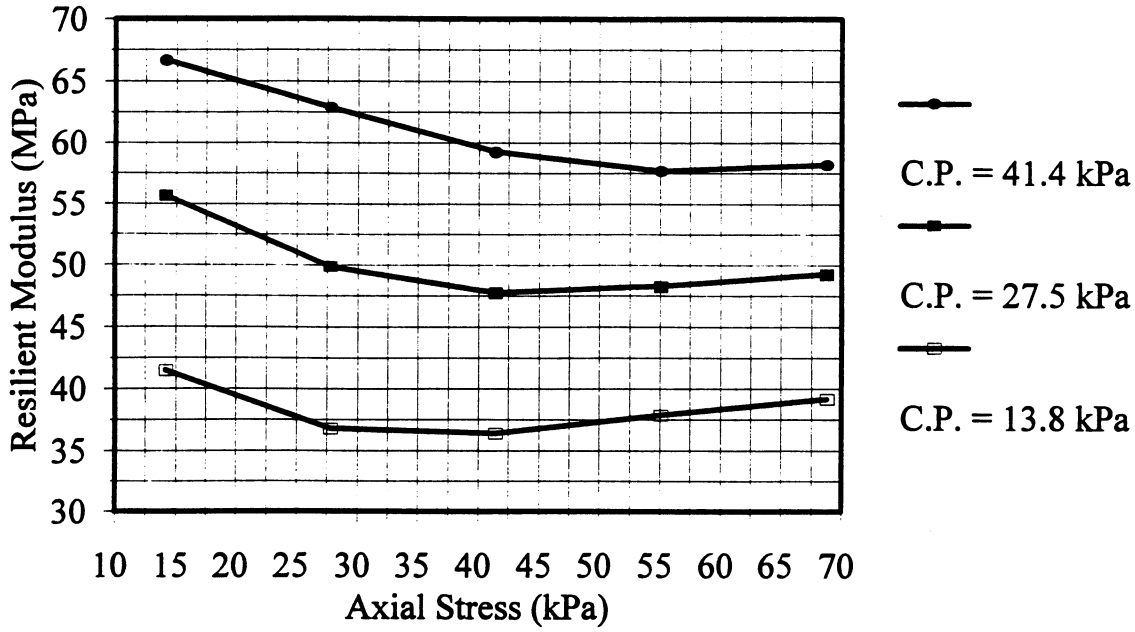

Figure 12b. Resilient Modulus Results: Loma Subgrade: γ_d = 17.1 kN/m^3 (109 lb/ft^3), ω = 12.0 %, S = 56.9 %

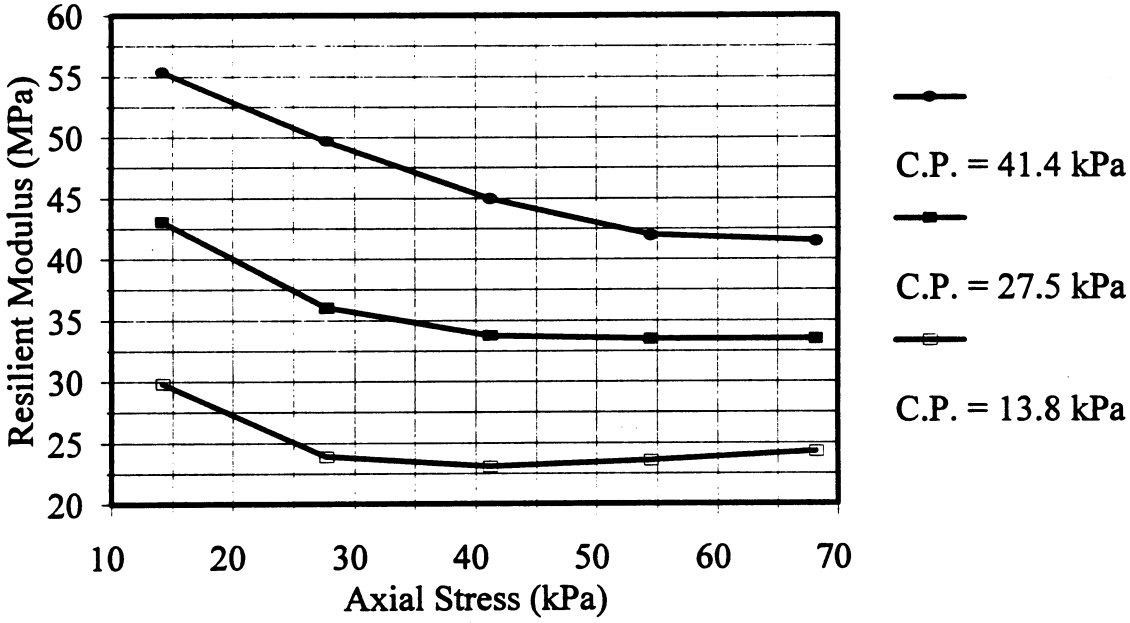

Figure 12c. Resilient Modulus Results: Loma Subgrade: γ_d = 17.1 kN/m^3 (109 lb/ft^3), ω = 20.0 %, S = 92.8 %

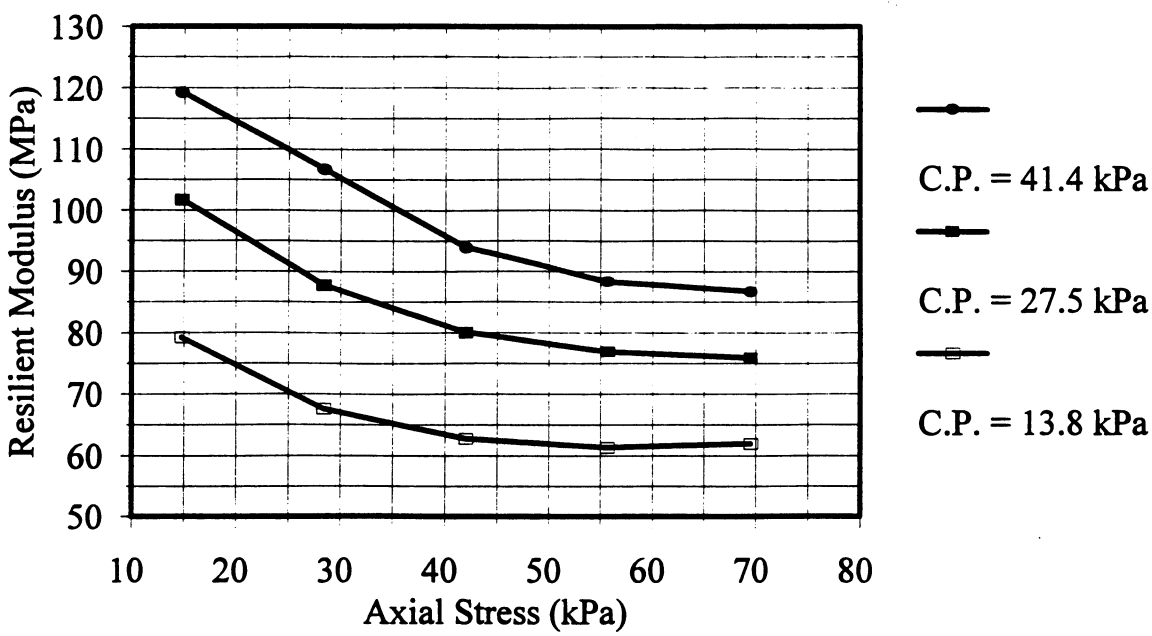

Figure 13a. Resilient Modulus Results: Swan Subgrade: γ_d = 17.1 kN/m^3 (109 lb/ft^3), ω = 8.0 %, S = 46.5 %

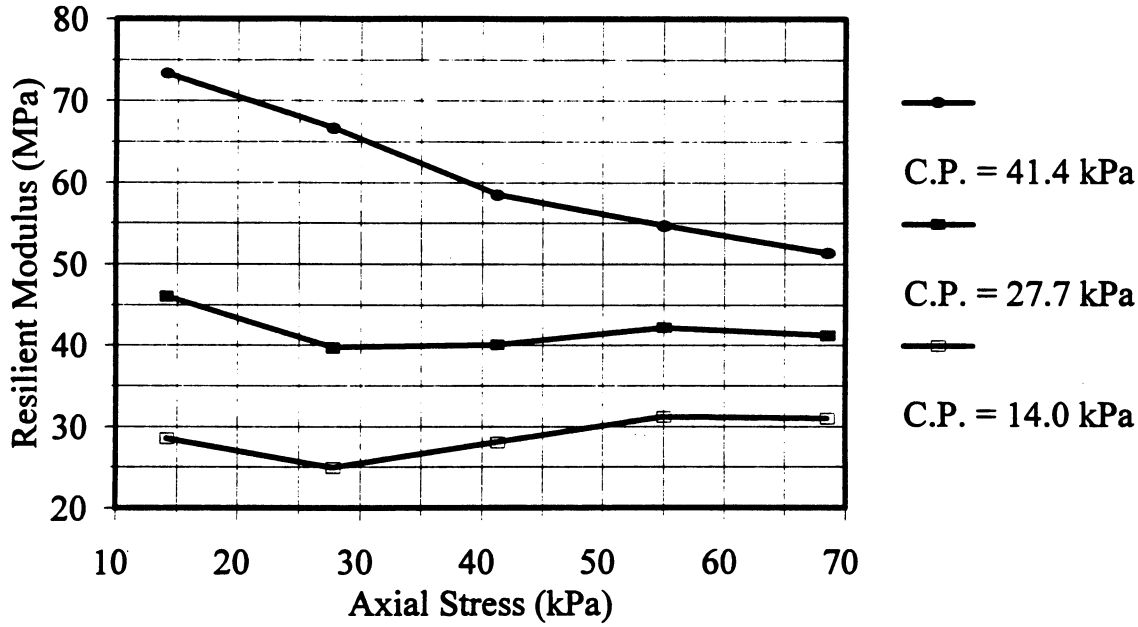

Figure 13b. Resilient Modulus Results: Swan Subgrade: γ_d = 17.1 kN/m^3 (109 lb/ft^3), ω = 13.0 %, S = 75.5 %

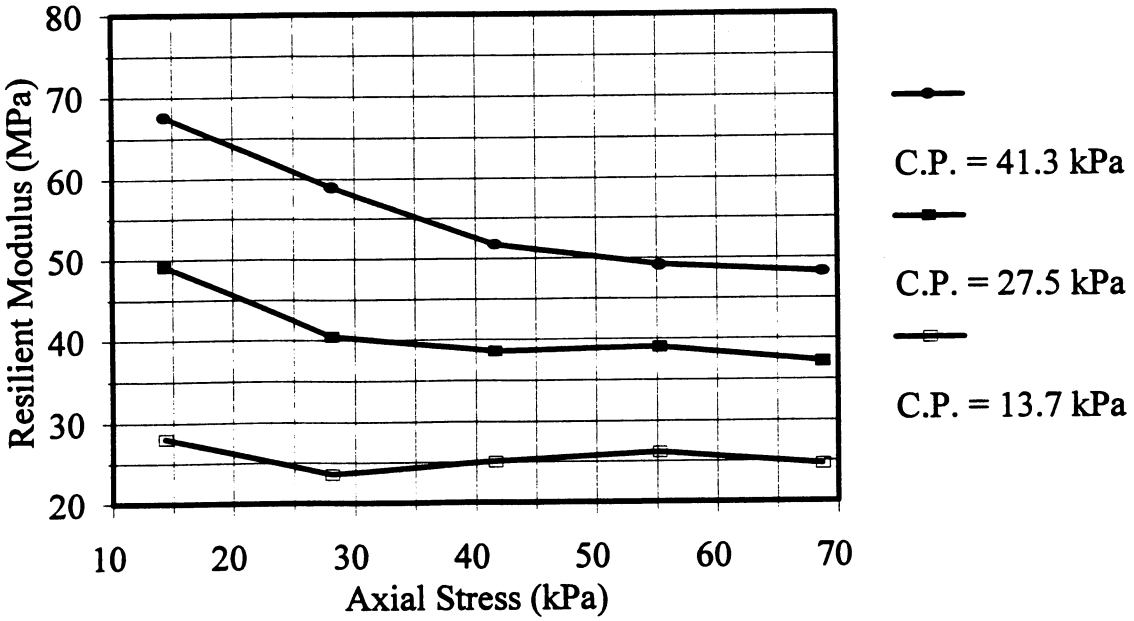

Figure 13c. Resilient Modulus Results: Swan Subgrade: γ_d = 17.3 kN/m^3 (110 lb/ft^3), ω = 20.0 %, S = 100 %

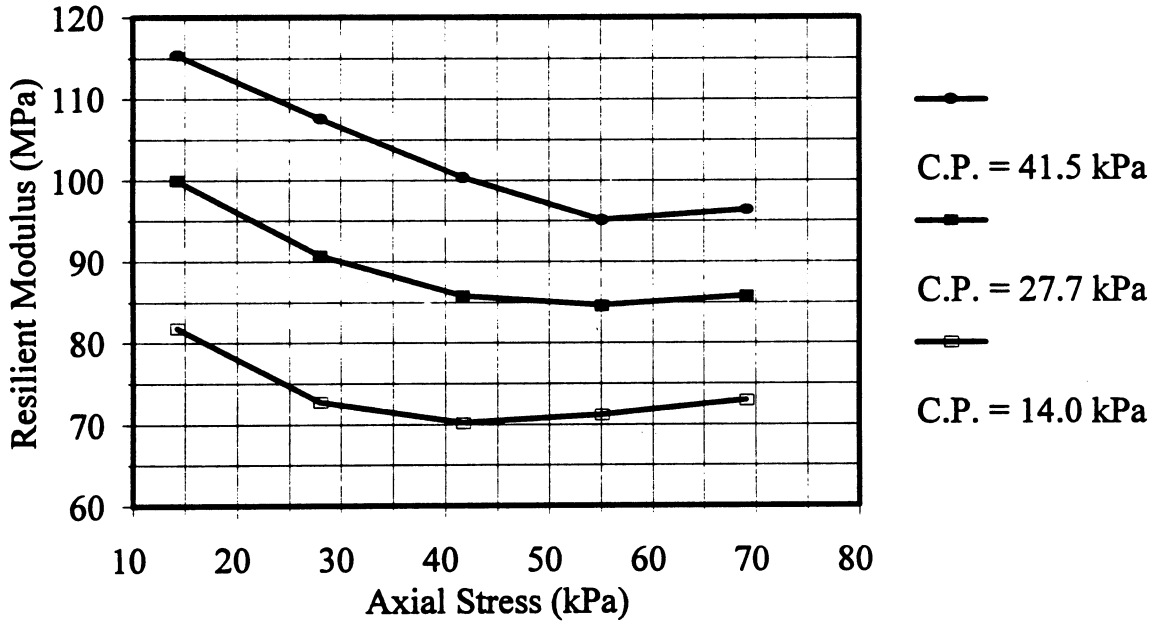

Figure 14a. Resilient Modulus Results: Dickey Lake Subgrade: γ_d = 17.3 kN/m^3 (110 lb/ft^3), ω = 7.0 %, S = 37.0 %

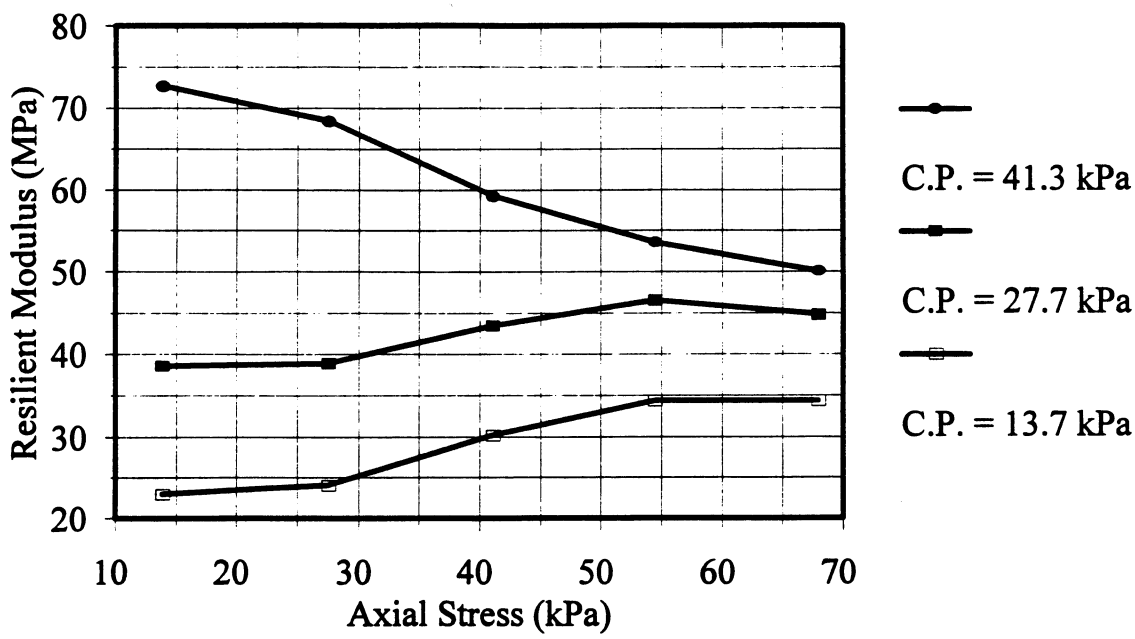

Figure 14b. Resilient Modulus Results: Dickey Lake Subgrade: γ_d = 17.3 kN/m^3 (110 lb/ft^3), ω = 12.0 %, S = 64.0 %

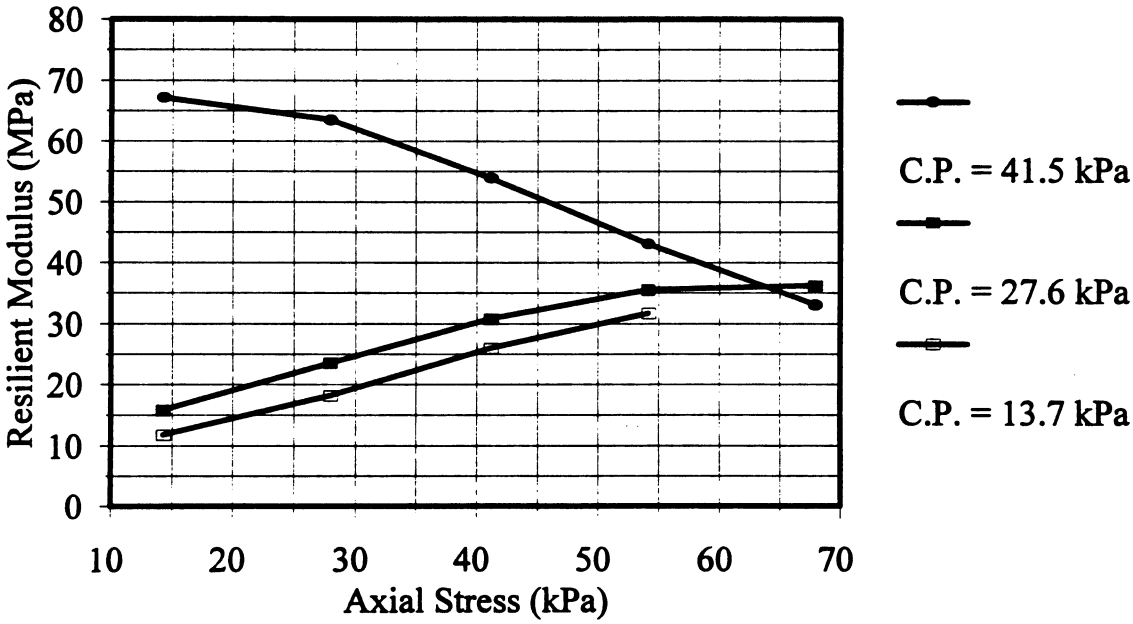

Figure 14c. Resilient Modulus Results: Dickey Lake Subgrade: γ_d = 17.3 kN/m^3 (110 lb/ft^3), ω = 13.0 %, S = 70.0 %

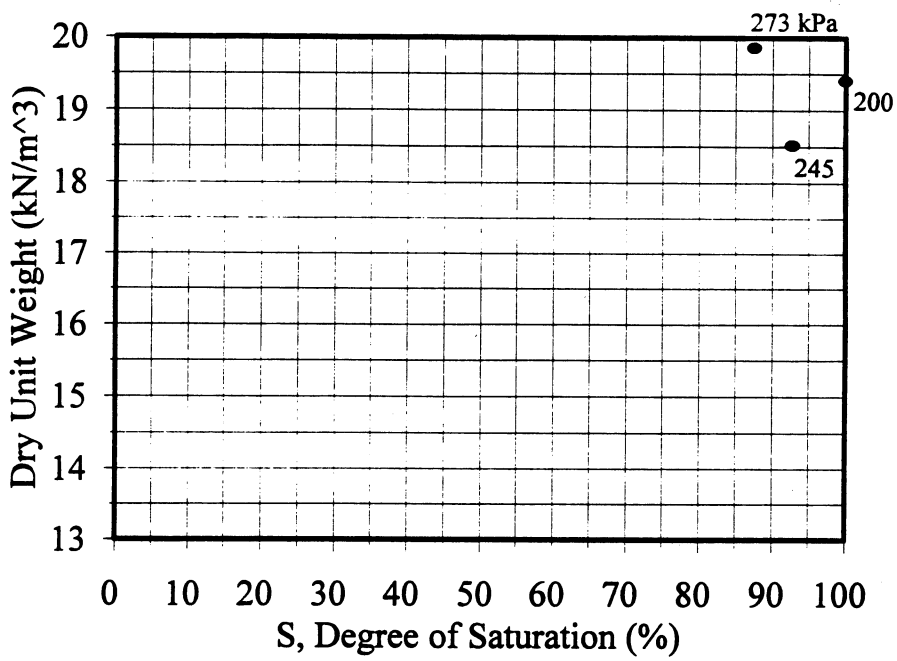

Figure 15a. Triaxial Ultimate Strength Versus Dry Density and Degree of Saturation: Sunburst Subgrade

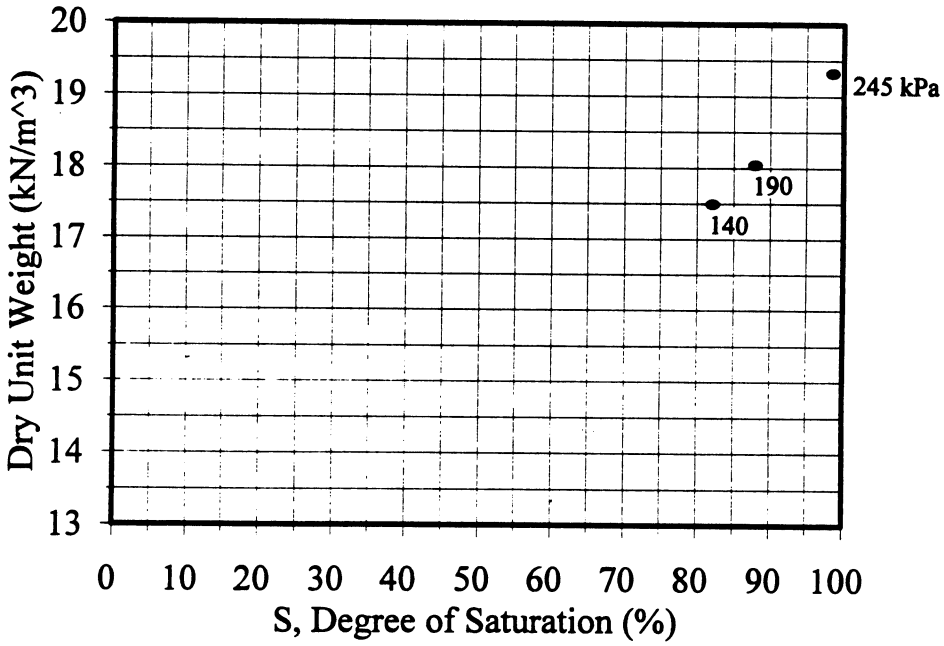

Figure 15b. Triaxial Ultimate Strength Versus Dry Density and Degree of Saturation: Alzada Subgrade

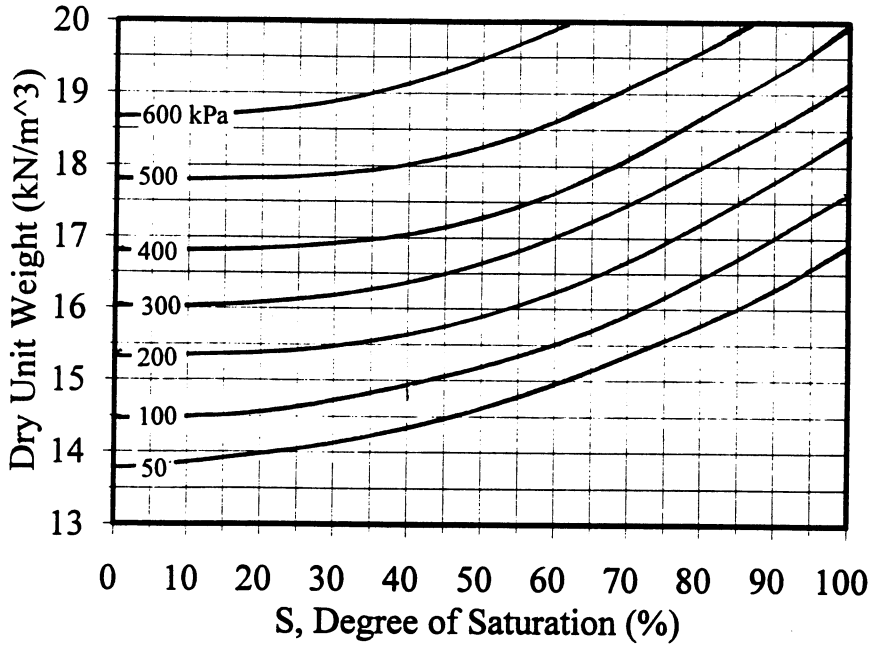

Figure 15c. Triaxial Ultimate Strength Versus Dry Density and Degree of Saturation: Loma Subgrade

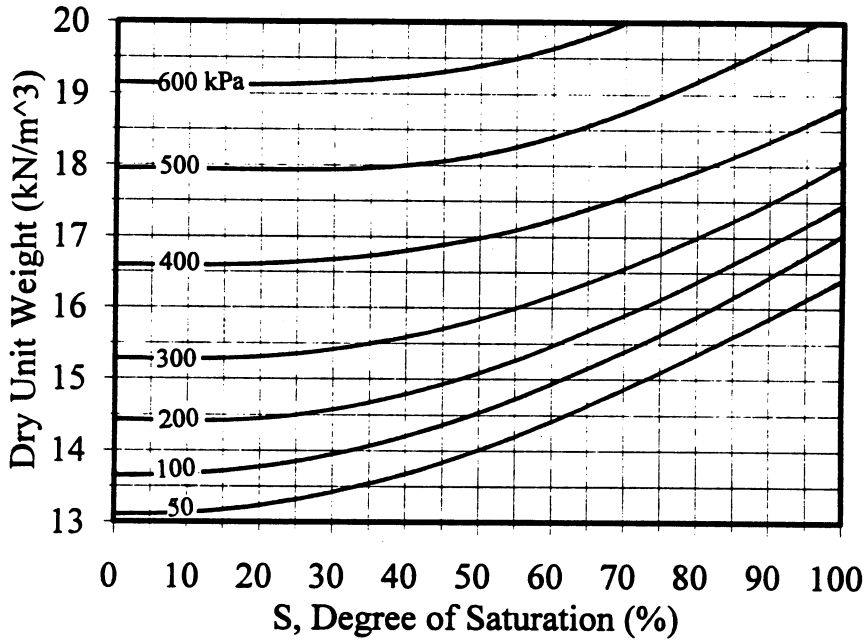

Figure 15d. Triaxial Ultimate Strength Versus Dry Density and Degree of Saturation: Swan Subgrade

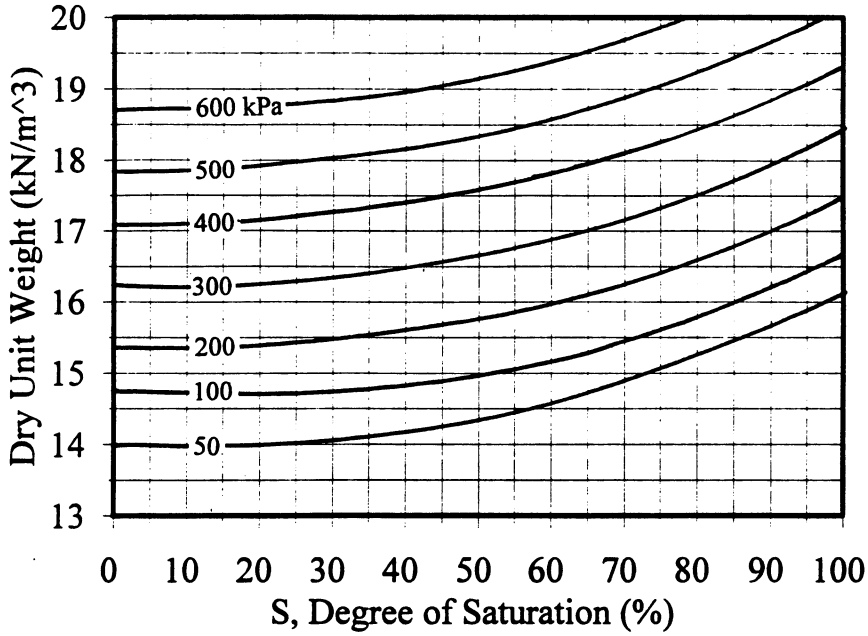

Figure 15e. Triaxial Ultimate Strength Versus Dry Density and Degree of Saturation: Dickey Lake Subgrade

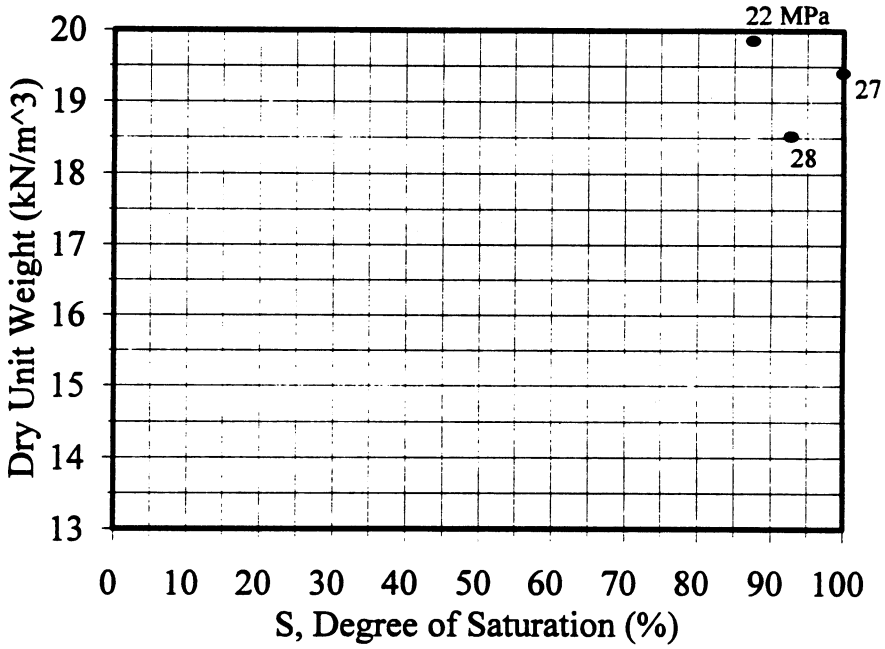

Figure 16a. Elastic Modulus Versus Dry Density and Degree of Saturation: Sunburst Subgrade

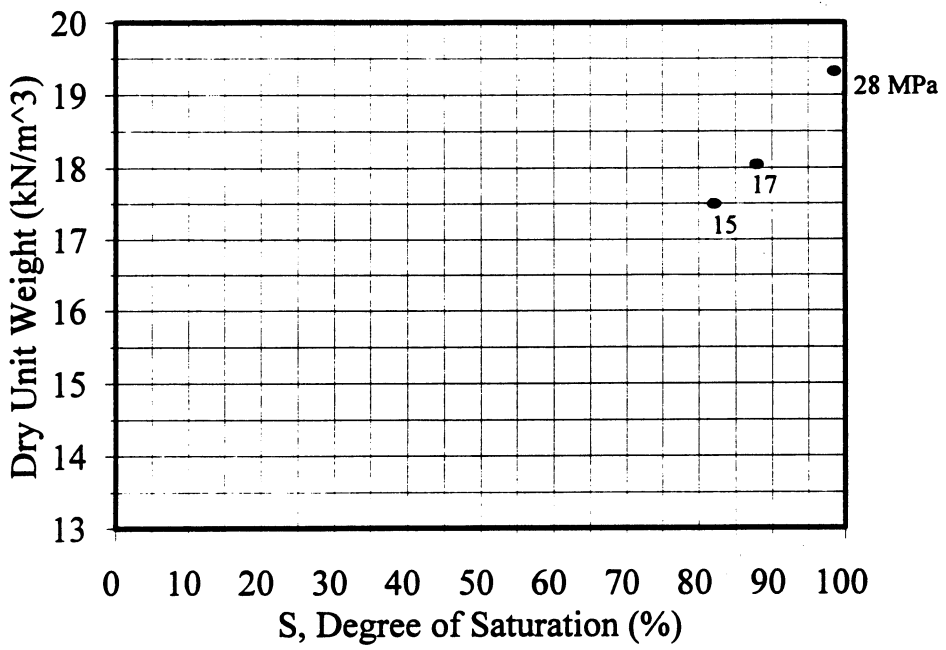

Figure 16b. Elastic Modulus Versus Dry Density and Degree of Saturation: Alzada Subgrade

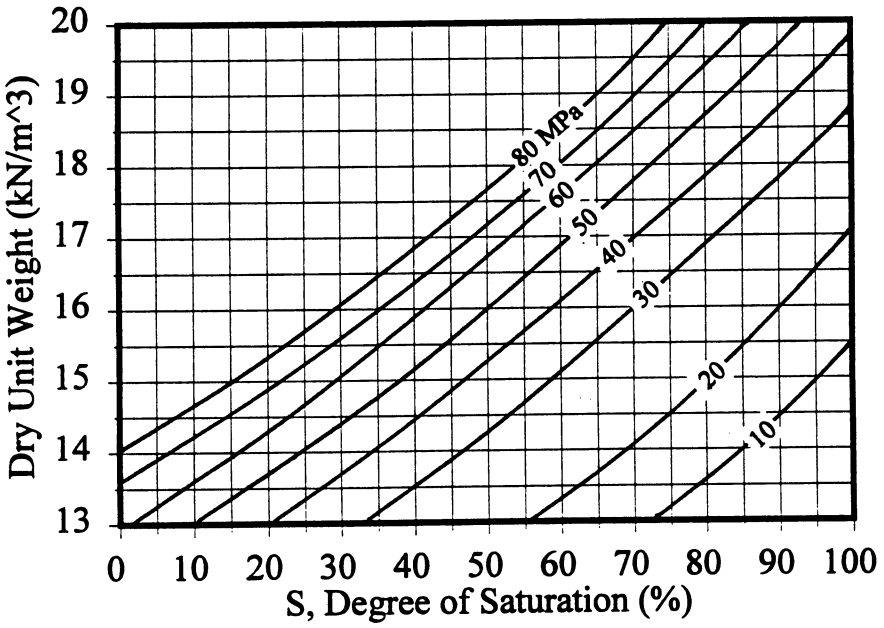

Figure 16c. Elastic Modulus Versus Dry Density and Degree of Saturation: Loma Subgrade

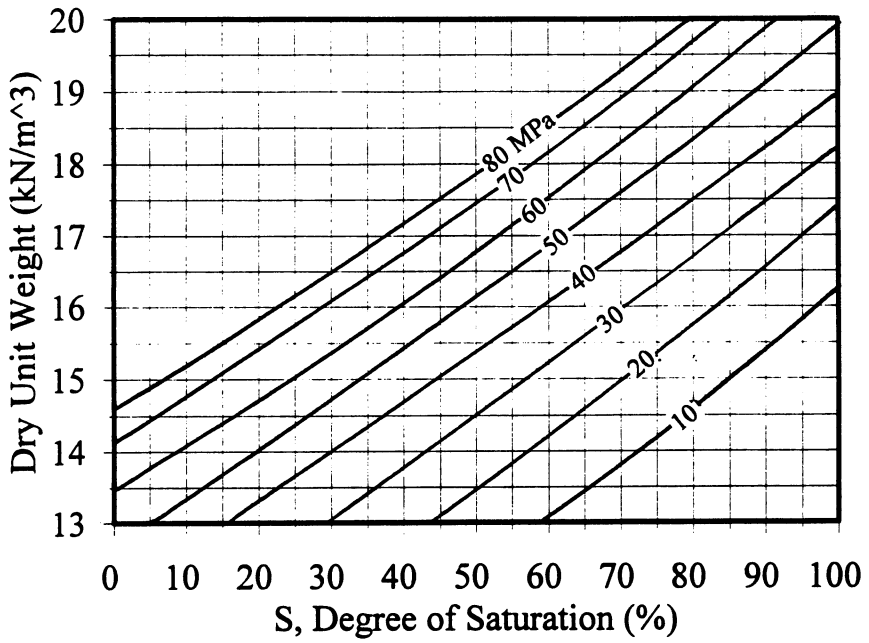

Figure 16d. Elastic Modulus Versus Dry Density and Degree of Saturation: Swan Subgrade

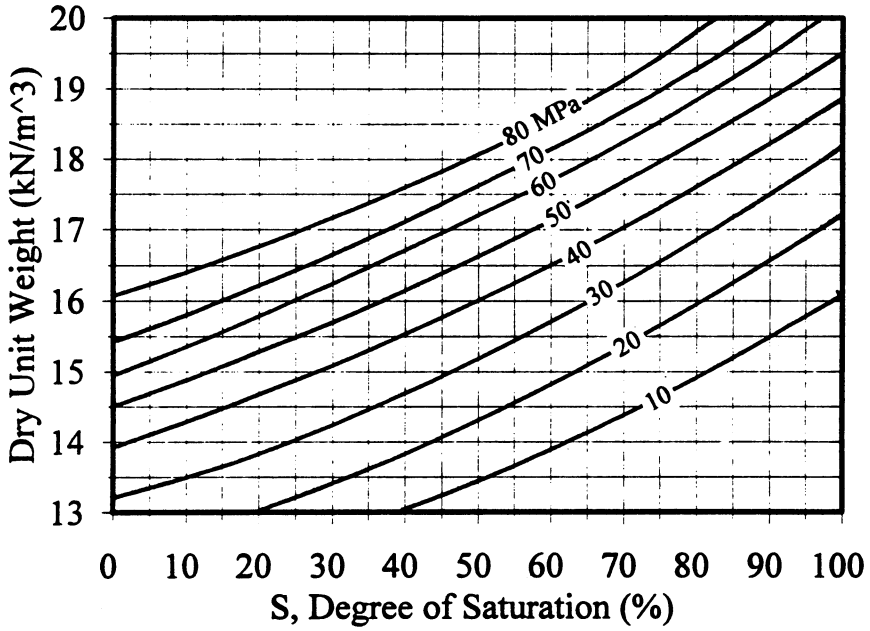

Figure 16e. Elastic Modulus Versus Dry Density and Degree of Saturation: Dickey Lake Subgrade

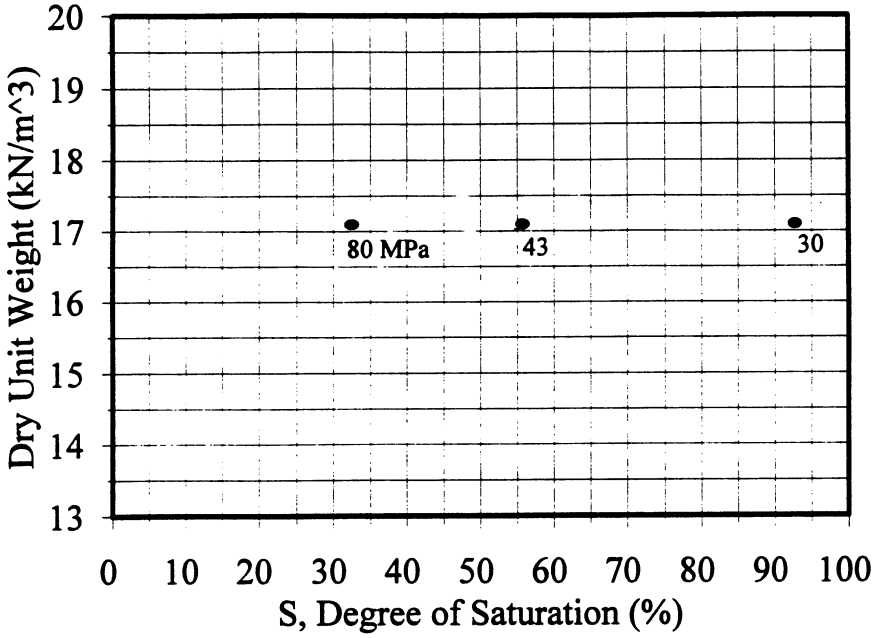

Figure 17a. Resilient Modulus Versus Dry Density and Degree of Saturation: Loma Subgrade

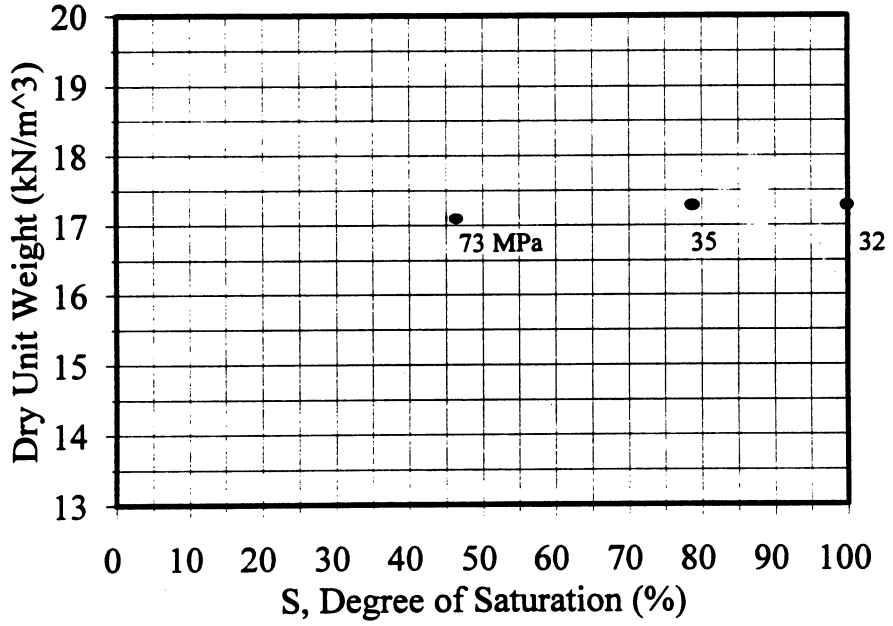

Figure 17b. Resilient Modulus Versus Dry Density and Degree of Saturation: Swan Subgrade

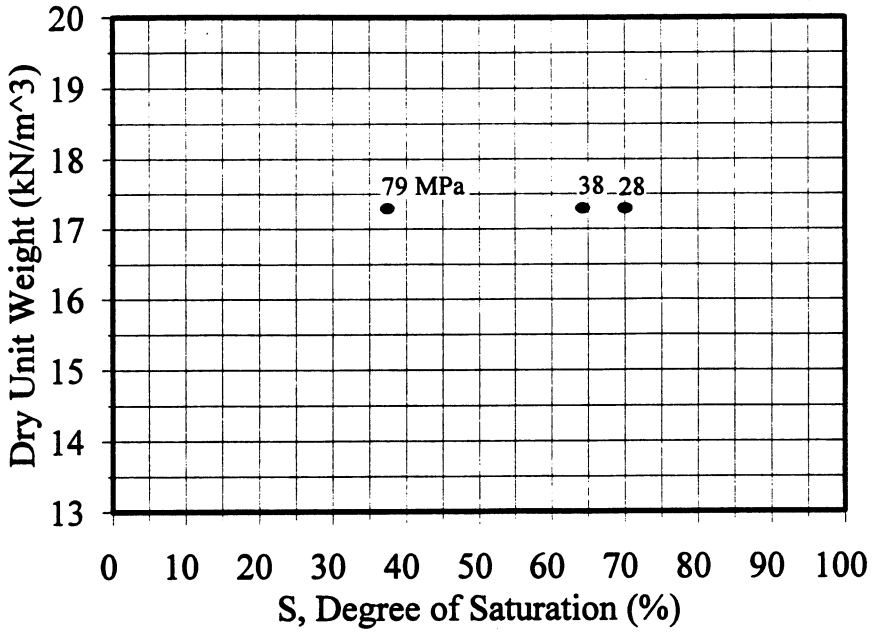

Figure 17c. Resilient Modulus Versus Dry Density and Degree of Saturation: Dickey Lake Subgrade

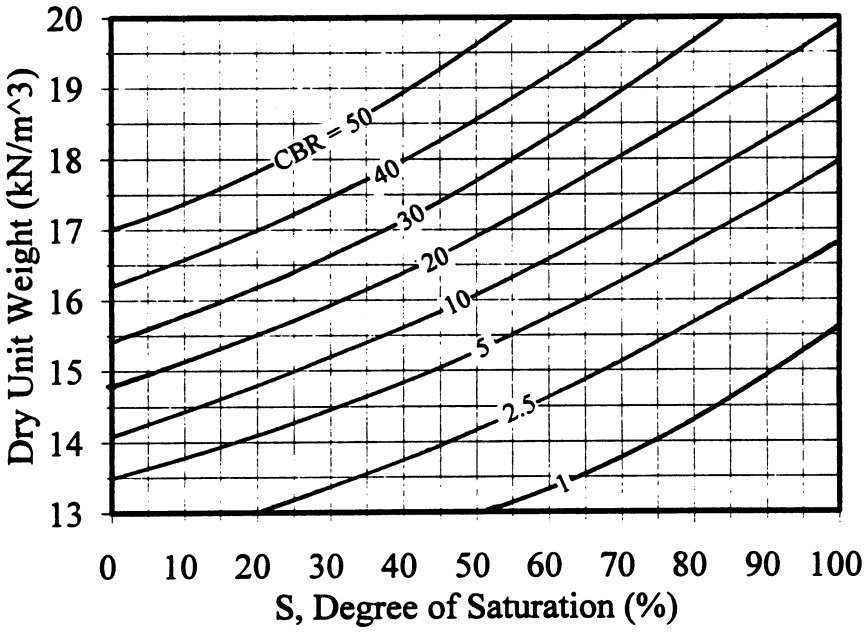

Figure 18a. CBR Versus Dry Density and Degree of Saturation: Sunburst Subgrade

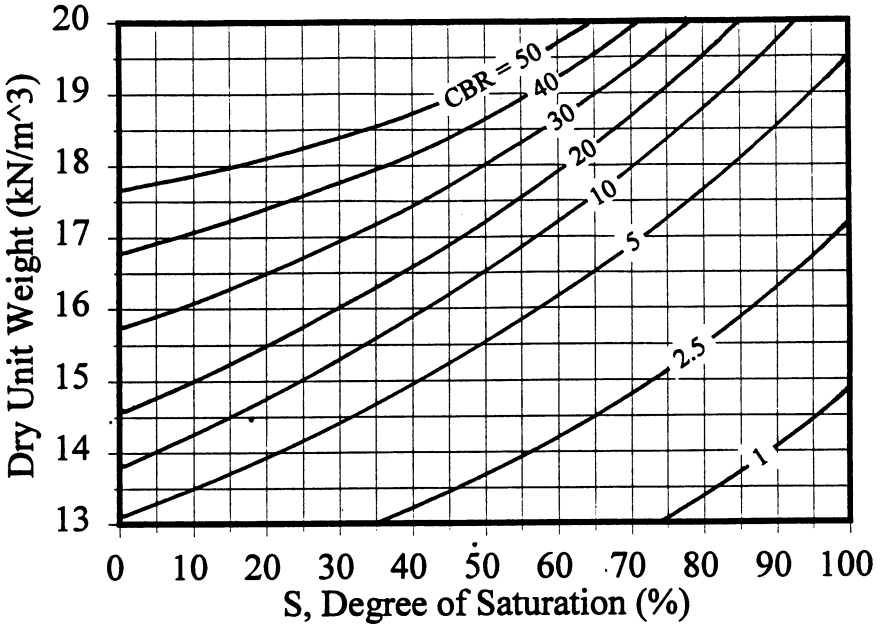

Figure 18b. CBR Versus Dry Density and Degree of Saturation: Alzada Subgrade

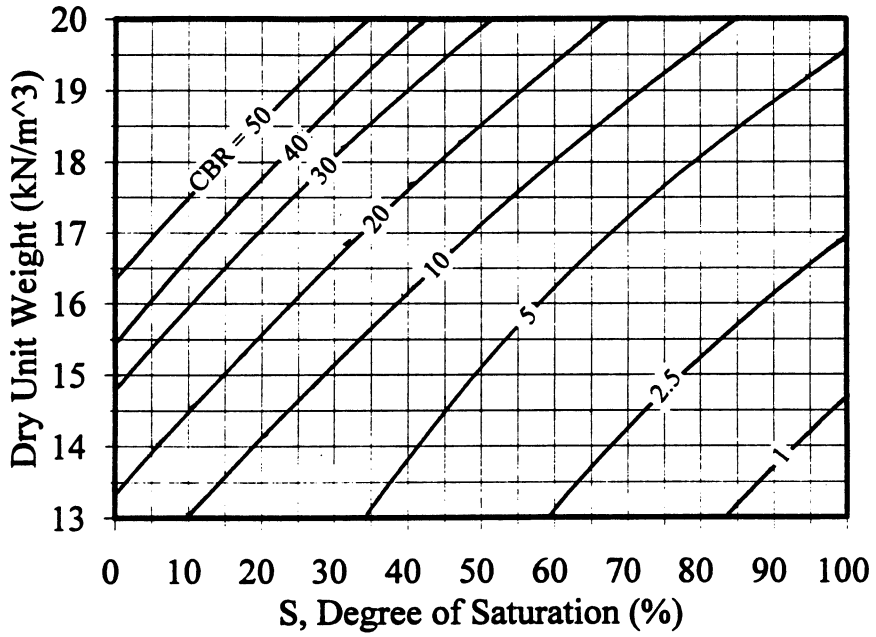

Figure 18c. CBR Versus Dry Density and Degree of Saturation: Loma Subgrade

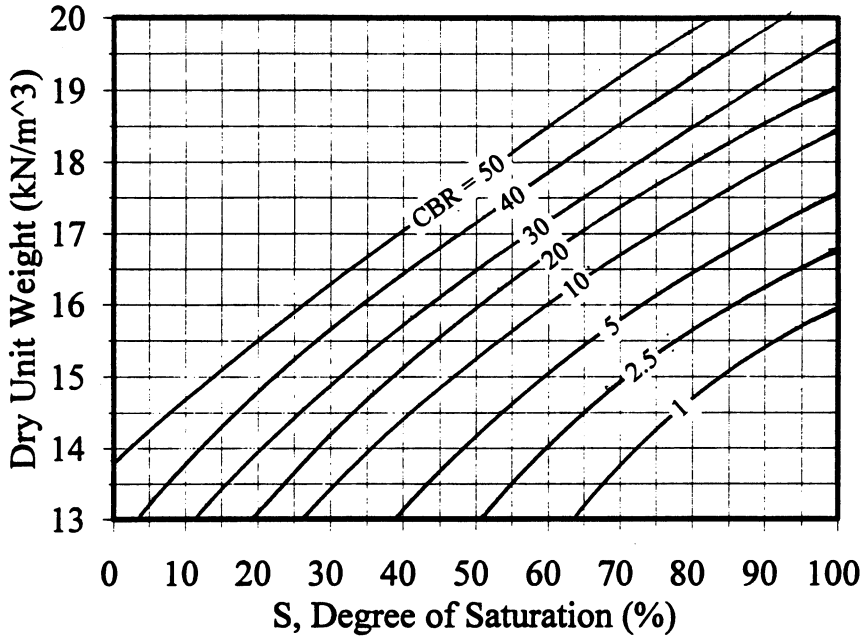

Figure 18d. CBR Versus Dry Density and Degree of Saturation: Swan Subgrade

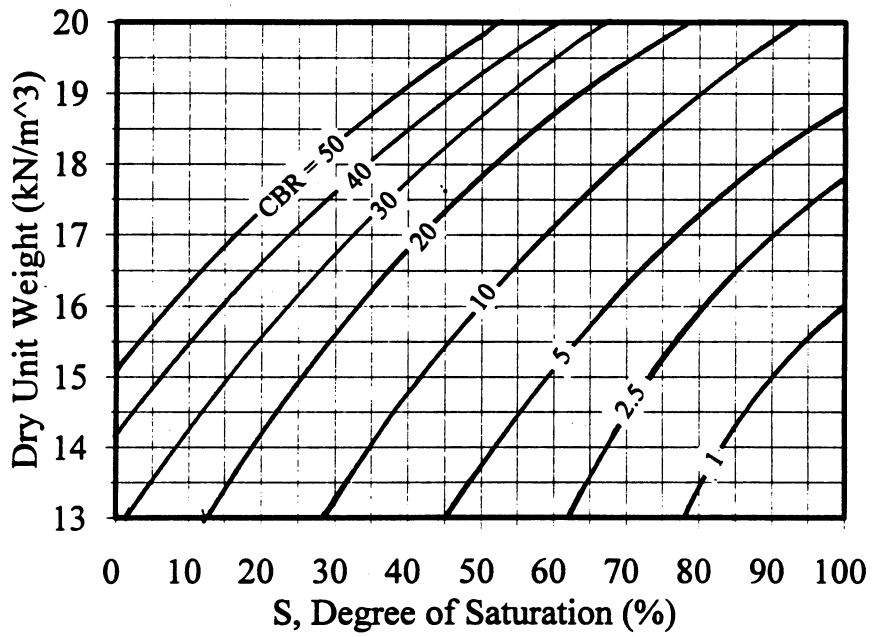

Figure 18e. CBR Versus Dry Density and Degree of Saturation: Dickey Lake Subgrade

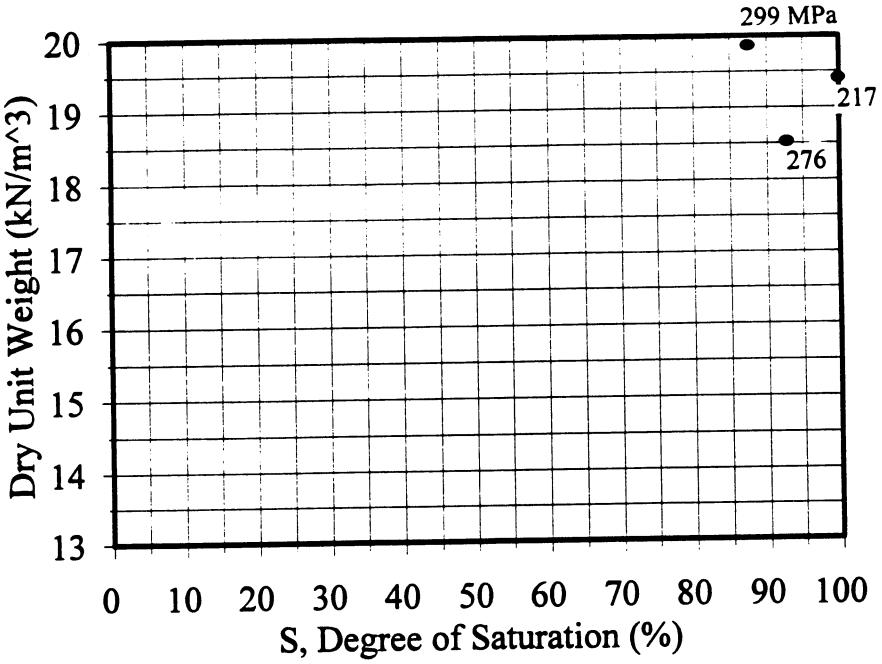

Figure 19a. Resilient Modulus Correlated From Triaxial Ultimate Strength Via Texas Triaxial Class: Sunburst Subgrade

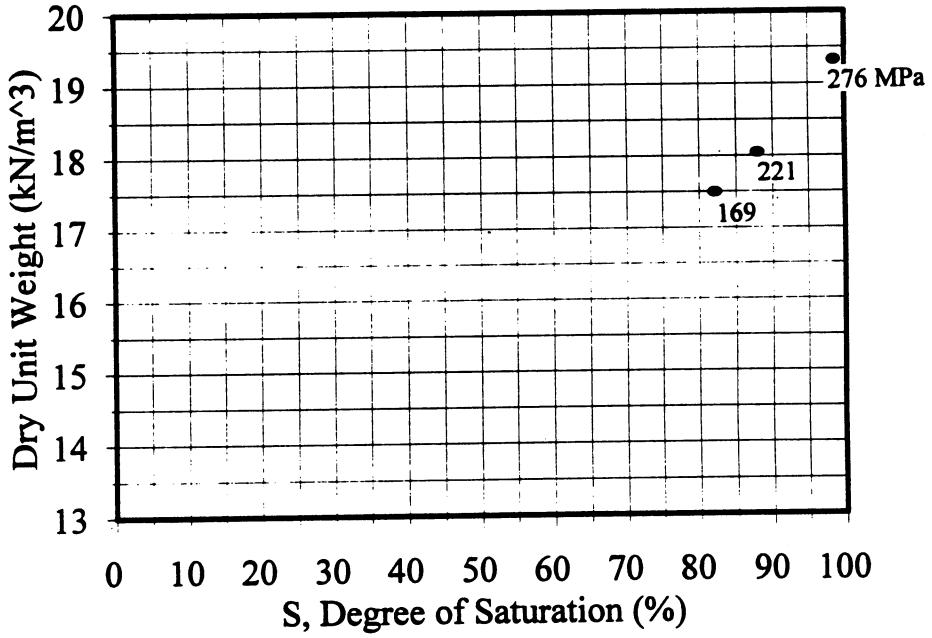

Figure 19b. Resilient Modulus Correlated From Triaxial Ultimate Strength Via Texas Triaxial Class: Alzada Subgrade

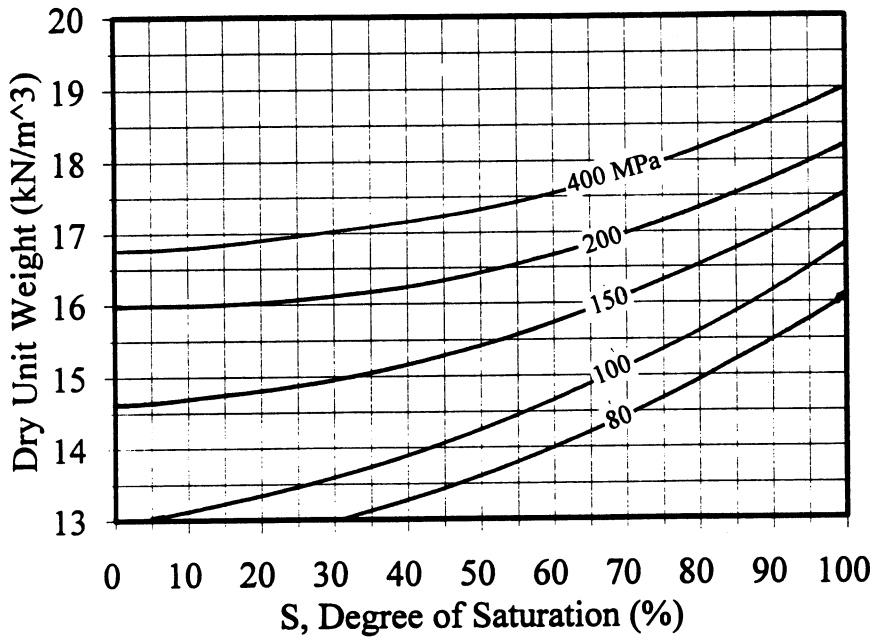

Figure 19c. Resilient Modulus Correlated From Triaxial Ultimate Strength Via Texas Triaxial Class: Loma Subgrade

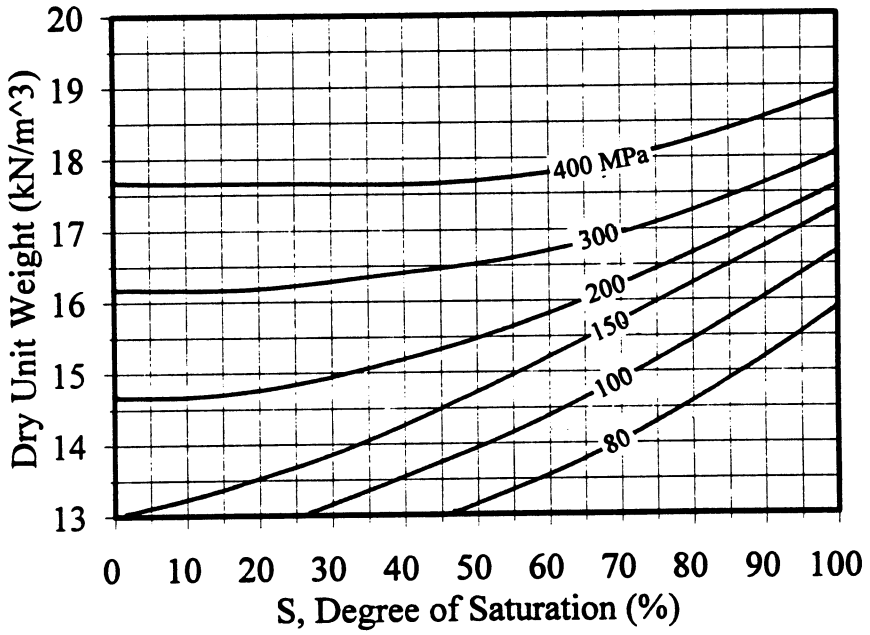

Figure 19d. Resilient Modulus Correlated From Triaxial Ultimate Strength Via Texas Triaxial Class: Swan Subgrade

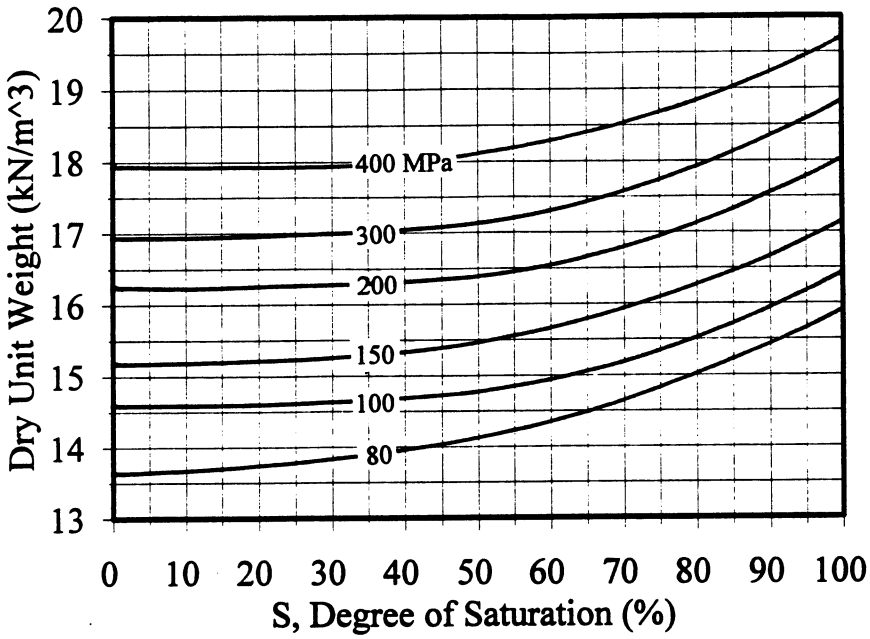

Figure 19e. Resilient Modulus Correlated From Triaxial Ultimate Strength Via Texas Triaxial Class: Dickey Lake Subgrade

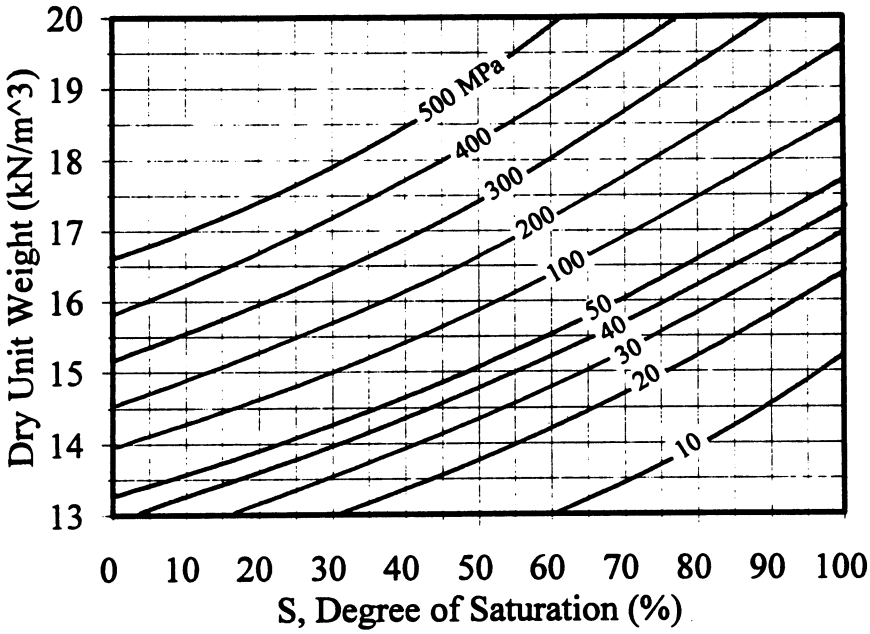

Figure 20a. Resilient Modulus Correlated From CBR (Heukelom and Klomp, 1962): Sunburst Subgrade

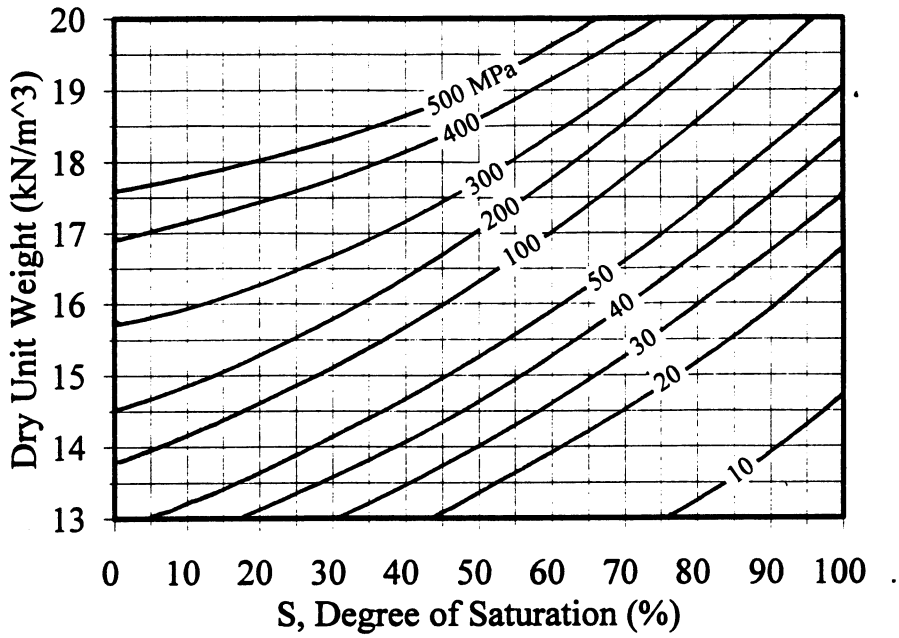

Figure 20b. Resilient Modulus Correlated From CBR (Heukelom and Klomp, 1962): Alzada Subgrade

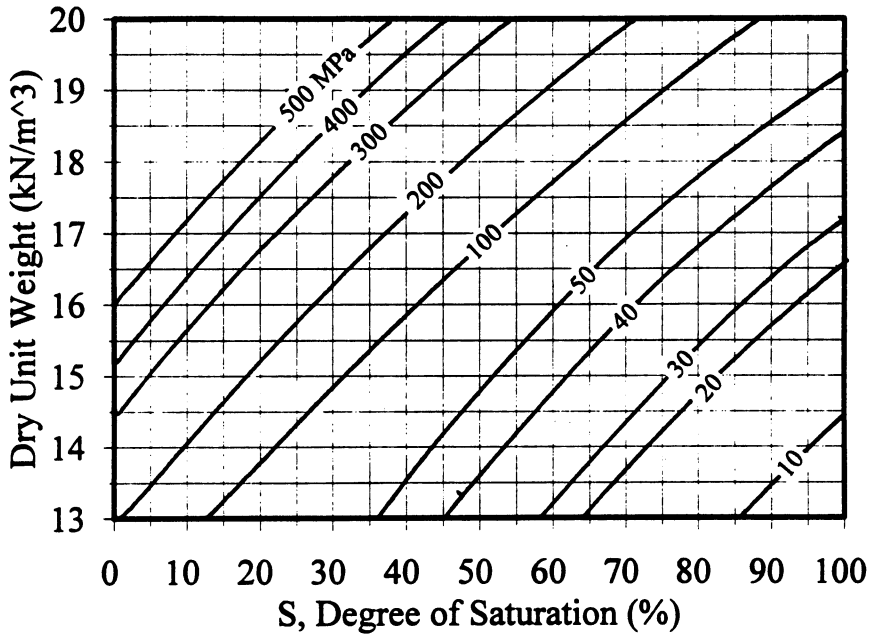

Figure 20c. Resilient Modulus Correlated From CBR (Heukelom and Klomp, 1962): Loma Subgrade

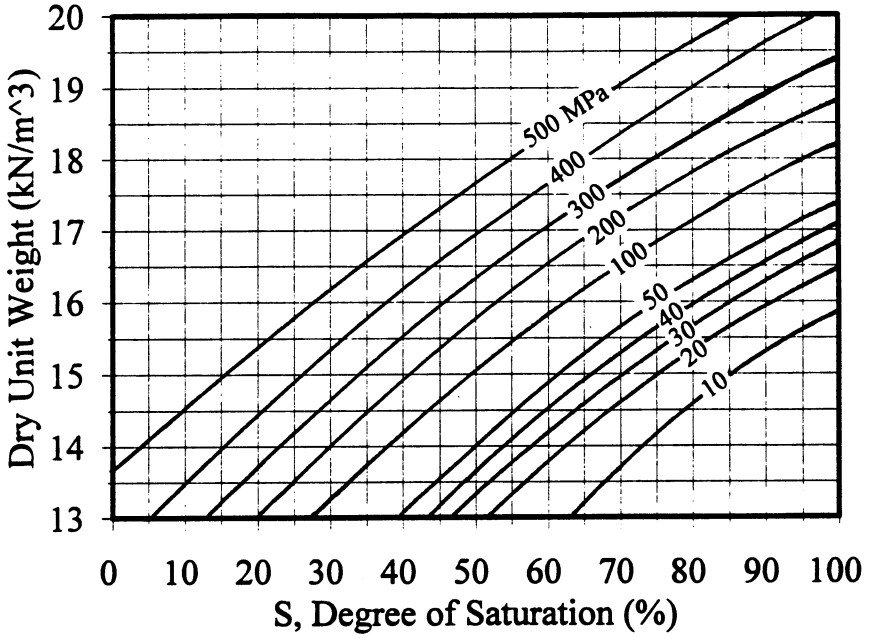

Figure 20d. Resilient Modulus Correlated From CBR (Heukelom and Klomp, 1962): Swan Subgrade

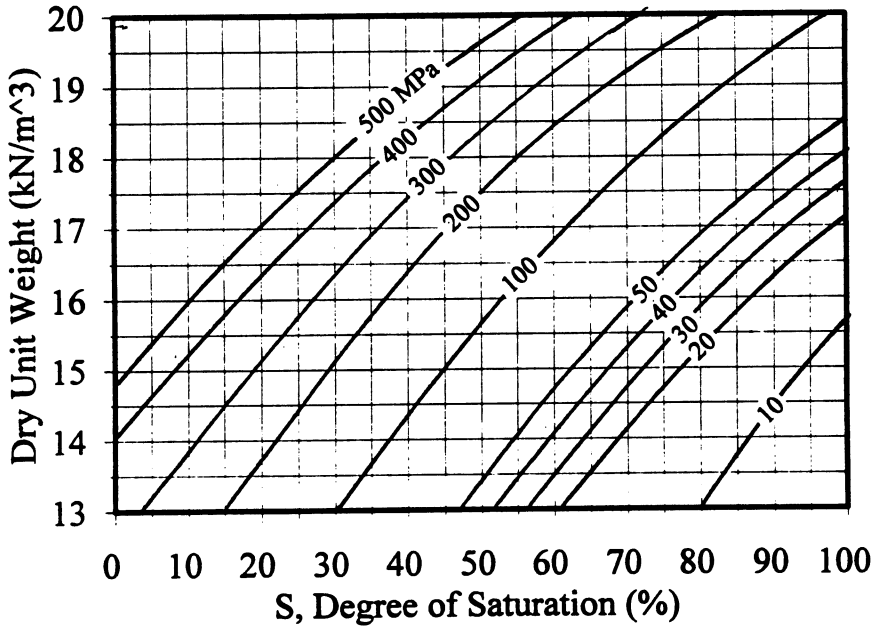

Figure 20e. Resilient Modulus Correlated From CBR (Heukelom and Klomp, 1962): Dickey Lake Subgrade

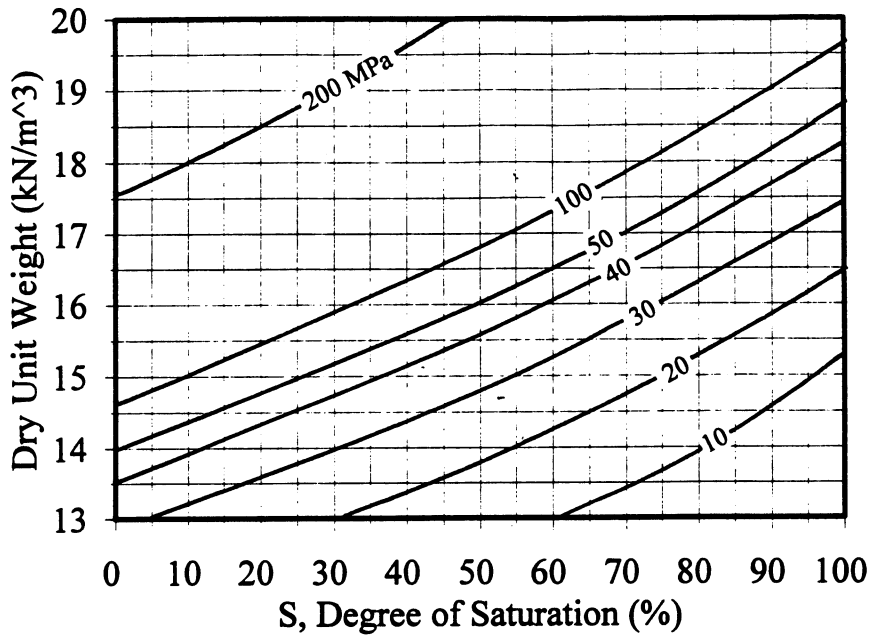

Figure 21a. Resilient Modulus Correlated From CBR (Van Till et al., 1972): Sunburst Subgrade

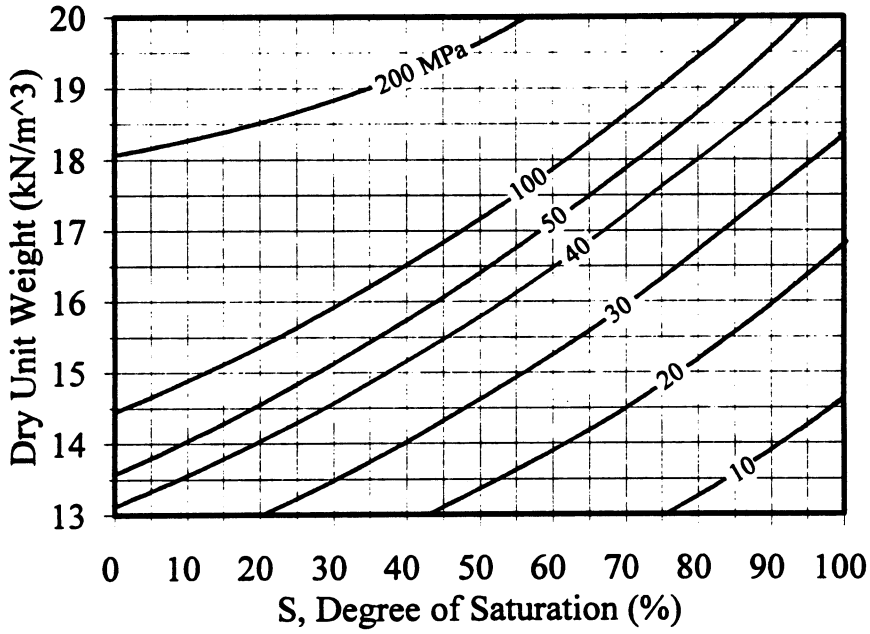

Figure 21b. Resilient Modulus Correlated From CBR (Van Till et al., 1972): Alzada Subgrade

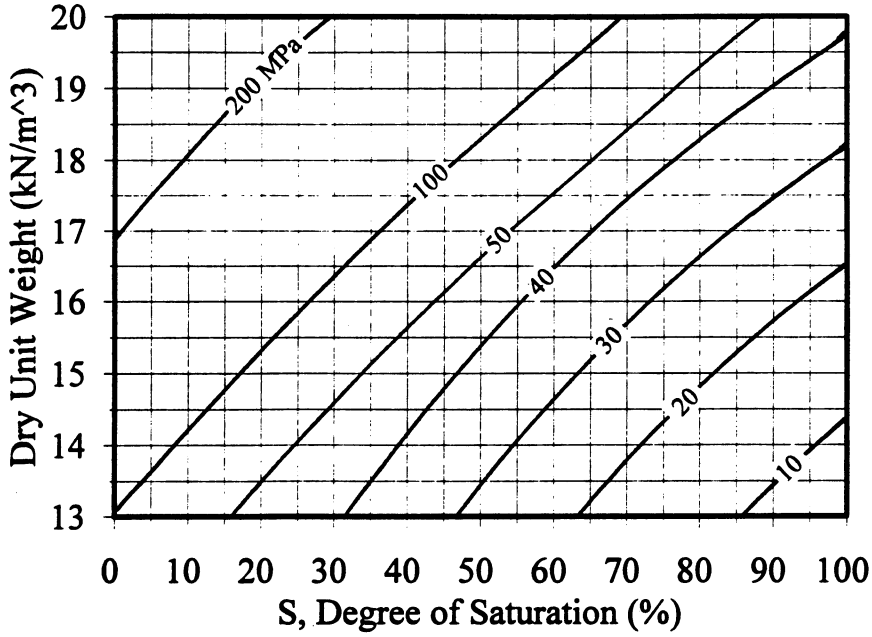

Figure 21c. Resilient Modulus Correlated From CBR (Van Till et al., 1972): Loma Subgrade

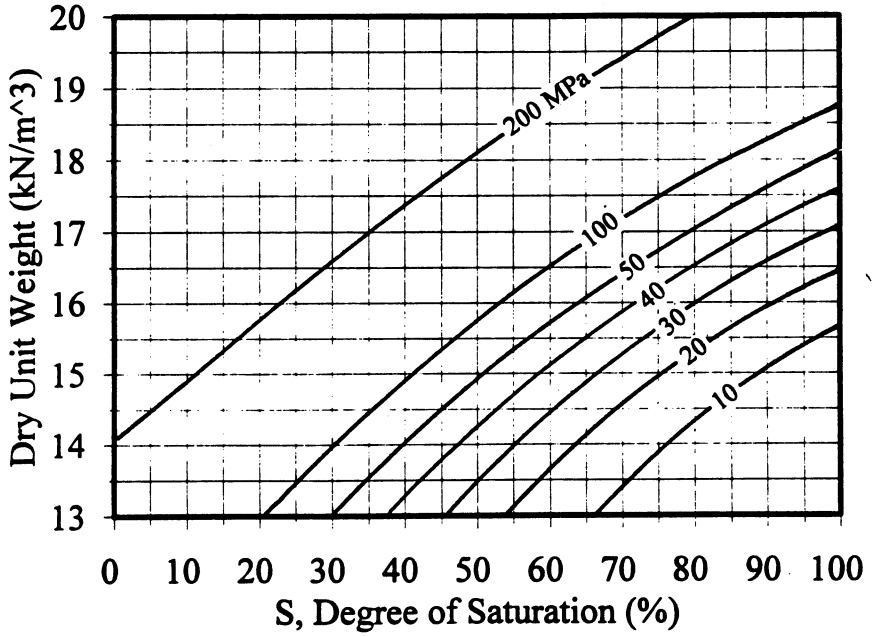

Figure 21d. Resilient Modulus Correlated From CBR (Van Till et al., 1972): Swan Subgrade

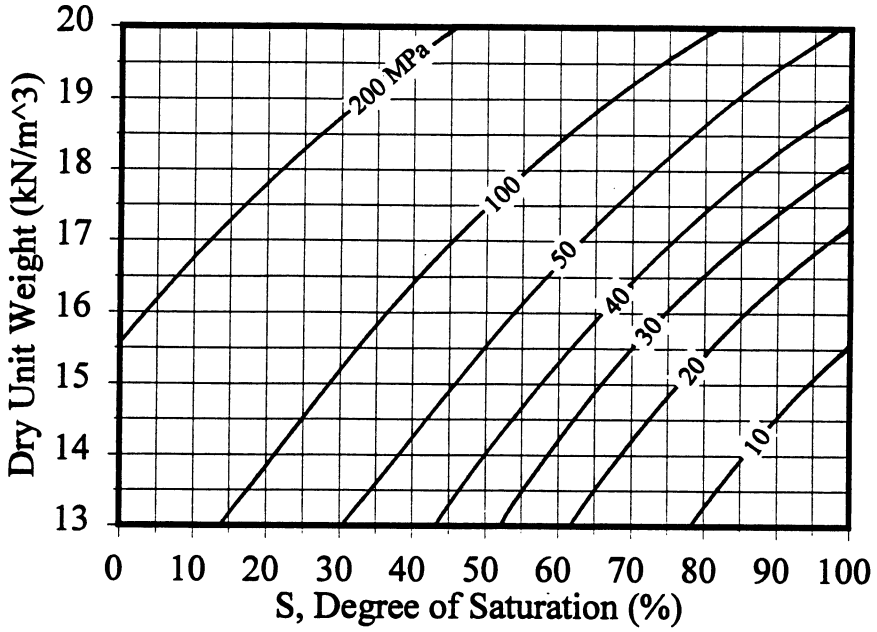

Figure 21e. Resilient Modulus Correlated From CBR (Van Till et al., 1972): Dickey Lake Subgrade